Scale growth study in a concentric reducer: Measurement of instantaneous velocity using Particle Image Velocimetry

By

Tabassum Rasheed

A thesis submitted in fulfilment of the requirements for the degree of

Master of Engineering

Process engineering and light metals (PELM) centre

James Goldstone faculty of engineering and physical systems

Central Queensland University

Gladstone, Australia

March, 2005

To my parents with respect

Table of Contents

Abstract

Gibbsite scale growth in pipe fittings is a major problem for an alumina refinery. A recent investigation into the scale growth mechanism at an alumina refinery found almost 60 % more scale growth in a reducer when compared with the connecting straight pipe sections for similar flow conditions.

Scale growth occurs where liquor (supersaturated solutions) come in contact with solid surfaces and it is affected by the liquor flow velocity besides other physical and chemical parameters. The present work is dedicated to study the hydro-dynamical aspects of the mechanism of scale growth. In particular, the role of the phenomenon of turbulent bursting, stream wise and cross stream fluctuating velocity components (U_x and U_y) was investigated as the flow moves through the reducer. Particle Image Velocimetry (PIV) technique was used to get a full view of the reducer and the readings close-to-the-wall of the reducer at Reynolds number of 27,000 and 44,000 upstream which corresponds to Reynolds number of 41,500 and 66,000 downstream of the reducer respectively.

The results showed an increase in cross stream and a decrease in magnitude of stream wise fluctuating velocity components, whereby we presume that the increased cross stream fluctuating velocity component increases the frequency of impacts of the scaling particles on the wall thus initiating excessive scale growth in the reducer when compared with the connecting straight pipe sections, for similar flow conditions.

List of figures

List of tables

List of acronyms

2D	Two dimensional
3D	Three dimensional
A/C ratio	Alumina to Caustic ratio
AIA	Analogue interface adapter
°C	Degrees Centigrade
CCD	Charge-Coupled Device
CCI	Charge Contrast Imaging
CFD	Computational Fluid Dynamics
CQU	Central Queensland University
DC	Direct Current
ρ_p	Density of Particle
ρ_f	Density of fluid
DNS	Direct Numerical Simulation
d_p	Diameter of particle
dt	Time separation between 2 pulses
e_r	Percentage error
FFT	Fast Fourier Transformation
g	Acceleration due to gravity
g/dm^3	Grams per decimetres
gpl	Grams per litre

HFA	Hot Film Anemometry
HWA	Hot Wire Anemometry
Hz	Hertz
kPa	Kilopascal
kW	Kilowatt
LDA	Laser Doppler Anemometry
LIF	Laser Induced Fluorescence
m/sec	Metre per second
mJ	Millijoule
mm	Millimetre
mm/sec	Millimetre per second
MQD	Mean Quadratic Difference
msec	Millisecond
NaI	Sodium Iodide
Nd:YAG	Neodymium: Yttrium Aluminium Garnet
nm	Nanometre
PELM	Process Engineering and Light Metals Centre
PIP	Pattern Image Matching
PIV	Particle Image Velocimetry
PLIF	Planner Laser Induced Fluorescence
POD	Proper Orthogonal Decomposition
ps	Pico second
QAL	Queensland Alumina Limited.

r	Radius at a certain distance "x" from the centre in a section
R	Full radius of the section
Re	Reynolds number
RPM	Revolution per minute
SEM	Scanning Electron Microscope
TB	Turbulent Bursting
TKE	Total Kinetic Energy
TPD	Transfer Pulse Delay
u	Velocity of fluid at a certain distance "y" from centre of section
U	Centre-line velocity
μm	Micrometer
μsec	Microsecond
U_0^2	Average velocity
U_x'	Fluctuating velocity component in x – direction (stream-wise)
U_y'	Fluctuating velocity component in y – direction (cross-stream)
v	Kinematic viscosity of fluid
VFD	Variable frequency drive
V_s	Sedimentation velocity
δ	Boundary layer thickness

List of Publication

Following conference papers were published as a result of this Masters in Mechanical Engineering,

1) ***Energy saving potentials in an Alumina refinery : A review***
   Central Region Engineering Conference" 5-6 Sept. 2003, Rockhampton.

2) ***Viability of steam injection in gas turbines (co-authored)***
   BSME-ASME,
   International conference on Thermal Engineering, 2-4th January 2004, Dhaka, Bangladesh.

3) ***Scale growth study in a concentric reducer: Measurements of instantaneous velocity using Particle image velocimetry***
   VSJ – SPIE
   International conference on advanced optical diagnostics in fluids, solids and combustion, 4-6 December 2004, University of Tokyo, Tokyo, Japan.

A journal publication is in progress to be published in a major fluid mechanics journal such as Journal of Fluid Mechanics, or Experiments in Fluids or Journal of Turbulence etc.

Acknowledgment

I won't be able to do justice with my words while writing this page but I will try in the following lines to accept the assistance of few outstanding individuals and institutes involved with the achievement of present study. Firstly, I am thankful to the CQU for a scholarship and PELM centre that provided me the means and resources to complete my work leading to Masters Degree in Engineering.

I would especially like to thank Professor Martin C. Welsh, who apart from being far away from the campus and having a very busy schedule helped me a lot in my work and guided me whenever I required his advice. Also I want to thank A/Prof. Masud Khan, Dr. Mohammad Rasul and especially Dr. Alex Deev who assisted me in every way he could even on weekends. I would like to show special gratitude to A/Prof. Masud Khan and Dr. Mohammad Rasul who supervised my work and corrected my write-ups. I am gratified to these people, especially Prof. Martin C. Welsh from the depths of my heart.

I am thankful to Professor Warren Thorpe whose time to time follow-ups and appreciative attitude helped me a lot and kept me on track. I owe thanks to Csabi Szeles (Chabi), Courtney Miles, Jason Connor (especially), and Benita Maudsley. Thanks to my colleagues, staff at the Office of Research at Rockhampton and staff at CQU Library, Gladstone.

In the end, I am obliged to the members of my family for their patience and who supported me a lot and never demanded an excursion whenever I was busy with my work.

Introduction and Background Chapter 1

We never know the worth of water 'til the well is dry.
-- English Proverb

1.1 An Introduction to the problem

A Bayer plant is principally a process for heating and cooling a large re-circulating stream of Bauxite-caustic soda solution under controlled conditions. In the first major process (Digestion) the Bauxite ore (max. size 20 mm) is dissolved in the caustic solution at elevated temperatures (250 ^{0} C) and pressures (3500 kPa). At a later stage after the removal of impurities (Clarification process) the crystallization of the alumina from the liquor is carried out by cooling the liquor and adding crystalline tri-hydrate alumina in the precipitation section of the Bayer plant. This dissolution and precipitation of Bauxite ore enables the gibbsite to be separated from other minerals and also ensures sufficiently pure hydrate product which is further refined by removing chemically bonded water molecules from alumina at high temperatures (1200 ^{0} C) – a process called Calcination.

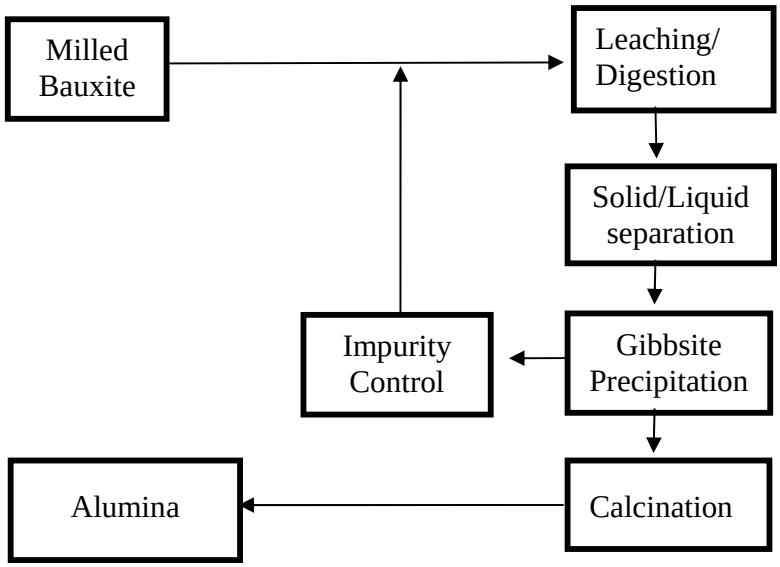

Figure 1.1 A generalized process schematic of a typical Bayer plant.

Scaling in different sections of the plant occurs as a consequence of heating at an early stage of the Bayer process and cooling at a latter stage, which results in the liquors becoming supersaturated with respect to Gibbsite and some other organic and inorganic substances (silicates, magnesium oxides oxalates and ferrous compounds etc). Scaling also occurs due to a high alumina to caustic ratio kept in the liquor for high yields. The total caustic content of Bayer liquor is typically in the order of 240 gpl (grams per liter) of Na_2CO_3 with about 140 gpL of this existing as free caustic soda.

This scaling phenomenon has been accepted as inevitable and inherent to many mineral processing and refining industries (e.g. lime, alumina and magnesium etc) for a long period of time. Although it is the largest refinery in the world with a maximum annual capacity of 3.7 million tons per year of alumina. Queensland Alumina Ltd. (QAL) is constantly challenged with the task of trying to remain competitive amongst the world's alumina producers. The need to

minimize costs and increase productivity has led to a demand for higher flow rates and caustic levels in the Bayer liquor with the associated risk of increased scale growth. With these economic pressures, it has become necessary to better understand the scale growth mechanism and factors affecting scale growth. The scaling problem is of particular importance to plants when tens of millions of dollars are spent annually to deal with it. It is estimated that direct cost of scale removal may contribute as much as one quarter of the operational costs of an alumina refinery (Thomas, 1997).

Scaling in plant equipment causes many problems like, reduction in heat exchanger efficiency, reduced residence time through decreased tank volumes, the need to construct spare equipment, production limitations from reduced flows, blockages from detached scale, the need for scale removal (both chemically and mechanically) and the need to construct spare equipment. All of these problems accumulate to generate high maintenance expenses and impact directly on the cost of production. Understanding the mechanism of scale formation can assist in reducing the scale growth problem. The present work is dedicated solely to the role of hydro-dynamics of fluid/liquor vis-à-vis the scale growth mechanism.

For the scale to be formed on the surfaces two important processes are “nucleation” and “growth”. The other contributing factors are super-saturated solutions and adherence of crystals to the already formed and deposited crystals on the surfaces. In the precipitation section the most rapidly forming scale is hydragillite or gibbsite scale or aluminum tri-hydrate–Al $(OH)_3$ scale. Organic compounds in the Bauxite dissolve and breakdown to form Oxalates and the liquor is often supersaturated relative to sodium oxalate. This oxalate scale growth reduces the efficient operation of precipitation tanks. It has been identified by recent investigations at an alumina refinery and studies of heat exchanger tubes that the fluid’s bulk velocity can play a vital role in

the formation of scale (Adomelt and Renz, 1995, Nawrath's thesis, 2004). This bulk velocity in turn determines the boundary layer conditions located very close to the wall where scale is deposited. Based collectively on a model of gibbsite scale growth, gibbsite dissolution and the scale crystallization process it was also proposed that the scale is a net result of the process of particle deposition and particles detachment or erosion in the wall bounded flows. Both processes are independent of each other. The scale can be formed and deposited at a steady rate whereas erosion or detachment of particles can be an intermittent process (Nawrath, 2004). For a fully developed turbulent pipe flow, the thickness of the viscous sub-layer is very small and is characterized by a high shear stress value. It is further assumed that there is a critical wall shear stress value below which the particle deposition process is dominant where as at above this critical shear stress value the particle detachment or erosion is more dominant (Beal, 1970, Cleaver *et. al.*, 1972, 1975). The net scale growth is the result of the difference between the particle deposition process and particle detachment process.

Firstly, understanding the scale growth mechanism can assist in reducing the scale problem, by

- Indicating how scale grows onto the surfaces in different physical and chemical conditions, and
- How scale attaches to the wall and solid objects.

These mechanisms will depend on saturation levels; flow conditions, solid object geometries, (fluid's rheology) like viscosity, temperature and density.

There is very little knowledge about how these parameters affect scale formation and deposition

The scaling problem in an alumina plant is complex and multi-faceted. There are many factors and parameters involved (both physical and chemical), which can play a crucial role in the mitigation of scale formation. The main factor in the scaling mechanism is the level of super

saturation, which the alumina refineries cannot lower or alter. The by-product is directly affected if the alumina to caustic ratio (A/C ratio, where A and C refer to aluminum and caustic concentrations expressed as Al_2O_3 and Na_2CO_3 in g/dm respectively) is lowered in a Bayer plant. The other scale-reducing options include process innovations and process optimization, which are long-term goals. The short-term possibilities include studying the effect of mainstream flow velocities and agitation levels

A series of experiments at an alumina plant (Queensland Alumina Ltd) was conducted in order to study the rate of Gibbsite scale formation on wall pipes. Among other findings one of the noticeable results were almost 60% more scale growth in a concentric reducer as compared with straight pipe sections under the same flow conditions.

1.2 Main Hypotheses behind More Scale Growth in a Concentric Reducer

Further investigation into the causes of enhanced scale in the concentric reducer leads to five hypotheses set forth by the investigation team at QAL. These hypotheses are based on fluid mechanics theory and alumina plant operational experience. The 5 hypotheses are,

1) The concentric reducer is connected with pipes sections through flanges. The two joined flanges have small notch (groove) in between them where the flow separation can take place. The flow separation can provide conditions ideal for scaling particles to have enough residence time to attach them to the wall.
2) The sudden contraction may cause boundary layer separation resulting in similar conditions perfect for scaling as explained above. This hypothesis was tested using dye injection method by Nawrath (2004) and he concluded that there is “no” boundary layer separation in the concentric reducer.
3) The instantaneous fluctuating velocity components in the near wall region are changing in magnitude and facilitating the scaling particles to form more scale in the reducer as compared with straight the pipe. As a result of these changes the scaling particles have better boundary layer penetration capabilities to initiate scale formation. This change in fluctuating velocity components is observed in the present work using Particle Image Velocimetry (PIV) technique. The role of turbulent bursting is also discussed.
4) The pipe section and concentric reducer are manufactured from different materials having different grain structure. It is possible that the grain structure of the concentric reducer is more suitable for the scale formation.

5) Fluid particles accelerate as the flow moves through the reducer. This flow acceleration can possibly increase the velocity of the suspended scaling particles to gain enough momentum to cross the boundary layer there-by increasing the chances of more scale formation in the concentric reducer as that of joining straight pipe sections.

Please note that here only third hypothesis is explained due to its relevancy with the present work.

1.2.1 Localized velocity effect

In a turbulent flow all three-velocity components are essentially nonzero. In the literature, we find that the behaviour of $U_x^{'}$ and $U_y^{'}$ (stream-wise and cross-stream) velocity components are changed as the flow passes through the contraction. For example, Torbergsen and Krogstad (1998) studied stream-wise, cross-stream and circumferential components experimentally using hot film anemometry technique in an axisymmetric contraction at Re = 35000. They measured the 3 velocity components along the whole length of an axisymmetric contraction. They found that the contraction caused a severe reduction in the stream wise components and a sudden gain in the cross-stream fluctuating velocity components. They also concluded that in the end the total turbulent kinetic energy remains conserved. The third hypotheses is based on the assumption that the decreased stream-wise fluctuating velocity components and increased cross-stream fluctuating velocity components may lead to the conditions ideal for more scale deposition and less scale erosion. This could be due to:-

- A decrease in the critical value of the shear forces required to maintain constant erosion in the near wall region, or,
- The particles suspended in the fluid have an increased ability to cross the turbulent boundary layer.

- The intensity of the turbulent bursting into the sub-layer reduces as the flow accelerates through the contraction.

The present work is related to the study of these fluctuating components (u and v) and the frequency of the "turbulent bursting" in the near wall region as the flow passes through the reducer using Particle Image velocimetry (PIV). The main advantage of the PIV technique is that the instantaneous flow velocity is recorded within the plane of a light sheet. Thus PIV is best suited for the measurement of global unsteady flow fields.

1.3 Turbulent Bursting Phenomenon

It is now known that a boundary suppresses the normal components of turbulent fluctuations due to the kinematic constraints and generates the organized structures if a mean shear is imposed on it. When the shear is increased alternating high-speed and low speed regions are observed near the boundary layer. These regions initiate turbulent bursting. It is a randomly occurring process consisting of a gradual local lift up of low speed streaks, sudden oscillations and ejection of low momentum fluid from the wall into the main stream. This is then followed by an in-sweep of high-momentum fluid into the wall region. This is called a turbulent bursting phenomenon

1.4 Aims and objectives of present research

The objective of the present study is to test the third hypothesis explained earlier. PIV is used to detect the quantitative change in the behaviour of the instantaneous fluctuating velocity components as the flow passes through the reducer. The frequency of "turbulent bursting" into the near wall region is also studied.

Theory and literature Review Chapter 2

A love affair with knowledge will never end in heartbreak.

Michael Garrett Marino

2.1 Introduction

In this chapter the mechanism of scale formation and types of scales formed in a Bayer process are discussed. The chapter also contains a review of fluid flow in an axisymmetric contraction (or concentric reducer), a review of the particle attachment and detachment processes, sections on the principle of PIV, review of PIV experimental methods flow, visualization and the phenomenon of turbulent bursting.

2.2 Mechanism of scale growth and types of Scales

Scale is a crystalline structure usually formed when in a saturated solution the physical or chemical conditions are changed. At one hand it is essential for the production of alumina crystals and on the other is unwanted in the form of crystalline deposits on equipments in an alumina refinery. As mentioned earlier the direct cost of scale removal may contribute as much as one quarter of the operational costs of an alumina refinery (Thomas, 1997).

Scaling occurs mostly when the liquor is super-saturated. In an industrial environment, it can occur both in liquor and in slurry systems. Within one liquor stream it is possible for the scale to form in one area, but not in other area, because of changes in process conditions, even without a

change in liquor composition. The scaling might occur either because the process change resulted in making the liquor super-saturated (a decrease in temperature) or by increasing the kinetics of precipitation (an increase in temperature). In a Bayer plant the most commonly occurring scale is gibbsite or tri-hydrate aluminate (also called hydragillite) scale. It forms during the precipitation from super-saturated caustic aluminate solution or pregnant liquor where liquor spends over half of its residence time in precipitation tanks due to the slow kinetics of crystallization.

At a local alumina plant (QAL - Gladstone) a test rig was designed, fabricated and installed along a tank in the precipitation section of the plant. The rig was installed in order to simulate the scale formation under industrial conditions in precipitation tanks with real liquor under different Re numbers i.e. 28,000, 40,000 and 66,000. The Re numbers were based on the pipe diameter and bulk velocity of the caustic liquor passing through each pipe section. These Re numbers were achieved by using different pipe diameters and connecting them with concentric reducers. (See figure in Appendix B).

Along with many other findings about the formation of scale growth in association with the same caustic liquor flow parameters the notable results are highlighted below. On average:-

- There was less scale (12 mm thick average) in the high fluid velocity regions in straight pipe sections
- Almost 60% more scale was deposited in the concentric reducers than in the straight pipes for similar flow conditions.

Figure 2.1 A typical pattern of Gibbsite scale growth in reducer (Nawrath's thesis, 2004)

For the scale to be formed on the surfaces two important processes are "nucleation" and "growth". Gibbsite crystal growth from caustic aluminate solutions has been studied extensively over the past few decades, from the single crystal to the bulk precipitation studies. Still much work is needed to fully understand the crystal growth mechanism. Based on an experimental study, Brown, (1972) showed that gibbsite growth is through two dimensional nucleation growth mechanisms. Where as studies by Lee and Parkinson, (1999) on a single gibbsite crystal showed that the crystal surface structure and the super-saturation levels play an important role in determining the crystal growth mechanism. Gibbsite precipitation studies have shown that gibbsite crystal growth is surface integration controlled. (Misra and White, 1971, Ilievski 2001). Li *et. al.*, (2003) studied the crystal growth from caustic aluminate solutions under different flow regimes at 80 degrees C. They concluded that hydrodynamics has little or no effect on growth

rates. The growth rate estimates from their experiments showed the gibbsite growth has second order dependency on super-saturation.

On the molecular level, the nature of gibbsite crystal-liquor interfacial layer, the surface forces involved and their consequent impact on the particle interactions which influence crystal growth and agglomeration (aggregation and crystal growth) have not been studied in detail. Direct measurement of the inter-particle interaction forces under Bayer precipitation conditions is a difficult task and has been only investigated recently (Addai-Mensah and Ralston, 1999, Roach *et. al.*, 1998 and few others). Strong repulsive structural forces were observed to account for the unusual colloid stability of gibbsite in fresh, super-saturated Bayer liquor. After some time these forces between gibbsite crystal showed adhesive properties (Addai-Mensah and Ralston, 1999). This conversion of repulsive forces into adhesive forces is believed to be due to the presence of Aluminum containing compounds. Addai-Mensah *et. al*., (1998 and 1999) conducted experiment on freshly prepared pure synthetic caustic aluminate solutions (with initial A/C ratio of 0.7). They used a quantum mechanics molecular modeling technique to investigate the inter-particulate forces and inter-facial structures occurring in gibbsite-sodium or potassium aluminate dispersions. Initial inter-particle repulsive forces decrease gradually with time where as adhesive forces subsequently emerge and grow upon further aging of liquor. They also concluded that higher order secondary agglomeration is the principle mechanism of enlargement for colloidal size particles rather than crystal growth. Scanning electron microscope (SEM) and crystal size studies of the crystallized product showed that agglomeration is more pronounced in sodium than in potassium based Bayer liquors and more prevalent between non crystal faces.

Roach *et. al.*, (1998) developed a new electron microscopic technique called Charge Contrast Imagining – CCI, This technique enables the study of the growth history of gibbsite particles

from the Bayer process. Growth of gibbsite on different crystal faces can be directly measured along with the initiation of nucleation can be detected with this technique. Prestidge *et. al.*, (2000) used Rheological methods and concluded that gibbsite agglomeration occurs by reversible aggregation followed by irreversible cementation.

Generally, there are two types of scales in a Bayer plant (Roach and Cornell, 1996). Growth scales and settled scale. A brief description is mentioned below.

2.2.1 Growth Scale

Growth scale is highly crystalline, non porous, hard and brittle with usually well defined crystal growth faces. The scale is often translucent. Growth rate is normally in the range of 0.1 to 1.0 mm per week. In pipes the moving liquor produces a more uniform and even scale as compared with the liquor in tanks where due to stagnant conditions at the tank walls, the scale is more dendritic/protruding in nature. (Nawrath, 2004)

2.2.2 Settled Scale

A settled scale is formed when slurry particles are settled and can be cemented by the super-saturated liquor. Settled scales are usually porous and soft. Actually the more porous or soft a scale is the more rapid is its formation. Such settling out and cementation occurs preferably in low velocity regions of plant equipment or during shut downs.

2.3 Review of fluid flow in an axisymmetric contraction

Most of the available literature on a flow through an axisymmetric contraction is for non-Newtonians fluids and flow of polymer melts. The work done by Torbergsen and Krogstad, (1998) studied fully developed turbulent flow through an axisymmetric contraction producing constant strain rate. They used hot wire anemometry to study three fluctuating components of velocity (stream-wise, cross-stream and radial components). They found a redistribution of energy between the three components as the flow moves through the contraction. The stream wise component is decreased and there is a similar gain in cross components in such a way that total turbulent kinetic energy remains constant in the initial section of the contraction. The stream wise component almost vanishes in the later section of the contraction. This results in a gradual increase in turbulent kinetic energy in the later section of the contraction. At the end the flow develops into a two component axisymmetric turbulence. Mainly their work is focused on the region not very close to the wall of the contraction. Their measurement lacks any data very close to the wall region.

Similarly, Kim-E *et. al.,* (1983) used finite element analysis for the generalized Newtonian fluid flow through an axisymmetric sudden contraction. They suggested that acting alone either increased shear-thinning of the viscosity or increasing fluid inertia suppressed the upstream vortex that surrounds the opening of a small section. They also showed that peaks in axial velocity were found for moderate and high Reynolds's numbers away from the centre of the tube and were enhanced by shear-thinning, which decreased the viscosity and consequently increase the local Reynolds number near the wall of the small section of the contraction.

Few other experimental observations were cited in the literature where the axi-symmetric is a part of the overall geometry for example in contraction-expansion geometry by Rothstein and McKinley, (1999, 2001). Laminar flow in a sudden axi-symmetric contraction was studied by Tachibana *et. al.*, (1987).

2.4 Phenomenon of Turbulent Bursting

A detailed investigation of the turbulent boundary layer has shown that the viscous sublayer is always changing (unsteady), and is continuously disrupted by turbulent "bursts". This phenomenon is associated with most of the turbulent energy production in this region and in the entire shear flow. Flow visualization experiments by Kline *et. al.,* (1967) led to one of the most important advances in turbulence research using hydrogen bubble wires in addition to the dye injection method. They showed that the inner part of the wall layer in the range of $5 < y^+ < 70$ is not at all passive as one might think. In fact it is perhaps dynamically the most active area in spite of the fact that it occupies only about 1 % of the total thickness of the boundary layer. Kovasznay (1967) divided the turbulent boundary layer into four distinct regions as sublayer, turbulent wall layer, outer region and super-layer. Persistent flow patterns or coherent wall structures have been observed by many investigators. (Cleaver and Yates, 1975, Corino and Brodkey, 1969, Grass, 1971, Kline *et. al.,* 1967, and Blackburn, 2001). They reported these basic sequence of bursts as, 1) The appearance of a relatively low speed region of fluid near the wall; 2) The lift-up of this low "speed streak" from the wall followed by some form of "oscillatory growth" and; 3) Ultimately the "break up" of any signs of coherency in the visual representations of this structure. This entire three stage process is called "bursting" or eruption process and is essentially an ejection of slower fluid into the mainstream flow. The flow into which ejection occurs decelerates, causing a point of inflection in the profile. The secondary flow associated with eruption motion causes a stretching of the span wise vortex lines, these vortex lines amplify due to inherent instability of an inflectional profile and readily breaks up producing a source of small scale-turbulence. The strengths of eruptions vary and the stronger ones can go right through to the edge of the boundary. This is "Sweep" or inrush of fluid during which high-speed fluid moves

towards the wall. Kline *et. al.*, (1967), found that the ejected fluid from the burst has a stream wise velocity equal to about 0.8 of the bulk velocity. Rao et al. determined the mean burst time period to be about $5\delta / U_0$ - where, δ is the boundary layer thickness and U_0 is the bulk velocity, (Rao et al. 1971). Thus the ejection process is responsible for some portion of the Reynolds stress, since a part of ejected fluid has $u' < 0$ and $v' > 0$, leading to a correlation of $u'v'$ of less than zero. It is widely suggested that virtually all turbulence production is a result of the bursting or ejection process, especially near the wall. Kline and Robinson, (1990) also reported hook shaped vortical structures in their work.

2.5 Mechanism of Particle attachment, particle detachment and turbulent bursting in relation to the scale growth

Experimental and direct numerical simulations (DNS) into the fundamentals of particle deposition enable us to determine operating conditions under which deposition can be significantly reduced. Flow rate has been found to be of large influence, since hydro-dynamic lift induced at sufficiently high shear rates prevents particles from depositing by transporting them back into the bulk flow. Based collectively on a model of gibbsite scale growth, involving the deposition and erosion of scale it was also proposed that the net scale growth is a result of the process of particle deposition and the erosion of particles in the boundary layer. Both processes are independent of each other. The scale can be formed and deposited at a steady rate whereas erosion or detachment of particles can be an intermittent process. It is further assumed that there is a critical wall shear stress value below which the fluid deposition process is dominant where as at shear stresses above this critical shear stress value the particle detachment or erosion is more dominant. The net scale growth is the result of the difference between the deposition process and the erosion process (Adomelt and Renz 1995). Hasan, (2002), modeled the deposition rate of small particles on a spherical collector under turbulent flow conditions. His study is based on three different cases for particle sizes. He showed that higher deposition rates results when the mean diameter of small particles get smaller and when the mean diameter of the collector particle gets larger. This study assumes that no detachment of particles took place during the experiment.

Narayanan and Lakehal, (2003) studied particle dispersion and particle deposition in the region near the wall of a turbulent open channel using direct numerical simulation (DNS). They divided the deposition particles in two categories 1) free flight deposition and 2) diffusional controlled deposition. Deposited particles with large normal velocities and small near wall residence times

are referred to as free flight deposition. Where as deposition induced by small near wall normal velocities and large near wall residence times is called diffusional controlled deposition. They concluded that the diffusional controlled deposition (small residual turbulent fluctuations) is the dominant mechanism for deposition. This result is contrary to the generally established opinion that free flight is the dominant mechanism of deposition in wall bounded flows. Their DNS study also revealed that diffusional controlled deposition occurs mostly along stream-wise oriented lines where as free flight particles deposit more evenly over the wall

Beal, (1970) described a method for predicting the deposition of particles entrained in turbulent flow. His method predicted the deposition of particles ranging from molecular size to approximately 100 microns in diameter.

Rashidi *et. al.*, (1990), experimented on particle-laden, fully-developed pipe flow. He conducted a series of experiments with different particle sizes, particle densities, particle loading and different Re numbers. They flow- visualised the boundary layer by successive photographic images for a turbulent pipeline flow. They stated that larger polystyrene particles of sizes1100 μm caused increased numbers of wall ejections. On the other hand the small polystyrene particles bring about decreased numbers of wall ejections. Wall ejections are basically the transport of low energy counter-rotating stream-wise fluid vortices from the boundary layer into the mainstream flow and in return the movement of high-energy vortices towards the boundary layer. These observations were first made by Kline *et. al.*, (1967) near a solid wall and later by Rashidi and Banerjee, (1990a) near a sheared gas-liquid interface. The bursting process is a randomly occurring event consisting of a gradual local lift up of low-speed streaks, sudden oscillation and ejection of low momentum fluid from the wall region into the main stream. This is then followed by an in sweep of high-momentum fluid into the wall region.

This spectacular phenomenon of bursting has been shown to be responsible for most of the turbulence energy production and to be the major contributor to the transport of Reynolds stresses. The above observation has been further confirmed in an experimental investigation by Kaftori *et. al.*, (1995) where the motion of particles was found to be intimately related to the action of the quasi-stream wise vortices populating the near wall region.

Dyer and Soulsby, (1988) have similarly shown the importance of bursting phenomena on the transport of particles on the ocean floor. The periodic ejection and in sweep events associated with the bursting process have been captured in the instantaneous measurements of the Reynolds stress. This is seen as a sudden rise in the Reynolds stress magnitude of up to 30 times the mean Reynolds stress. In the ocean these events are visible as swirls of sand that are lifted up above the ocean floor. Furthermore it is observed that the particle movement affects the fluid velocity profile (Taylor and Dyer, 1977, Itakura and Kishi, 1980 and Soulsby and Wainwrights, 1987).

Another very important contribution by Yung *et. al.*, (1989) was the study of interaction between turbulent burst activity and deposited particles within the viscous sub-layer of a wall bounded turbulent flow (Re from 17000 to 47000). They carefully placed micro-glass and polystyrene particles (50 μm diameter) on the surface such that the average particle layer is no more than single particles. In this way particles were completely submerged in the viscous sublayer. It was shown that only 1% of the particles are lifted up into the flow by bursts. However as the size of particles increased the number of re-entrained particles also increased. Though they failed to get any particle re-entrainment at low velocities of 0.2 to 0.5 m/s and Re numbers of 17000 to 47000, but they strongly believe that there is a *threshold* of local flow conditions (like shear stress and localized velocity or high energy fluid - vortices) at which particle re-entrainment can occur. They concluded that the ability of turbulent bursts to create sufficient lift force may be possible

with large-sized particles and with higher bulk or mean velocities. Present work is based at a Re numbers of 27000, 41500, 44000 and 66000 and flow velocities from 0.7 m/s to 1.3 m/s to study the penetration of the turbulent bursting into the boundary layer and to study the change in values of velocity fluctuating components, since it is assumed that the intensity of the bursts reduces in the contraction as the flow moves through it. This causes more scale to be grown in the contraction as compared to the straight pipe sections.

Kaftori *et. al.,* (1995), investigated the motion of solid particles near the wall in a turbulent boundary layer using flow visualization and LDA techniques. They used polystyrene particles with diameters ranging from 100 to 900 μm. Their work showed that the coherent wall structures are the dominant factor affecting particle motion near a solid boundary in turbulent flow. They affect deposition and entrainment also. They found “funnel” type vortices. These vortices generate high speed regions relative to the fluid in the viscous layer, sweep along the wall, pushing particles out of the way. In doing so they create conditions where particles may be entrained if they are light enough. If the particles are too heavy to be entrained, then they are pushed aside and form particle streaks, which are infact avenues along sides of the path traced by the vortices.

Marchioli and Soldati, (2002) using Direct Numerical Simulation (DNS) study reported a particle transfer mechanism due to strong coherent sweep and ejection events and specifically points out the effect of small stream wise vortices very close to the wall in promoting particle accumulation under the low speed streaks. Similarly, Corino and Brodkey, (1968) exposed images using a high speed motion picture camera moving with the flow of fluid. They observed regions very near to the pipe wall, including the viscous sub-layer, without injecting dye or disturbing the flow by the insertion of probes. They concluded that in a turbulent pipe flow the motion has a distinct

character which is a function of the distance from the wall. Within the distance of $y^+ \leq 5$ the flow is not laminar but is disturbed by velocity fluctuations of small magnitude and by the intrusion of bulk elements of fluid from the adjacent region. Where y^+ is the dimensionless distance from the wall expressed as $y^+ \equiv y\, u_* / \upsilon$, where "y" is distance from the wall, "u_*" is the frictional velocity and "υ" is the kinematic viscosity of the fluid. The region from $5 \leq y^+ \leq 70$ contains the position of origin of fluid ejection. The region beyond $y^+ \geq 70$ has reduced intensity of velocity fluctuations and a large scale of turbulence. They also pointed out that ejection of 3-dimensional disturbances occurs in the wall region randomly. The interaction of these disturbances (or ejections) with the mean flow creates turbulence.

Cleaver and Yates, (1972, 1975) quantitatively studied the effect of particle removal. They developed a model of the deposition of particles, which incorporates re-entrainment effects. In an earlier paper they described the mechanism of particle detachment and concluded that if the hydro-dynamical force is large enough to overcome adhesion, the particle will be detached from the surface and will be entrained in the main flow. They categorised deposition into two mechanisms (1) Diffusion controlled deposition and (2) Inertial controlled deposition.

Diffusion controlled deposition is for very small particles in turbulent flow. For larger particles diffusion becomes insignificant. Deposition is mainly controlled by inertial impact with the surface. They concluded that wall shear stress is a controlling parameter for particle removal and critical wall shear stress might be useful for estimating adhesion forces for re-deposition problems.

On the same grounds Adomelt and Renz, (1995) while studying the effect of fluid flow in the heat exchanger tubes study showed both experimentally and theoretically that deposition

decreases with increasing flow rates. This is due to the hydro-dynamical lift forces acting on particles caused by both flow confinement and shear in the vicinity of the heat exchanger tube surface. Their numerical simulation study showed that increased shear rates are an efficient means to prevent particles sizes between 0.4 to 1.5 μm from depositing by enhanced hydrodynamic lift. Very small particles of diameter 0.4 μm are hardly affected by lift forces. Sufficient shear forces can be achieved by high flow rates or by using relatively small diameter tubes to decrease particle deposition. This effect may be caused by high fluid's shear stresses induced by turbulent bursting activity. Further prediction of erosion in pipes was carried out by McLaury and Shirazi, (1998). They divided the flow into two regions, turbulent core and sub-layer buffer region. Their model predicts the ability of the particle to pass through each of these regions and to impinge on the wall.

2.6 Flow visualization and Particle Image Velocimetry

Flow visualization is the study of methods to display dynamic behaviour in liquids and gases under different flow conditions. It also studies behaviour of heat transfer through fluid and wall bounded motions. Its objective is to render a flow and/or temperature field visible in some way. (Many fluids are transparent, so motion and temperature are ordinarily invisible to the eye). But by using dye, tracer particles, and interference techniques it is possible not only to display these fields, but also to collect quantitative information about them. This field dates back at least to the mid-1400, where Leonardo Da Vinci sketched images of fine particles of sand and wood shavings which have been dropped into flowing liquids. Since then, laboratory flow visualisation has become more and more exact, with careful control of the particulate size and distribution. Advances in photography, large scale electronic integrations and advancements in computers have also extended our understanding of how fluids flow under various circumstances. More recently, computational fluid dynamics (CFD) has extended the abilities of scientists to study flow by creating simulations of dynamic behavior of fluids under a wide range of conditions. The result of this analysis is usually a 2-D or 3-D grid of velocity vectors, which may be uniformly or non-uniformly spaced. The goal is then to analyze this vector field to identify features such as turbulence, vortices, and other forms of structure. There are several variations on the structure of the field data which is generated by these experiments. A static field is one in which there is only a single, unchanging velocity field. Time-varying fields may either have fixed positions with changing vector values or both changing positions and changing vectors (for example, when modeling rotating turbine blades or pitching airfoils). These latter types are refered to as unsteady flows.

2.6.1 Principle of Particle Image Velocimetry (PIV)

In PIV, the velocity vectors are derived from sub-sections of the area under consideration. The flow is seeded with seeding particles. Keane and Adrian (1990) recommended a particle concentration of about 15 particles per interrogation volume for high quality PIV measurements. The distance between the two seeding particles is measured using two light pulses. The light pulses could be ordinary light or laser light. The laser light is used commonly since it's a highly coherent beam of light with single wavelength and is easy to form into a bright sheet of light for the illumination of the targeted area. The CCD camera images the target area onto the CCD array of a digital camera. The CCD is able to capture each light pulse in separate image frame. Once a sequence of two light pulses is recorded the images are divided into small sub-sections called interrogation areas, using specialized software. The interrogation areas from each image frame, I_1, and I_2 (figure 2.2), are cross-correlated with each other pixel by pixel. A pixel is defined as the smallest resolvable rectangular area of an image on the screen or stored in memory. Cross-correlation is a statistical approach for the analysis of PIV images. The correlation produces a signal peak, identifying the common particle displacement, "Δx". An accurate measure of the displacement and eventually of the velocity is achieved with sub-pixel interpolation. A velocity vector map over the whole targeted area is achieved by repeating the cross-correlation for each interrogation area point by point over the two image frames captured by the CCD camera (Figure 2.2).

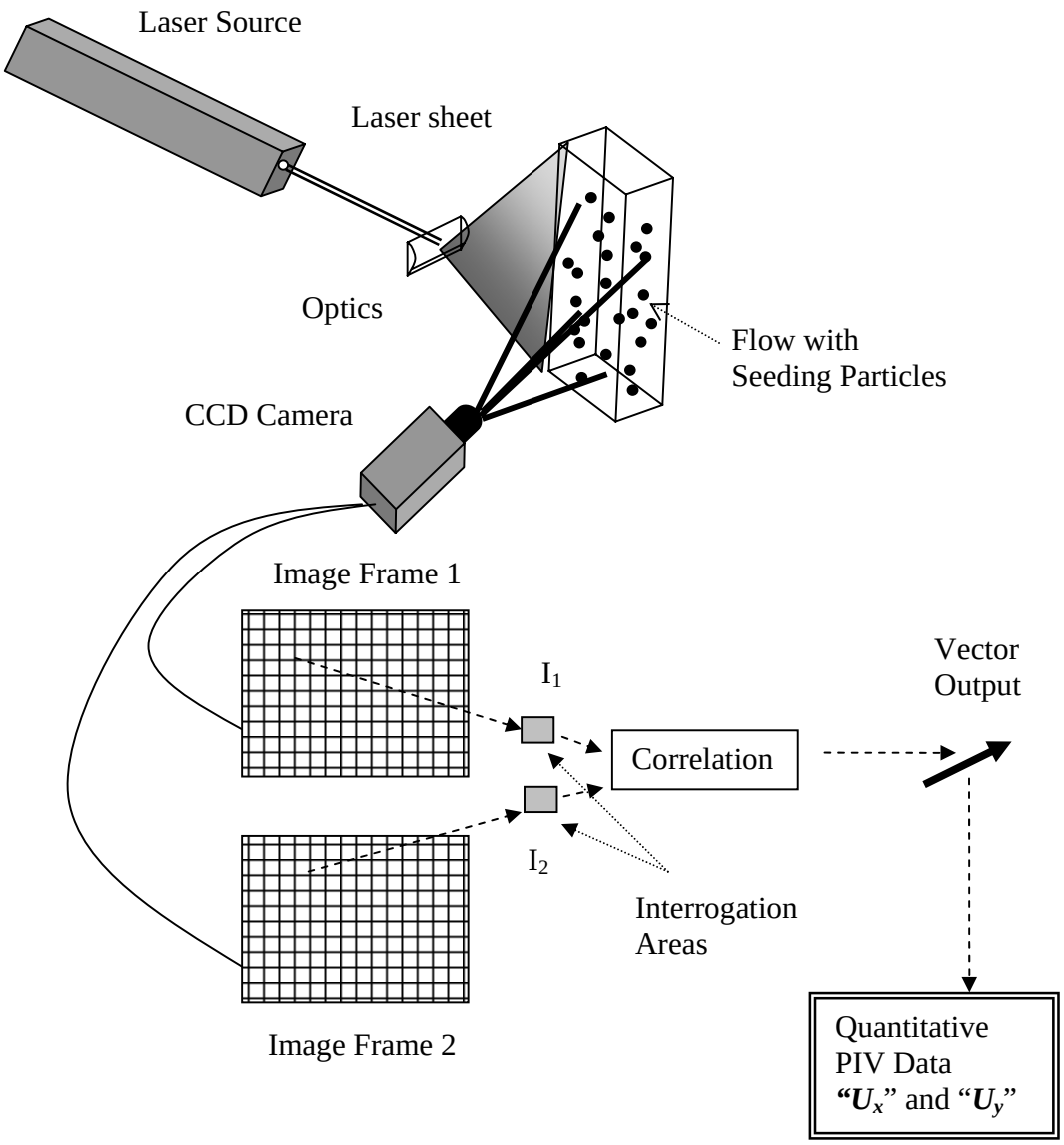

Figure 2.2A lay-out of a PIV system, where "U_x" is the stream wise fluctuating velocity component and "U_y" is the cross stream fluctuating velocity component.

2.7 Review of PIV experimental method

One of the challenges of fluid flow is the measurement of turbulence in a channel or pipe flow from wall to wall with a resolution sufficient enough to resolve the small scale motions. In addition to this, the measurement error needs to be small enough in order to measure the small velocity fluctuations near the centre-line and close to the wall region. The Particle Image Velocimetry or PIV is the method of choice. There are other options available (like Hot Wire Anemometry, Hot Film Anemometry, Laser Doppler Anemometry, Laser Fluorescent Anemometry and Laser Induced Fluorescence) but PIV is a full field quantitative method of measuring the velocity fields instantaneously. (Simpkins and Dudderar, 1978, Barker and Fourney, 1977, Dudderar *et. al.,* 1988 and many others).

Westerweel et al. (1996) studied turbulent flow at Re = 5300 in a fully developed pipe flow using PIV. They compared the PIV and LDV measurements with the direct numerical simulation-DNS. They found that the results are quite comparable. While studying the zero-pressure-gradient-boundary layer using PIV Adrian *et. al.,* (2000) detected hair pin vortexes in the boundary layer. They performed their experiment at three different Re nos. with a maximum of 6845 and showed that the boundary layer is densely populated by velocity fields with hair pin vortices. These hairpin vortices found in the outer layer occur in stream-wise aligned “packets” with small velocity dispersion. The number of hairpin vortices also increases in these packets with increasing Re no. Later on similar hair pin vortices were confirmed by Adrian and Liu, (2002) using both flow visualization and PIV method. They used DNS also to confirm the existence of hairpin vortex packets. Visualization of the DNS velocity field and vortices also shows the close association of hairpin packets with long low-momentum streaks and regions of high Reynolds shear stress

Similarly, (Ranade *et. al.,* 2001 and Escudie and Line, 2003), studied the trailing vortices behind the blades of a standard Rushton turbine using PIV. Angele and Muhammad, (2001) demonstrated that PIV was an important tool to investigate the mean velocity in the near wall region of a turbulent boundary layer. They performed measurements down to $y^+ = 8$ at high Re no. of turbulent boundary layer (see page 22 for explanation of y^+). Bugay *et. al.,* (2002) and Baldi *et. al.,* (2003) used PIV to analyze the flow field in a stirred tank with particular attention to the production and transport of turbulence and dissipation rate of turbulent kinetic energy. On similar grounds, in a stirred tank the CFD modeling was done by Ma *et. al.*, (2003). Comparison between the predicted and the experimental data measured by PIV show that all the major flow patterns are well produced in a CFD study. The quantitative comparisons showed encouraging agreement. Lastly, Papadopoulos and Hammad, (2000).developed PIV based flow meter for measuring seeded fluid flow in a straight pipe.

Limited number of researchers used the technique of refractive index matching for PIV studies (Uzol *et. al.,* 2002). Uzol et al. studied the flow of fluid through rotors and stator in an axial turbo-machinery using PIV. The rotor and stator was made of a transparent material (acrylic) that has the same optical index of refraction as the working fluid, a 64 % by weight NaI solution. This fluid has the specific gravity of 1.8 and a kinematic viscosity of 1.1×10^{-6} m^2/s .i.e. very close to that of water. Thus the rotors and stators become almost invisible, do not obstruct the field of view and do not alter the direction of the illuminating laser sheet. The draw backs of this technique are that the NaI solution needs to be protected from direct light and should be kept in oxygen free environment. Along the same lines Ciu and Adrian, (1996), used LDA and a refractive index matching technique to measure velocity vectors in a centrifugal pump. They used

a mixture of tetraline and turpentine as a working fluid to match the refractive index of the pump casing made from acrylic.

At the end different authors used different PIV post processing data evaluations methods. Among the various PIV evaluation methods correlation based algorithm plays a major role. Almost all algorithms for the estimation of the displacement of a group of tracer particles use cross-correlation techniques. We also used cross-correlation techniques for the evaluation of the PIV data. Another method to accelerate the PIV evaluation process is to use Fast Fourier Transformation or FFT. While using the FFT technique for post processing, interrogation windows of random sizes can be can utilized.

Gui and Merzkirch and Lindken et al (1999) used the minimum quadratic difference method (MQD) to evaluate vector plots from PIV images. The MQD technique is in principle a tracking of particle image patterns and therefore is more comparable with the correlation based tracking algorithm than with evaluation by using fixed interrogation windows for relatively small displacements less than one pixel. Huang (1998) described a post processing technique called particle image pattern-matching (PIP-matching). He concluded that the PIP-matching technique is good for boundary layer analysis when compared with the auto-correlation PIV post processing technique. PIP-matching showed a better spatial resolution than the auto-correlation technique. Liberzon *et. al.,* (2001) used the proper orthogonal decomposition technique (POD) for the post processing of PIV images to study coherent structures in a wall bounded flow. They constructed the vorticity field with the POD method which was masked by the effect of background vorticity for which coherent features could not be revealed by using conventional PIV post-processing methods.

2.8 Conclusion

- There are two types of scales reported in the literature, 1) Growth scale and 2) Settled scale. Growth scale grows onto the surface due to crystallization of gibbsite and oxalate from over-saturated liquor where as settled scale grows mainly due to the agglomeration (aggregation and binding of liquor particles) of particles from a solution.
- In a scale growth study at a local alumina refinery excessive scale was found in the concentric reducer as compared with connecting straight pipe sections for similar flow parameters.
- Hydrodynamics or agitation of liquor has little or no effect on the precipitation of growth scale, whereas agglomeration (first step in settled scale formation) of caustic liquor particles is flow dependent. Hence a study of fluid flow in a concentric reducer is necessary to understand why there is additional scale growth in a concentric reducer.
- Liquor velocity has a non-monotony effect on the scale growth. At lower liquor velocities it could be the increase of scale growth rate. However, if flow accelerates, at high bulk velocities in pipes, scale may disappear which has been explained earlier. It is also noticed that close to the wall shear stress value plays a dominant role in the particle removal phenomenon.
- Near the wall velocity decreases and velocity fluctuating components (stream-wise, cross stream and radial) start playing a prominent role in scale formation or otherwise. Study of flow through an axisymmetric contraction revealed that there is a redistribution of the three fluctuating components in such a way that total kinetic energy (TKE) remains constant and eventually at the end of the axisymmetric contraction the stream wise

component almost vanishes. Hence it is necessary to learn the behaviour of these components through a concentric reducer.

- We found that for the present study PIV is the method of choice when compared with other techniques since it can give an instantaneous full field quantitative velocity vector information of the flow from which fluctuating components can be evaluated and categorized. Other techniques provide velocity values at a single point in the flow.

Experimental Procedure Chapter 3

> It is best to learn as we go, not go as we have learned.
>
> Leslie Jeanne Sahler

There are number of techniques and procedures available to flow visualize and measure flow parameters (mostly fluid's velocity) in a fluid flow both as an average and instantaneous values. Few of the main techniques are hot wire anemometry (HWA), hot film anemometry (HFA), laser induced fluorescence (LIF), planner laser induced fluorescence (PLIF), particle image velocimetry (PIV) and laser doppler anemometry (LDA). Each technique is different in terms of principle of operation and its application and is used for diverse flow visualization requirements. As an example where high frequency repeatability is required with a single point measurement values in the bulk flow, HWA is used where as HFA is used for wall shear stress measurements on the wall. Similarly LIF and LDA have different application requirements. Some techniques are single point measurements like HWA and LDA. We used PIV for our flow measurements because it is the only technique, which can measure full field instantaneous velocity.

3.1 Introduction to PIV

Particle image velocimetry or PIV is a whole-flow-field technique providing instantaneous velocity vector measurements in a cross-section of a flow. Two or three velocity components (stream-wise, radial and circumferential) can be measured. A CCD camera and dedicated computing hardware and software enable real-time velocity vector maps to be developed.

3.1.1 Main features of PIV

The technique is non-intrusive and measures the velocities of micron sized particles following the flow.

1. Velocity range from zero to supersonic.
2. Instantaneous velocity vector maps in a cross-section of the flow are obtained.
3. All three velocity components may be obtained with the use of a stereoscopic arrangement, but in our case we analysed only 2 components of velocity. i.e. stream-wise and cross-stream components.

3.2 TSI's PIV 200 Experimental setup

The TSI's PIV 200 experimental test facility at PELM centre, CQU, comprises of the following basic systems.

1. Nd:YAG laser source (with mirrors and lenses and laser positioning device)
2. CCD camera (with cables)
3. Personal computer with post-processing software
4. Seeding system
5. Delay generator, Power supply and Water chiller.

3.2.1 Nd:YAG laser source

The layout of the components used in PIV measurement is shown in figure 3.1. The PIV laser system used is a Quanta-Ray PIV pulsed series system, which generates a class 4 Nd:YAG laser beam. The laser wavelength is 532 nm in green spectrum and output of this system is specified at 350 mJ per pulse with their polarizations aligned in standard configuration. The PIV system is designed to be externally triggered by a high quality delay generator. Usually the Nd:YAG laser is operated in a repetitive mode. We operated the laser system at 10 Hz. The minimum pulse separation between two light sheets can be as little as 9 nano-seconds. The laser source used is manufactured by Spectra-Physics. The timing diagram of the laser source controlled by the delay generator is shown in figure 3.2.

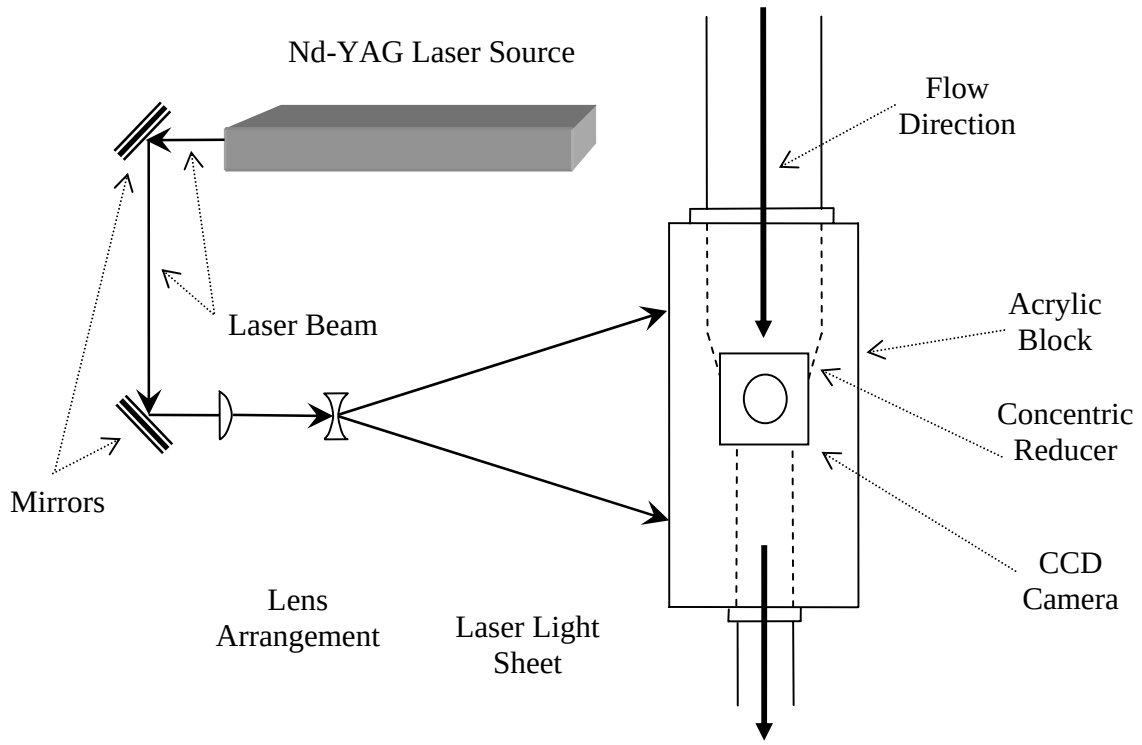

Figure 3.1 Nd-YAG laser system layout and acrylic model of a concentric reducer

3.2.2 CCD Camera

The camera used in our PIV application was KODAK MEGAPLUS Model ES 1.0. The AIA interface connector at the back panel of the camera sends digital output video to the computer and receives commands from the computer. The camera has an interline CCD sensor array with 1008(H) x 1018(V) light sensitive elements (pixels). The pixels are 9 microns square with a centre to centre spacing of 9 microns. The camera can be operated in a continuos mode or one of several “triggered” double exposure modes. Image exposure times as small as 125 microseconds is possible with the camera’s electronic shutter and the frame rate is unaffected by the exposure

time. The CCD camera was triggered by the same delay generator which controls the pulse separation time between the two consecutive laser pulses.

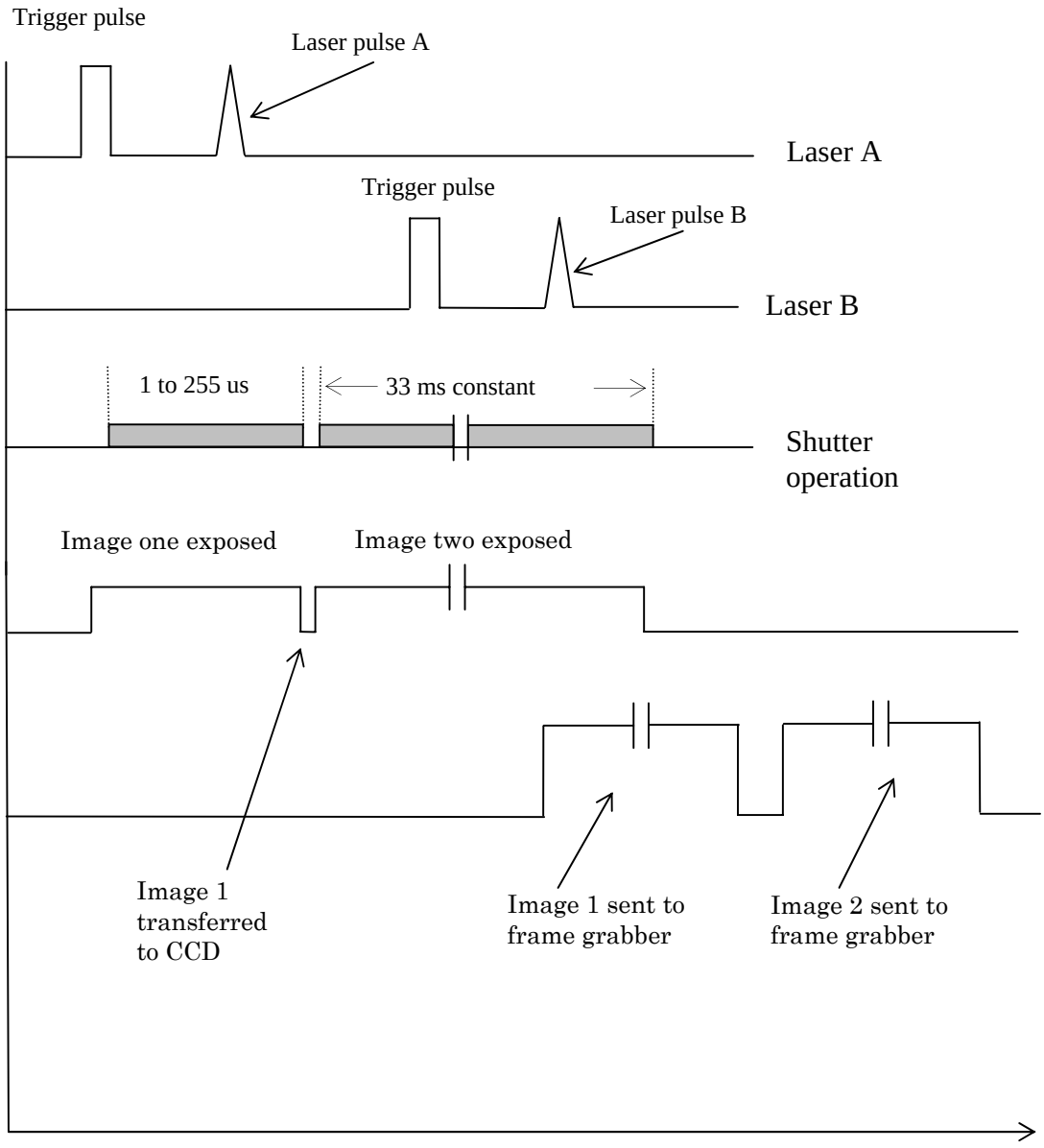

Figure 3.2 Nd-YAG laser and CCD camera timing diagram for the TSI's PIV 200 set up

We operated the camera in Triggered Double Exposure Mode. As it was mentioned in the section describing PIV technique, two successive images of a seeded flow are captured in rapid succession. This can be done in triggered double exposure. In the triggered double exposure two images are captured in rapid succession by the camera. This is accomplished by capturing the first image in diode array of the CCD camera, transferring the first image into the CCD array camera and then capturing the second image in the photo diode array. The first image is transferred from CCD to the frame grabber card while the second image is being captured by the diode array. The second image is then transferred into the CCD array and then on to the frame grabber card. In our experiments the first image had an exposure period of 175 micro-seconds, as set by transfer pulse delay (TPD) through software. The second image has fixed exposure of 33 milli-seconds. As shown in figure 3.2. We set our TPD at 175 micro-second and exposure time for 2^{nd} image was fixed at 11.0664 milli-seconds. The frame grabber transfers the recorded images from the camera to the hard disk of the host computer used to further analyse PIV images.

3.2.3 Personal Computer and PIV post processing software

The computer (with i486 micro-processor) is used to store the PIV images it receives from the frame grabber and to process the images and obtain quantitative data. The operating system is NT based. The software used to post process PIV images is TSI's "INSIGHT ^{TM} version, 1.01 software". The Insight software is high performance software designed to digitize and process multiply exposed PIV images. It is graphical based software and uses a high resolution monitor and display card mounted in the host computer. The software accepts images acquired through Kodak Mega plus 1.0 CCD camera. The system uses electronic capture for the recording of flow field images. The image acquisition is under PIV software control. Commercially there are two

modules available, (a) the acquisitions and processing module INSIGHT and (b) the post processing and presentation module or DATASHOW. We used only INSIGHT ™ software which contains features such as image file open, save, delete, image zoom, camera control, delta ‘t” (time separation) setting between two consecutive laser pulses, vector scaling, velocity calibration, Grid setup and generation of quantitative values of vector in stream-wise and cross stream directions along with their “x” and “y” location in the field of view.. The vectors are processed at a range of 10-40 vectors per second.

3.2.4 Seeding system

The single most important feature of a meaningful PIV data is the proper selection and use of seeding particles. As mentioned PIV is a method of visualizing a flow by tracking seeding particles within that flow. Therefore it is very important for the seeding particles to precisely follow the movement of fluid. This condition requires that the seeding particles be neutrally buoyant in the fluid and they must have acceptable light-reflective properties. After all it does not matter how well the particles follow the movement of the fluid if they do not reflect enough light to be captured by the camera. Apart from these an appropriate seeding density must be achieved. We used silver coated hollow glass sphere particles average size 10 microns for PIV images very close to the wall and polystyrene seeding particles, size range from 25 to 38 micron, for the whole images of reducer. The sedimentation velocity or settling velocity of these micro-spheres was calculated using Stokes’ law which is

$$Vs = \frac{g d_p^{\,2}}{18 \upsilon_f} \left\{ \frac{\rho_p}{\rho_f} - 1 \right\} \quad \text{..... (3.1)}$$

Where, "V_s" is the sedimentation or settling velocity of seeding particles, "g" is the gravitational acceleration, "d_p" is the diameter of particle, "υ" is the kinematic viscosity of the fluid (in our case water), "ρ_p" is the density of particle and "ρ_f" is the density of fluid. A particle is neutrally buoyant if its sedimentation velocity is nearly zero. The 10 micron hollow glass sphere particles sedimentation velocity and polystyrene seeding particles was close to 0.54 millimetres per second. Since this velocity is much smaller we assume that the motion of particles closely represents the fluid motion.

3.2.5 Delay generator, Power supply and Water chiller.

The delay generator (model DG535 of Stanford Research systems, Inc. USA) is a device used to control the timing order of the 2 laser pulses from the laser source, for maximum power output of the laser. It has a range from 0 seconds to 999.999,999,999,995 seconds with a resolution of 5 ps (Pico-seconds). The device is used to change the time separation between pulses for different flow velocities. Since for high speed flows (high Re nos.) the time separation between two laser pulses should be small, where as the time separation for low speed flow are relatively high to get good PIV vector plots. As a rule of thumb the time separation between the two consecutive PIV images should be 3-5 diameters of the seeding particles divided by the average velocity at that point. The power unit supplies un-interruptible supply of regulated power to the laser source generator and control panel of the laser. The water chiller keeps the water circulating through the laser source at a pre-determined temperature in the range of 6 to 20 degree Celsius. We set the temperature in the range of 16-20 degrees Celsius.

3.3 Flow visualization test rig

Schematic of flow visualization test rig is shown in figure 3.3. The test rig comprises mainly of the followings

- A water tank
- A variable frequency drive motor operated pump
- A water flow meter
- Flow straightening tube bundle
- An acrylic block (for flow visualization)

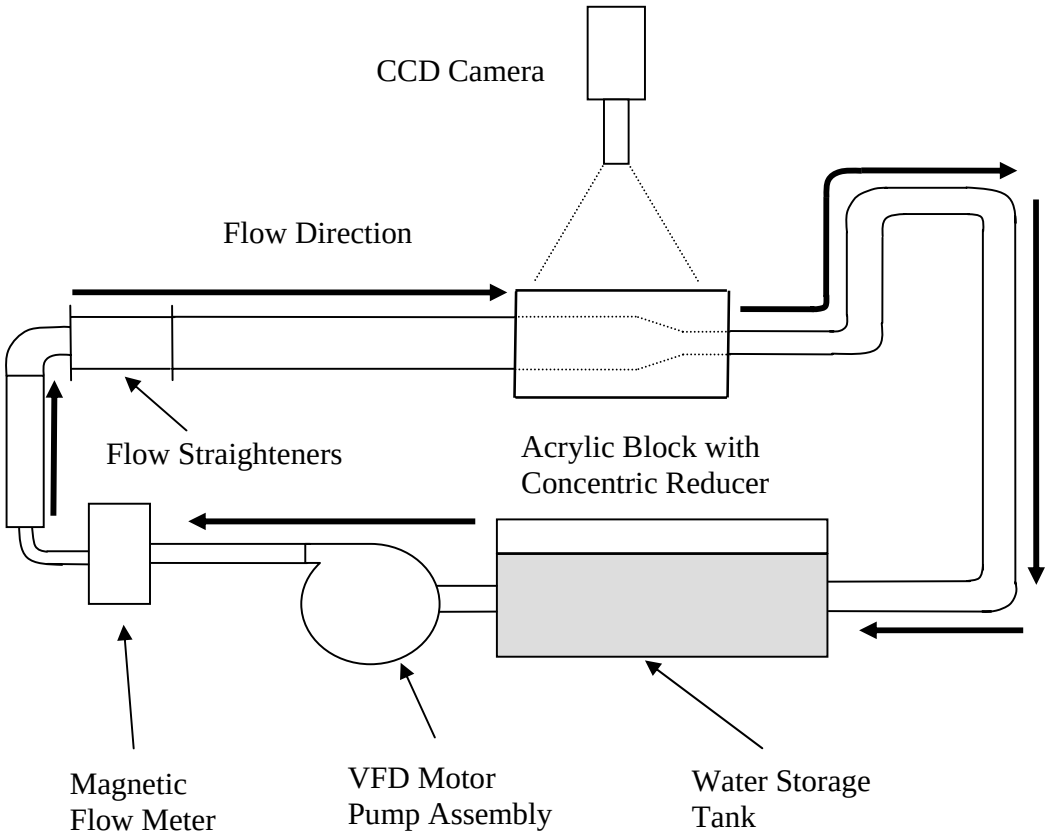

Figure 3.3 Water flow path through flow visualization test rig

3.3.1 Water tank

A rectangular PVC tank with 450 liters of capacity is used for water storage. We used the tank to mix the seeding particles for PIV application also.

3.3.2 VFD Motor – Pump assembly

The pump used in the rig is an Onga Hi-flo model 112, rated nominally at 300 liters per minute of discharge rate at 2800 rpm. It is mounted below water level in the tank for trouble free priming. The variable frequency drive (VFD) motor; a Danfoss model 6004, 2.2 kW, is powered by a 3 phase power supply. Centre-line velocities of up to 1.6 m/sec and Re nos. of almost 87,000 (downstream of the reducer) can be achieved when the VFD motor is operated at 47 Hz.

3.3.3 Magnetic Flow meter

It is an, electro-magnetic water flow meter (ABB Magmaster) with a remote display having an accuracy of 0.5 % over the range of 0.35 to 1.5 liters per second.

3.3.4 Tube Bundle Flow Straightener

The flow straightener comprises of 20 diameters PVC tubing bundled together in the 300 mm length of 100 NB PVC pipe. Its function is to prevent the entry of any swirling flow of fluid into the acrylic block.

3.3.5 Acrylic Block with Concentric Reducer

It is the heart of the rig, used to flow visualizes the fluids in the concentric reducer. The block shown is fabricated by gluing together rectangular slabs of acrylic material and then machining precisely a concentric reducer similar in shape to the one used in the vertical test rig at QAL site. The photograph and dimensions of the machined reducer are shown in the figure 3.4. The reducer

dimensions were closely matched with the outlet pipe dimensions in order to avoid any step or notch formed at the inlet which may disturb the fully developed pipe flow condition. The reducer in the acrylic block is located at a length equal to almost 19 diameters of straight pipe. The 19 diameters pipe is not sufficient for the flow to be fully developed (the required length for the fully developed pipe flow is 26 diameters) but we hope that this insufficient pipe length has minimal effect due to the following reasons.

- We took readings in a region very close to the wall due to the limitations of our 2-D PIV equipment, mismatching refractive indices of the block material (acrylic) with water and due to the circular geometry of the pipe. (Please see page 84 last point, page 28 second paragraph etc).

- The main aim of our study was to compare the near-wall turbulent patterns in the reducer with those in the straight pipes upstream and downstream of the reducer. The difference in the near wall flow patterns was even affected less by the incomplete development of the pipe flow, then the flow patterns themselves.

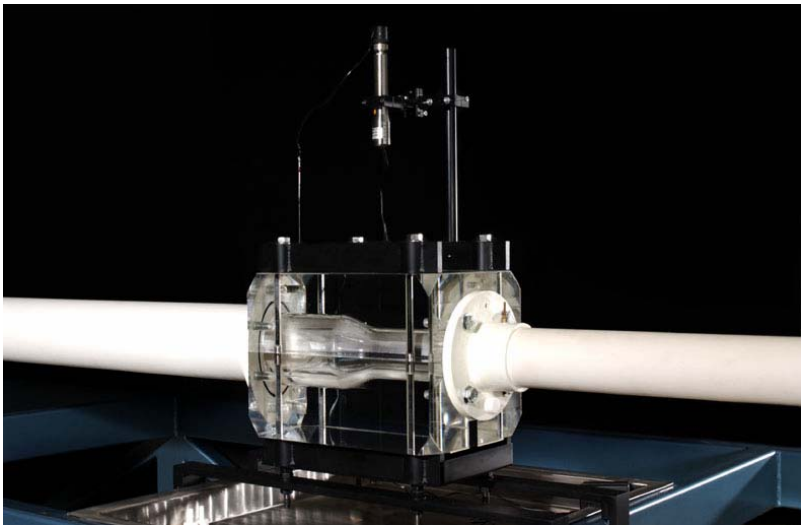

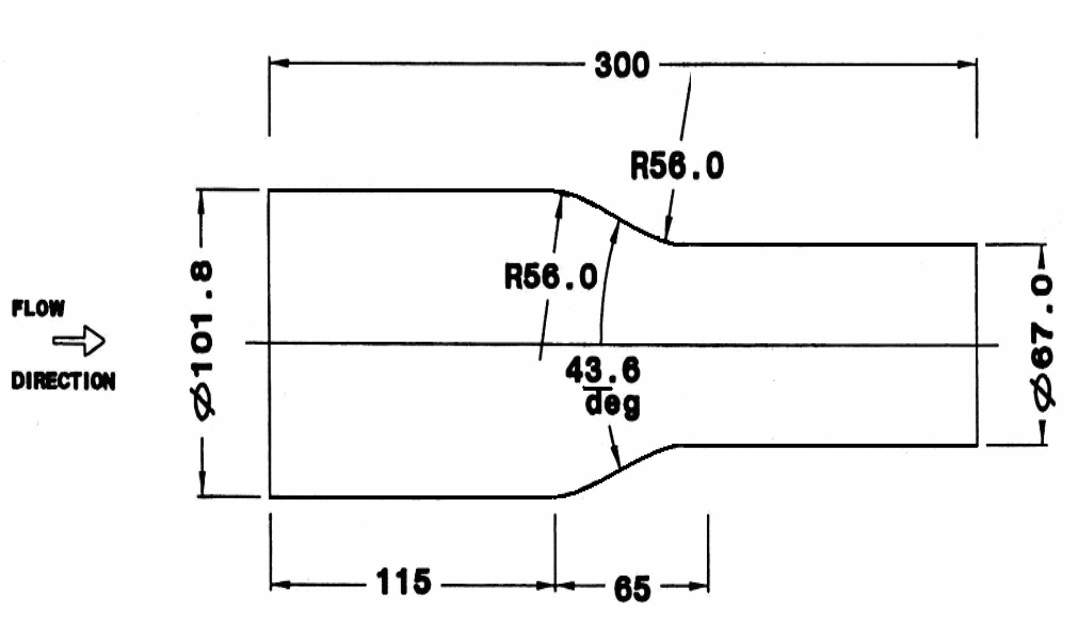

Figure 3.4 Photograph of Acrylic Block mounted on the test rig and its dimensions in mm

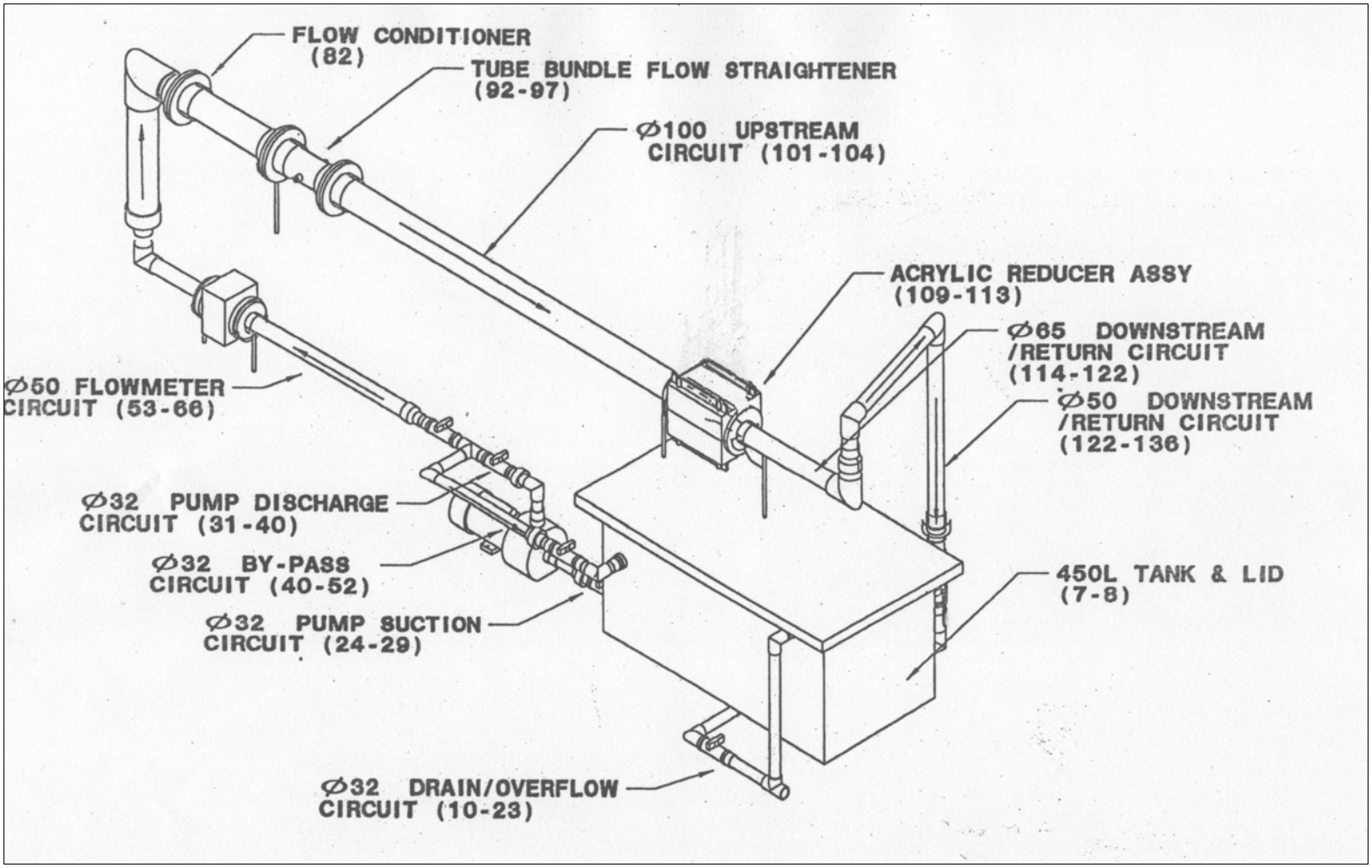

Figure 3.5 Flow Visualization test rig in a PIV laboratory at Process Engineering and Light Metals (PELM) Centre

3.4 Measurement sections

PIV images of the flow in the concentric reducer were exposed for two different views,

1) Full view of the Reducer (Figure 3.6)
2) Close to the wall view of the reducer (Figure 3.7)

3.4.1 Full view of the reducer

This view was selected to categorize the change in the instantaneous velocity fluctuations along the x and y-axis of the reducer as the flow moves from the larger diameter section to the smaller diameter section over a total axial length of 68 mm. The rig's motor-pump assembly was operated at two frequencies 23 Hz and 36 Hz. Operation of the rig at 23 Hz produced Re = 27,000 (based on flow velocity of 0.27 m/sec and pipe diameter of 101.8mm) at the upstream of the contraction and Re = 41,500 (flow velocity of 0.62 m/sec and pipe diameter of 67mm) at the downstream of the contraction. Operation of rig at 36 Hz generated Re = 44,000 (flow velocity of 0.432 m/sec and pipe diameter of 101.8mm) at the upstream the contraction and Re = 66,000 (flow velocity of 0.998 m/sec and pipe diameter of 67 mm) at the downstream of the contraction. These Re numbers are the closest match to the flow conditions studied earlier on a test rig at a local alumina refinery (Nawrath thesis, 2004 – See figure in appendix B).

Quantitative measurements of stream-wise (x-axis) and cross-stream (y-axis) fluctuating components at seven different sections A, B, F, C, G, D and E perpendicular to the flow direction were performed. The distance between each section was 8 mm with the exception of section E which is 28 mm from section D (exit of the contraction) to minimize the after effect of the contraction on the fluid flow.

In total 700 PIV images were recorded, 350 images for Re = 27000 upstream of the reducer and Re = 41500 downstream of the reducer and 350 images for Re = 44000 upstream of the reducer and Re = 66000 downstream of the reducer. For section A, B, F, C, G, D and E 50 images were exposed for each section. Out of 50 images for each section 25 pairs were post processed and time averaged for the evaluation of the average velocity. This average velocity is used to estimate the fluctuating velocity components (stream wise and cross stream).

These components were non-dimensionalized by dividing them with the bulk velocity of the fluid flow. "U^2_x / U_0^2" versus "y/R" plots for the stream wise fluctuating velocity components and "U^2_y / U_0^2" versus "y/R"plots for cross stream fluctuating velocity components were produced. Where "U^2_x"is the stream-wise fluctuating velocity component squared and averaged, "U^2_y"is the cross stream fluctuating velocity component squared and averaged, "U_0^2" is the average flow velocity squared, "y" is the perpendicular distance from the wall and "R" is the "U_0^2"radius of the section.

In total 28 plots were produced. 7 plots for 7 sections A, B, F,C, G, D, and E for stream wise and 7 plots for cross stream fluctuating velocity components were produced at Re = 27000 and Re = 41500 upstream of the reducer and downstream of the reducer respectively. Similarly 7 plots for 7 sections were produced for Re = 44000 and Re = 66000 upstream and downstream of the reducer respectively.

The horizontal field of view (HFV) of the CCD camera was 121 mm for velocity calibration purposes. This corresponds to 120 μm per pixel of the CCD camera resolution. The camera lens aperture was set at f = 8 for all the PIV images. The laser pulse separation between the successive images was fixed at 600 μsecond for Re = 27000 and Re = 41500 upstream and downstream of

the reducer respectively and 350 μsecond for Re = 44000 and Re = 66000 upstream and downstream of the reducer respectively. Detailed explanation of the generation of 1 out of 28 plot in MS – Excel is outlined in appendix A, a CD is attached with the thesis containing complete Excel files used to plot these graphs.

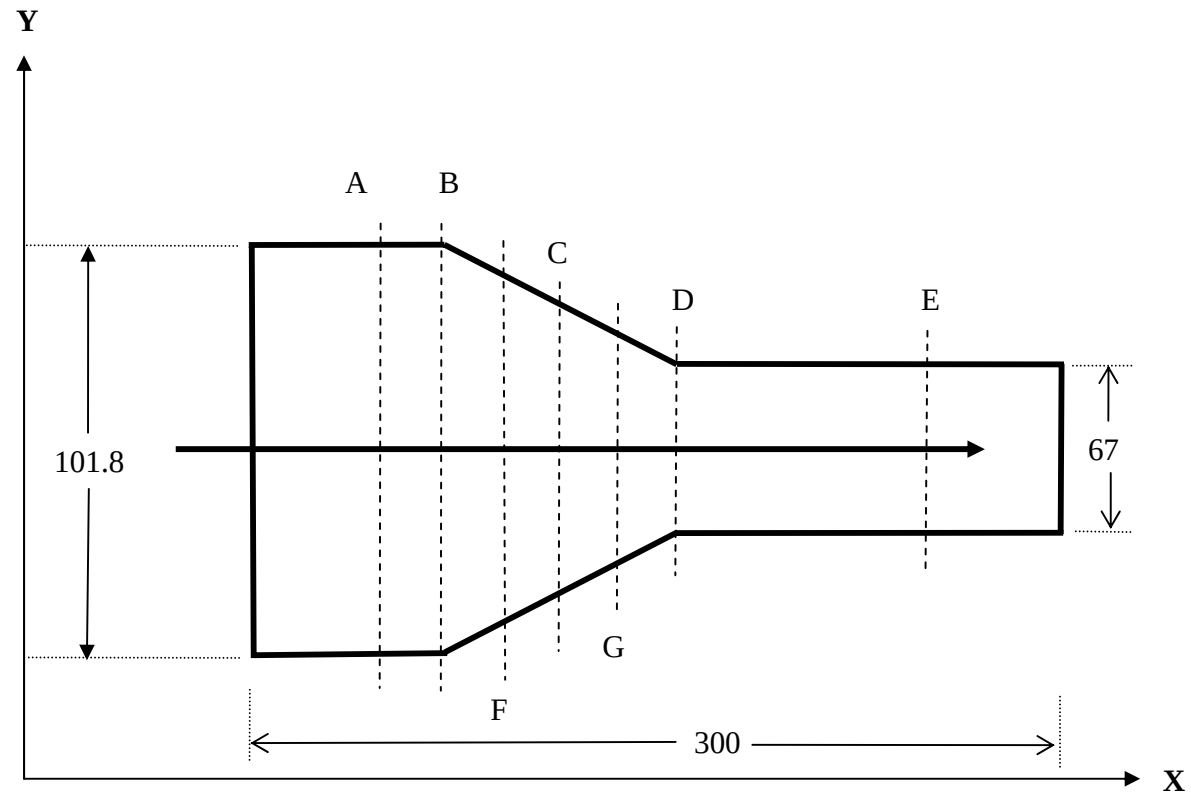

Figure 3.6 Seven-measurement sections for full view of the reducer. Distances between sections are A to B is 8 mm, B to F is 8mm, C to G is 8mm, G to D is 8 mm and D to E is 28 mm.

3.4.2 Close to the wall view of the reducer

These views were selected to magnify the region very close to the wall in order to detect "turbulent bursting" (TB) activity. PIV images were recorded as close to the wall as permissible by the system. These magnified PIV images were exposed utilizing spacers between the CCD camera body and lens. The horizontal field of view for velocity calibration purposes was 46 mm for first section AA and 27 mm each for the remaining two sections i.e. BB and CC. (Figure 3.7). Fifty PIV images for each of the three sections AA, BB and CC at a distance of 2-3 mm away from the wall were recorded at Re = 27000 and Re = 41500 upstream and . Re = 44000 and Re = 66000 downstream of the reducer respectively.

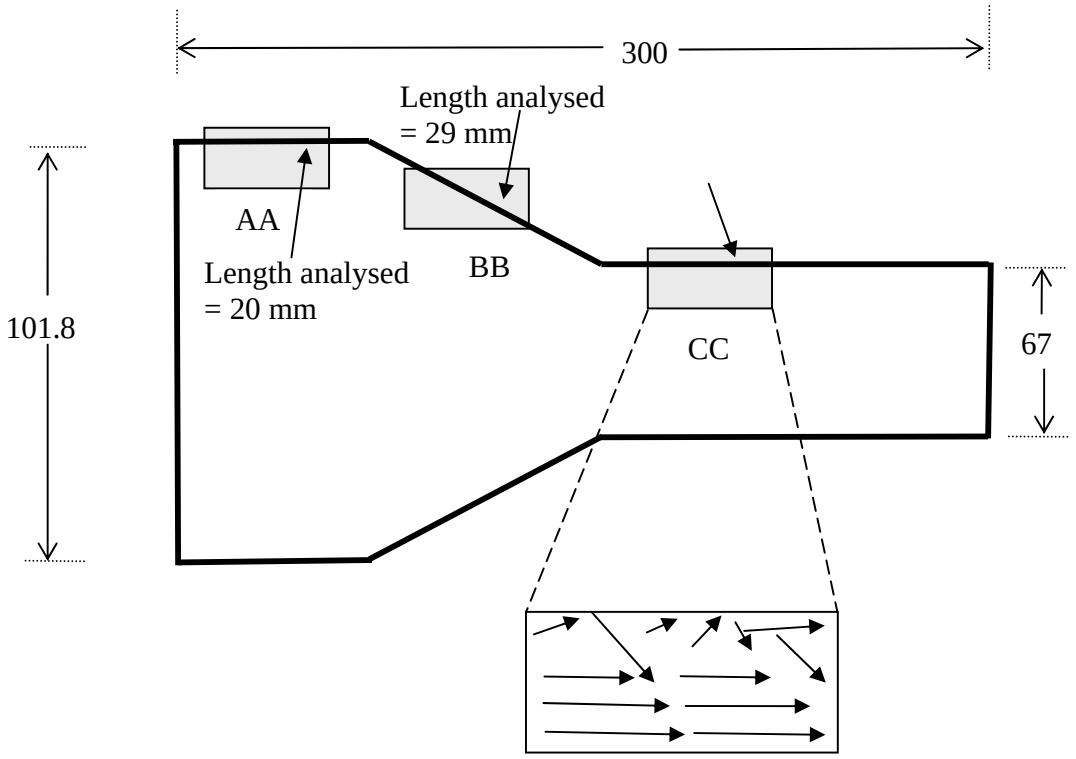

Figure 3.7 Measurement sections for close to the wall readings (all readings are in mm)

The laser pulse separation for Re = 27000 upstream of the reducer and Re = 41500 downstream of the reducer was 600 μs and 350 μs for Re = 44000 upstream of the reducer and Re = 66000 downstream of the reducer. The camera aperture was set at f = 8 for all the images. In section AA and CC 15 numbers of vectors were analysed at 2-3 mm distance from the wall and for section BB the number of vectors analysed was 12 due to the angular placement of the contraction in front of the camera. The axial length of the wall region exposed for AA section (upstream of the contraction) was 20 mm and for sections BB was 19 mm (in the contraction) and for CC it was 11 mm (downstream of the contraction) see Figure 3.7. A total of twenty five images were time averaged to estimate average velocity and to calculate stream wise and cross stream fluctuating velocity components. The analysis is carried out by separating the fluctuating velocity components (stream wise-U_x and cross-stream-U_y) and then taking magnitude or absolute value of the fluctuating components as $\sqrt{\left(U_x^2 + U_y^2\right)}$. The angle of the resultant vector was calculated by taking the inverse of the tangent of U_x and U_y as $Tan^{-1}\ U_x/U_y$. We assume that if we can point out pairs of the vectors where first instantaneous vector pointing towards the wall and the very next one pointing towards the main stream flows (away from the wall region) then a single occurrence of TB has been detected. (Please see page 16 chapter 2 for more details on TB). In isolating TB from the PIV data another criterion was to look for pairs of vectors whose angle of "incidence" were greater than 45^0 and angle of "reflection" from the wall as little as $25^{0.}$ In total 19 images were evaluated for the detection of TB in section AA and CC and 18 for section BB. A file (named CW DATA) is attached with the thesis for the ease of the reader. The results obtained are explained in the next section.

3.5 Sources of Error in PIV

There are three main sources of error in a PIV measurement. These are enumerated below,

1. Errors due to Seeding Particles
    - Non uniform size of seeding particles
    - Velocity lag of seeding particles due to high velocity gradients in a flow
    - Locally varying concentration of tracer particles due to the centrifugal forces in vortices
    - Non-uniform displacement of particle images within an area corresponding to the size of interrogation window
    - Low particle concentration, which offers different possibilities of combining images to pairs
2. Errors due to Recoding of Images
    - Geometrical distortion due to lens aberration or out of recording plane motion
    - Light reflected from the surface of the model or faults in the model
    - Recording not focused properly
3. Errors due to Evaluation of PIV Images
    - Noise of CCD camera
    - Signal to noise ratio from the PIV image
    - Poor velocity calibration through software

3.6 Estimation of Experimental Error

The TSI's PIV 200 system was checked for accuracy and experimental error using two methods

- Rotating disc experiment
- Center-line velocity check at Laminar flow
- PIV accuracy check using instantaneous velocity and flow meter

3.6.1 Rotating disc experiment

A 180 mm cardboard disk was painted black and sprinkled with 1 mm polystyrene seeding particles. The disc was then mounted onto a DC motor, and the rotational speed was measured with a tachometer before and after the experiment. Power supply to the DC motor was fed from a variable DC voltage supply (Figure 3.9) and its rotational speed was maintained at about 550 revolutions per minute (RPM). The following equation was used to calculate the velocity values at each point on the circular disc. The camera was positioned directly over the disc with seeding particles sprinkled on it.

$$Velocity = \frac{RPM\ of\ motor\ x\ Radius\ of\ velocity\ vector}{9.55} \quad \text{..... (3.2)}$$

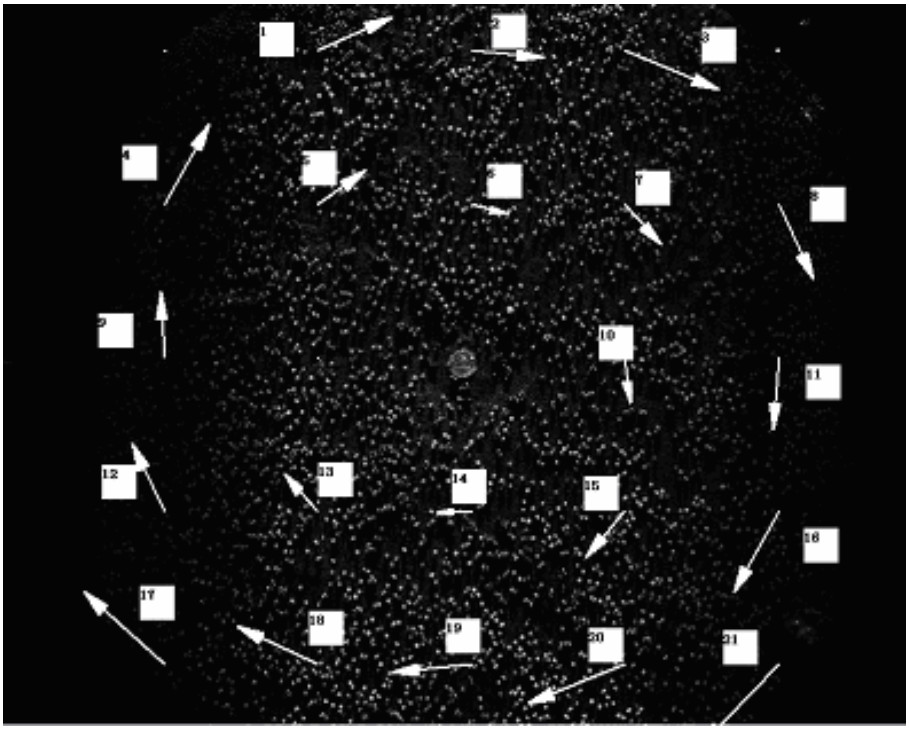

Figure 3.8 PIV image of disc rotating at 550 rpm with velocity vectors and their numbers

The disc was tilted slightly towards the laser light beams (figure 3.9) so that the entire disc was illuminated. Since the angular velocity of the disc was measured by a tachometer, the velocities of seeding particles attached to the disc could be calculated.

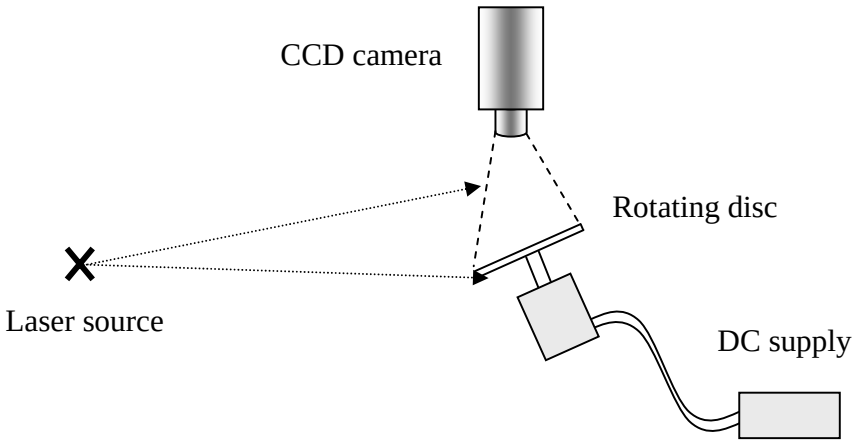

Figure 3.9 PIV calibration set up for rotating disc

Tables 3.1 & 3.2 A comparison of velocities measured by the PIV System with calculated linear velocities shown below separately for the ” Outer and inner circle of vectors” in figure 3.8

Outer Circle of Vectors

No	Distance from the Centre of rotating Disc (mm)	Calculated Velocity (m/sec)	PIV Measured (m/sec)	Percentage Relative Error e_r (%)
1	840	4.1849	3.6974	11.649
2	750	3.7365	3.2849	12.087
3	860	4.2845	4.6295	8.052
4	820	4.0852	4.1636	1.918
8	860	4.2845	3.741	12.686
9	720	3.587	2.9724	17.135
11	770	3.8361	3.2989	14.004
12	810	4.0354	3.4063	15.589
16	850	4.2347	4.163	1.6933
18	800	3.9856	4.0264	1.025
19	730	3.6368	3.5967	1.1031
20	830	4.135	4.7208	14.17
Average Relative Percentage Error				9.26

Inner Circle of Vectors

No	Distance from the Centre of the rotating Disc (mm)	Calculated Velocity (m/sec)	PIV Measured (m/sec)	Percentage Relative Error e_r (%)
5	530	2.6404	2.6968	2.134
6	390	1.943	1.7304	10.939
7	560	2.7899	2.4747	11.297
10	40	1.9928	2.0977	5.263
13	50	2.491	2.2805	8.4509
14	350	1.7437	1.5862	9.0304
15	520	2.5906	2.7142	4.77
Average Relative Percentage Error				7.4

The camera acquired several pairs of images. The images were processed by software to produce velocity vector plots. A sample of such a plot is shown in figure 3.8. These velocities were compared to the velocities calculated in a manner described above. The results obtained are presented in the tables 3.1 and 3.2. As it can be seen from Fig. 3.8, the velocity vectors may be divided into two groups – the inner circle, for the vectors lying at a distance from 300 mm to 500 mm from the disk centre, and the outer circle, for the vectors lying at the distance between 700 mm and 900 mm from the disk centre. The time separation; "*dt*" was estimated at a displacement of 4 times seeding particle diameter divided by local velocity. It was found, that the average of the percentage relative error for the velocities lying in the outer cycle was 9.3%, and that for the velocities lying in the inner cycle, was 7.4%. It is important to note here, that the time delay between two images captured by PIV camera ("*dt*"), used for the subsequent generation of the instantaneous velocity field using cross-correlation method, was also set to 4 seeding particles diameter also. This confirms the recommendation by TSI Inc., the PIV manufacturer, to set the time delay “dt” such, that the displacement of seeding particles over this time "*dt*" should be 3 to 5 particle diameters. Thus in our subsequent experiments we calculated the time delay in accordance with the TSI recommendation. The time separation between the two images ("*dt*") was calculated on the basis of 4 diameters separation of the seeding particles (4 mm) taken at half of the radius of the disc. The average of percentage relative error for outer circle vectors values is 9.3 %, whereas the error for inner circle vectors is 7.4 %. The same value of time separation between images ("*dt*") is maintained in the experimental set-up for exposing PIV images of the reducer model.

3.6.2 Centre-line velocity check at Laminar flow

A centerline velocity check was also performed along with rotating disc experiment to check the accuracy of the PIV system for the measurement in the actual fluid flow conditions. A fully developed laminar flow was established at the upstream of the contraction at Re = 2049 in 101.8 mm section at a flow rate of 0.165 liters per second using following expression.

$$\mathrm{Re} = \frac{v D}{\upsilon} \quad \text{..... (3.3)}$$

Where, "v" is average velocity, "D" is diameter of the pipe section and "υ" is kinematic viscosity of the water.

The measured centre-line velocity at point B (or velocity calculated from flow meter readout) was 0.0405 m/sec, figure 3.5. The centre-line velocity is twice the value of average velocity under laminar flow conditions. The average velocity was calculated by dividing the flow rate taken from the digital read-out of the magnetic flow meter (having an accuracy of 0.5 %) and dividing the flow rate with the cross sectional area of the pipe (101.8 mm). This measured value was compared with the values obtained quantitatively from the PIV Insight software after necessary velocity calibration. The calculated velocities at both points A and C is 0.03037 m/sec. The parabolic velocity profile given by equation 3.4 for fully developed pipe flow is sketched in figure 3.10.

$$\frac{u}{U} = 1 - \left(\frac{y}{R}\right)^2 \quad \text{..... (3.4)}$$

Where "u" is the velocity at a perpendicular distance "y" from the wall and "U" is the centre-line velocity at the radius upstream of the reducer (Figure 3.10). The velocity data from PIV software and measured values is tabulated below; (Table 3.3) corresponding to the localised

velocity vectors as shown in the diagram below. The value of localized velocity from PIV software at points A, B and C are 0.03286, 0.04311 and 0.03320 m/sec respectively. The percentage relative errors between the measured values of the velocities from flow meter based calculations and the values from the PIV software for the points A, B and C are 7.6 %, 6 % and 8.5 %. This is within acceptable range.

X – Location	Y – Location		Vel. From Flow Meter Reading (m/sec)	PIV Measured velocity (m/sec)	Percentage Relative Error (%)
55.692	101.682		0	0.00023	
55.692	98.53201	**A**	0.03037	0.03286	7.6 %
55.692	95.256	**B**	0.04050	0.04311	6.0 %
55.692	92.106	**C**	0.03037	0.03320	8.5 %
55.692	88.956		0	0.00068	

Table 3.3 A comparison of flow meter based measured velocities and PIV Insight softwares based velocities along with x and y locations

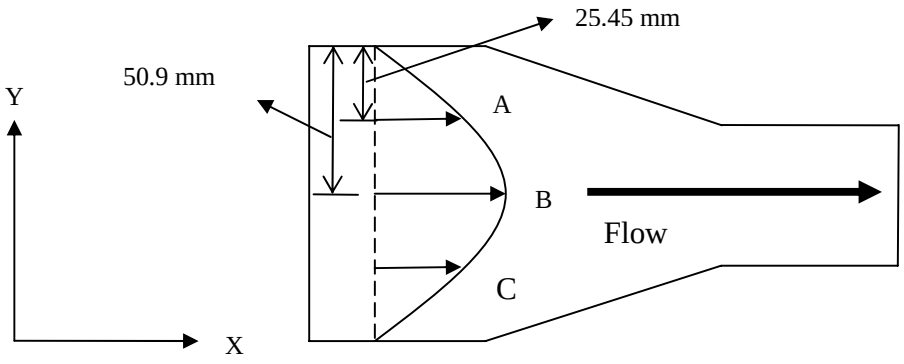

Figure 3.10 Centre-line velocity check at Laminar flow in the reducer

Close to the wall the PIV measurements are biased towards high velocity values, mainly the relatively large interrogation windows that define the size of the measuring volume cause this.

The uncertainty of the PIV measurements also increases due to the degree of curvature of the pipe (the PIV camera was positioned at the top of the block to keep it at 90 degrees from the laser light sheet - figure 3.1, page 35) and the difference of the refractive index between water and the acrylic block. Few of the investigators used refractive index matching techniques, which eliminates this error (Uzol *et. al.,* 2002, Ciu and Adrian, 1996). In this method a refractive index matching fluid is used for PIV measurements instead of water. For the acrylic model of reducer we need to use a strong solution of NaI (62-64 % by weight) to effectively match the refractive index with the acrylic block. The refractive index of this solution varies with temperature, concentration and the wavelength of light passing through it. There are some problems associated with the maintenance of the NaI solution due to which we could not use this refractive index matching technique for our close to the wall readings using PIV method. The main problem is the storage of the fluid in a tank under vacuum in order to avoid its contact with the oxygen present in the air.

In the method of "Centre-line velocity check at laminar flows", we noticed that the percentage error increased as we approached the wall, (page 55 and 56). At the centre we had a percentage error of 6% where as at points A and C lying relatively close to the wall; the percentage error is increased to 7.6% and 8.5% respectively. This certainly validates the difficulty arises when using PIV for curved surfaces enclosed in acrylic block and exposed from the top by CCD camera.

3.6.3 PIV accuracy check using instantaneous velocity and flow meter

The mass flow rate passing through the reducer sections AA and EE were estimated using flow meter reading and mass flow from instantaneous stream wise velocity values and formula as narrated in the next paragraphs at Re = 27000 and Re = 41500 for upstream of the contraction and Re = 44000 and Re = 66000 downstream of the contraction.

Assuming symmetrical flow the flow rate is estimated using formula as, (the flow is divided into five annular rings passing through the concentric reducer each having a velocity value "V" at its centre at a distance "R" from the centre).

$$Q = R_1 * V_1 + R_2 * V_2 + R_3 * V_3 + R_4 * V_4 + R_5 * V_5 \quad \text{.....(3.5)}$$

Where,

Q = Volume Flow rate

R_n = Area of nth ring (please refer to figure 3.11 page 59)

V_n = Nth instantaneous velocity through the centre of the ring (figure 3.11 page 59)

The ratio of the flow meter reading (actual flow) to the calculated flow using above equation (3.5) is a direct measure of the accuracy or the experimental error of the PIV system. The percentage error found using above method is presented in a tabulated form below and the procedure is explained in appendix C.

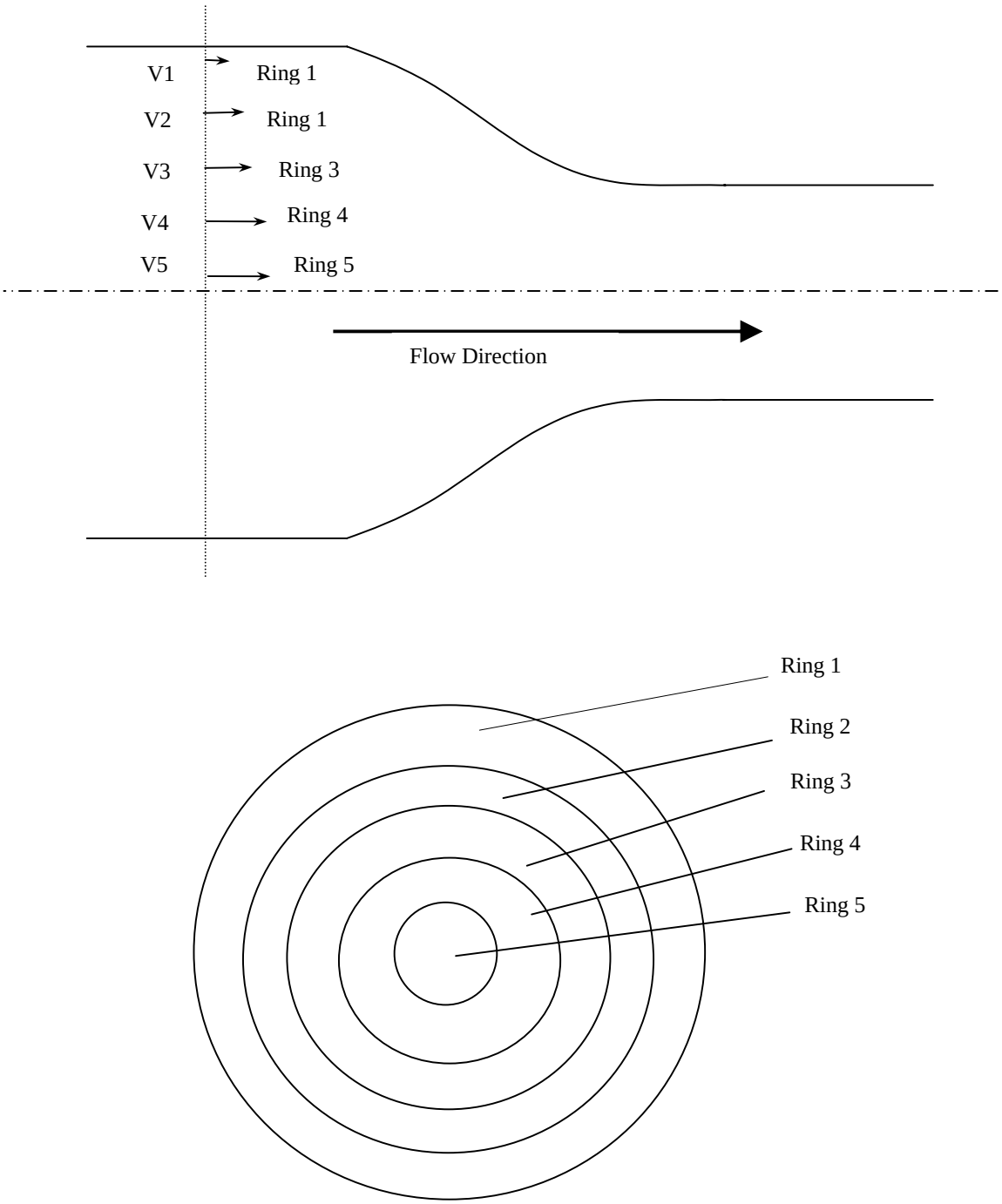

Figure 3. 11 PIV accuracy measurement using instantaneous velocity and flow meter reading

Table 3.4 Percentage error using instantaneous velocity and flow meter

Sr. No.	Flow Rate from Flow meter on the rig (Liters/sec)	Flow Rate value from the formula (Liters/sec)		Re no. in 101.8 mm pipe section	Re no. in 67 mm pipe section	Percentage Relative Error	
		Section AA	Section EE			Section AA	Section EE
1	2.2	1.83	1.95	27000	41500	16.85	11.5
2	3.5	3.83	4.11	44000	66000	9.4	17.5

Note: - The reader is also referred to the page no. 50 on “sources of errors” in PIV.

3.7 Conclusion

- PIV was utilized because it is the only technique, which can give instantaneous velocity values of the whole field of view from which instantaneous fluctuating components can be derived and plotted; other techniques give the flow velocity at a single point or average values.
- Two views such as the full view of reducer and close to the wall view of the reducer were selected to check the overall change in the stream-wise and cross-stream fluctuating components of the flow as the flow moves through the reducer.
- The full view of the reducer was selected to observe the overall changes in the instantaneous fluctuating components in the straight pipe sections (101.8 mm diameter), in the contraction and after the contraction in small pipe section (67 mm diameter).
- Close to the wall PIV images were exposed and analyzed to detect the frequency and intensity of the turbulent bursting activity in the near wall region of the flow and to track changes of the components of the flow velocity in the near wall region. Each setup of PIV images was analyzed by taking 50 images and post processing the data to get instantaneous values.
- Measurement error of PIV system was checked by using two methods such as

  1) Rotating disc method and 2) Centre-line velocity check, at laminar flow. Error in the observed and measured readings was found to be within in acceptable ranges. Error sources in a PIV method were also discussed.

Results and discussion Chapter 4

Better to understand a little than to misunderstand a lot.
-- Anonymous

In the previous sections 2 views were selected for PIV measurement of the reducer; 1) Full view and 2) Close to the wall view. This chapter contains the information deduced from the PIV images to further understand the role of localized velocity of fluid flow with the scale formation.

4.1 Full View of the reducer

The view of the reducer along with seven sections, perpendicular to the flow, exposed to PIV measurement is shown (Figure 4.1, 4.2, 4.3 and 4.4). On the whole 50 pairs of images (100 PIV photographs) for each section (total 700 PIV images at Re = 27000 and Re = 41500 upstream of the reducer and downstream of the reducer respectively for first batch of PIV measurements and at Re = 44000 and Re = 66000 upstream of the reducer and downstream of the reducer respectively for the second batch of PIV measurements were time averaged to calculate the fluctuating components of velocity in the direction of flow (stream-wise components or U_x) and perpendicular to the direction of flow (cross stream components or U_y).

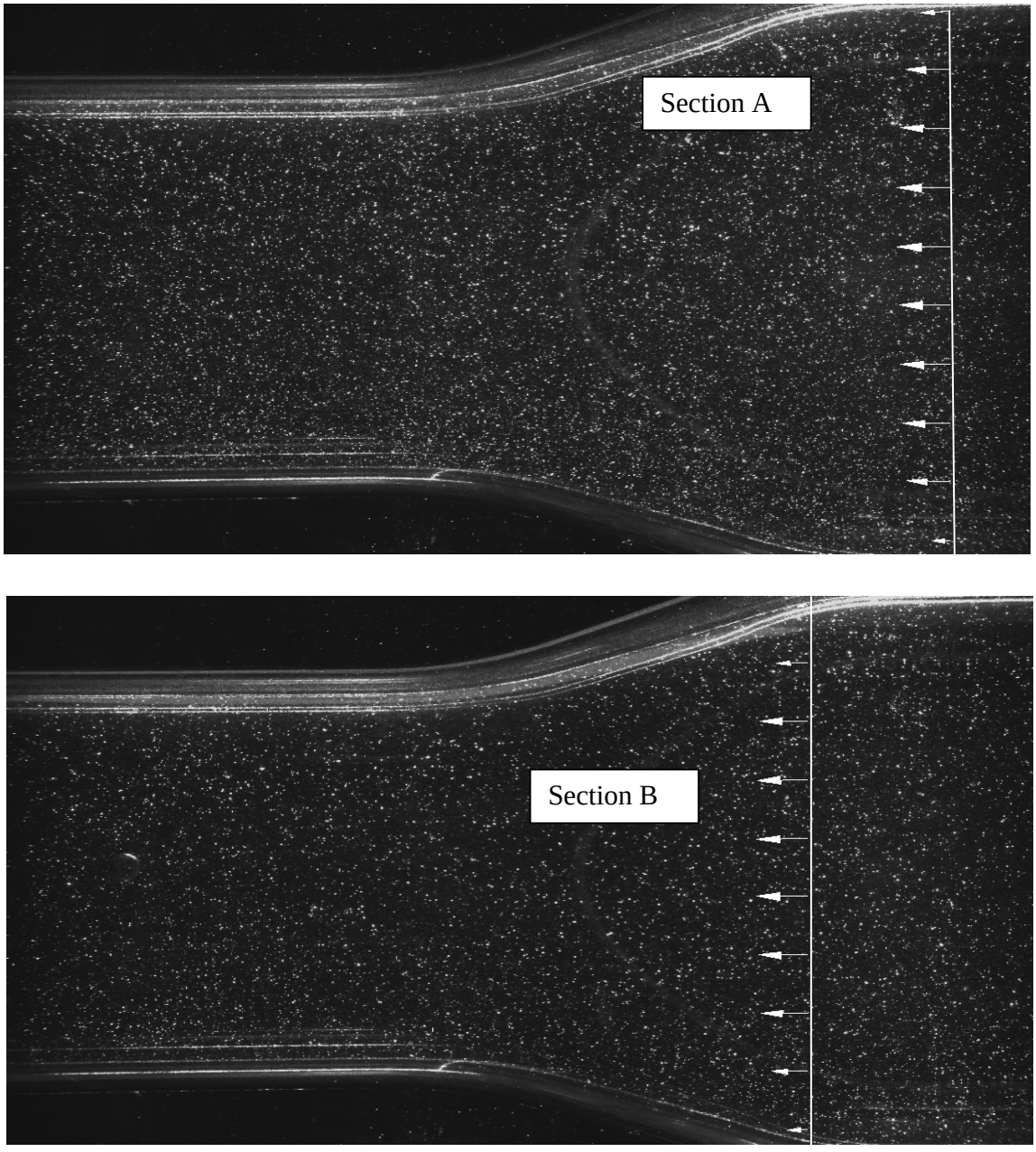

Figure 4.1 Sections A and B

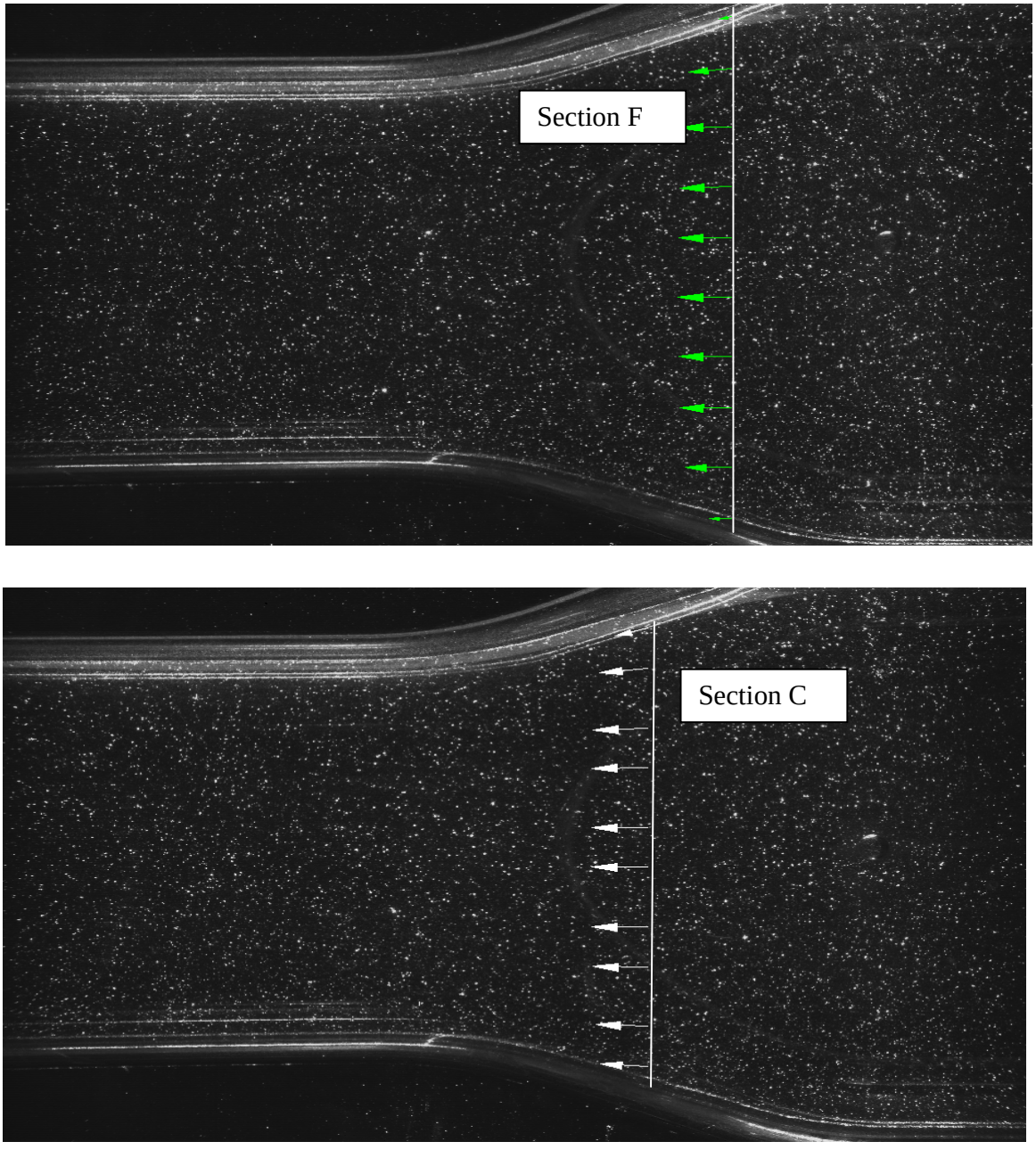

Figure 4.2 Sections F and C

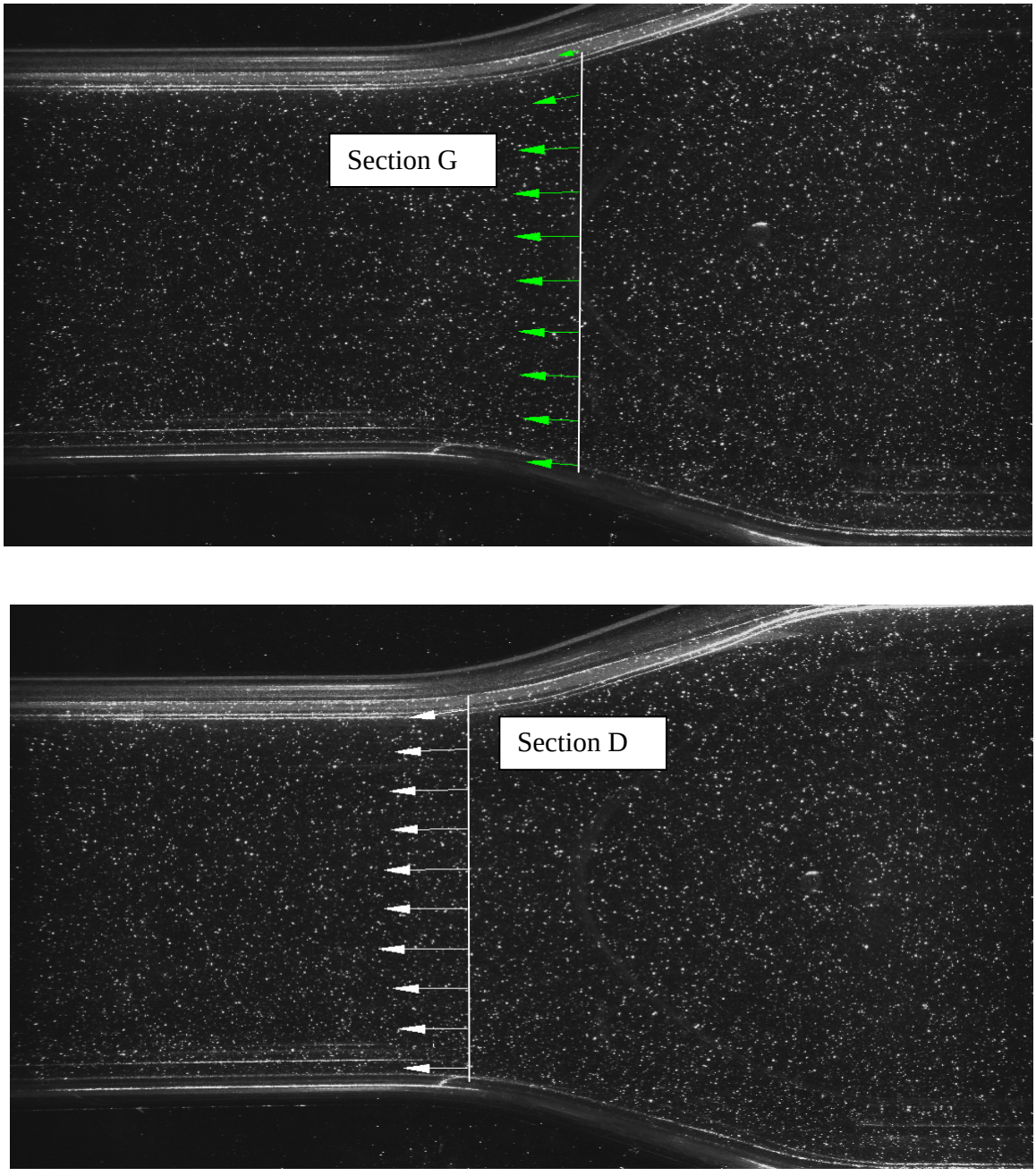

Figure 4.3 Sections G and D

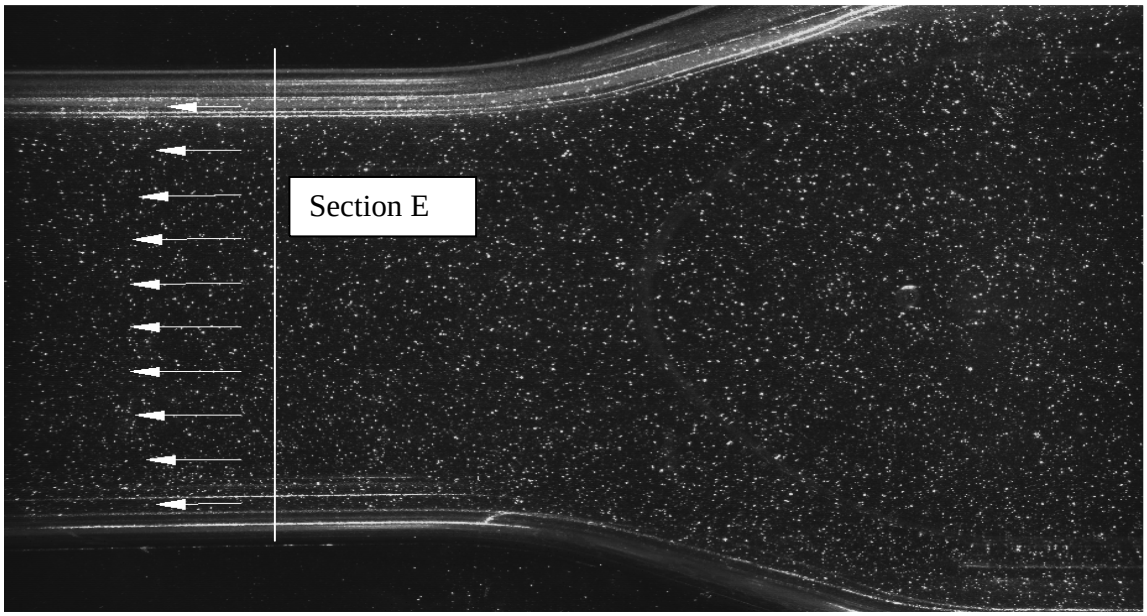

Figure 4.4 Section E

4.2 Results and discussions for Re = 27000 and Re = 41500

Figure 4.5 shows all the 7 plots of stream-wise fluctuating components (U_x) for each section A, B, F, C, G, D and E. As is evident from the plots the stream-wise component is almost of the same value when comparing section A and B since both sections are at the upstream of the contraction with the same flow conditions and Re numbers. As the flow enters the contraction there is a decrease in the magnitude of the stream wise fluctuating components from a value of 0.038 to around 0.004, which is approximately a decrease of 10 times. Further in the contraction at section "C" there is an increase in the stream-wise fluctuating components which is contrary to the earlier finding by Torbergsen and Krogstad (1998). They found a gradual decrease in stream wise components and a corresponding increase in cross-stream components.

In the next section G, the last section in the contraction, we again observe a decrease in the stream wise component to almost the same value as that noticed in section F (0.004). The remaining two sections D and E have almost similar value of the stream wise components. The discussion presented above is for values very close to the wall region, y/R = 0 to 0.2, since scale growth is an event affected by the "close to the wall" readings of the fluctuating velocity components.

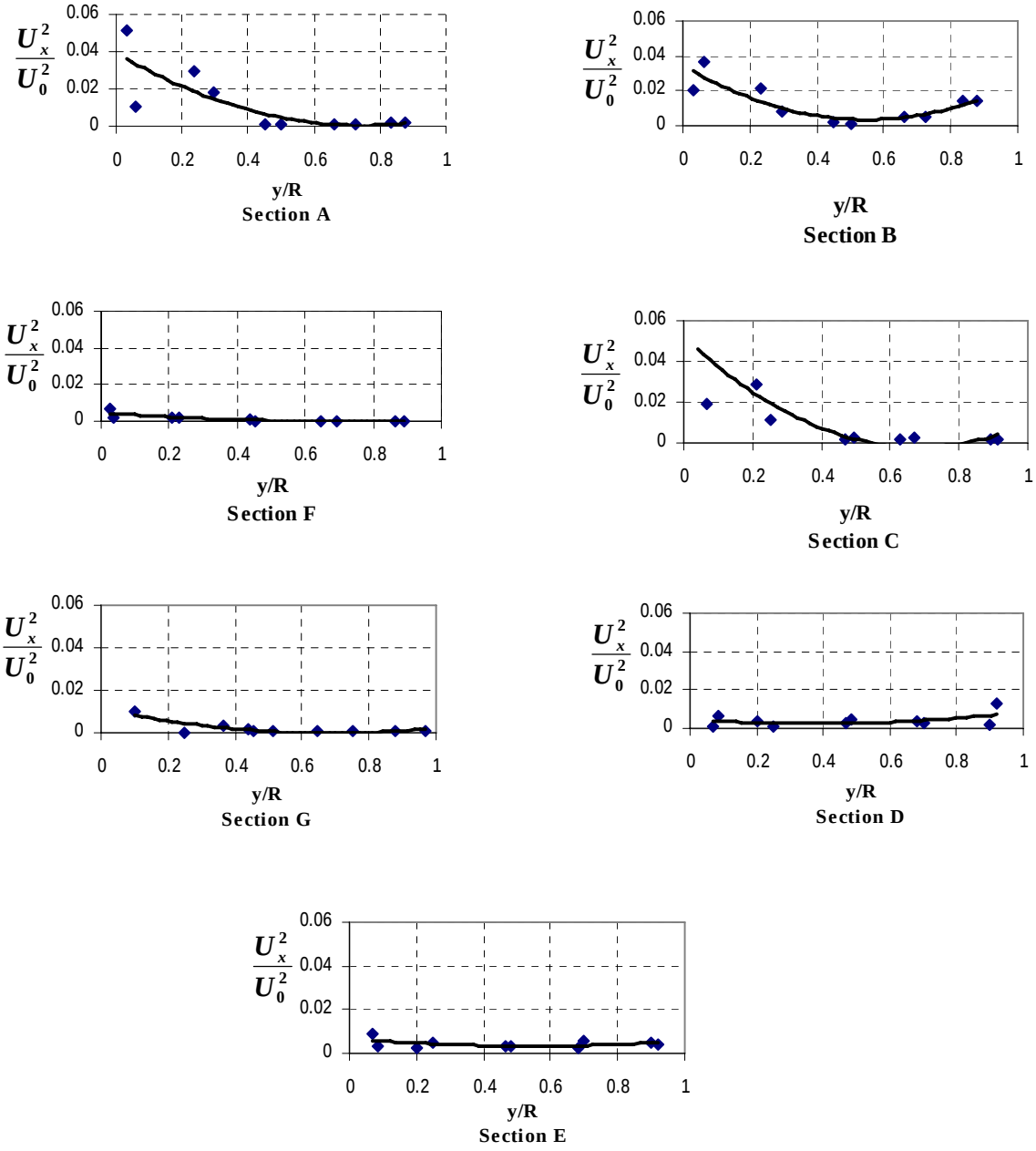

Figure 4.5 Variation of stream wise components ($U_x^{'}$) at Re = 27000 upstream of the reducer and Re = 41500 downstream of the reducer through sections, A, B, F, C, G, D and E.

The reason for suppression of stream wise fluctuating velocity components at section F could be the difference of Re number or difference of geometry used by Torbergsen and Krogstad (1998) or both. The reason for the rise of the stream wise component at section C could also be the same as mentioned above (the difference of the rate of change in contraction diameter and Re number). Torbergsen and Krogstad (1998) used contraction that produces constant strain rate and they conducted their experiment at a Re = 35000 and their work lacks the data in the region very close to the wall, where as our geometry does not intend to make constant strain rates and we have Re = 27,000 at the upstream of the contraction and Re = 41,500 at the downstream of the contraction. The concentric reducer studied in the present research is the exact dimensional replica of the reducers used in the process industries for pipe works.

Another reason for the deviation from the expected result could be the difference in the experimental technique employed. Torbergsen and Krogstad (1998) made use of hot wire anemometry technique but we used 2D PIV method. Close to the wall the PIV measurements are biased towards too high velocity values, this is caused mainly by the relatively large interrogation windows that define the size of the measuring volume.

Similarly, a closer look at plots in figure 4.6 revealed that there is almost no change of the cross stream component as the flow moves through the reducer at Re = 27000 and Re = 41500 upstream and downstream of the reducer respectively. In section A the value of the cross-stream fluctuating velocity components is approximately 0.001 and we observe that in section B the value is increased from 0.001 to 0.004 (a 4 time increase). It could be due to the effect of contraction on the incoming flow. In the next sections F, a noticeable drop in the value of the cross-stream fluctuating velocity components is observed, from an initial value of 0.0039 to around 0.0007, (not visible in the graph for section F in figure 4.6 due to y-axis truncation).

From F to E we noticed a rise in the value of the cross-stream components from 0.0007 to 0.018 which remains at this value in the contraction up to the section D and downstream of the contraction. At section E we found a sharp decrease in the value of cross-stream fluctuating velocity components (75 times) at a value of 0.0004. This is true for close to the wall readings and for bulk flow also. These results are contrary to the study by Torbergsen and Krogstad (1998), probably due to the difference of geometry and difference of Re numbers.

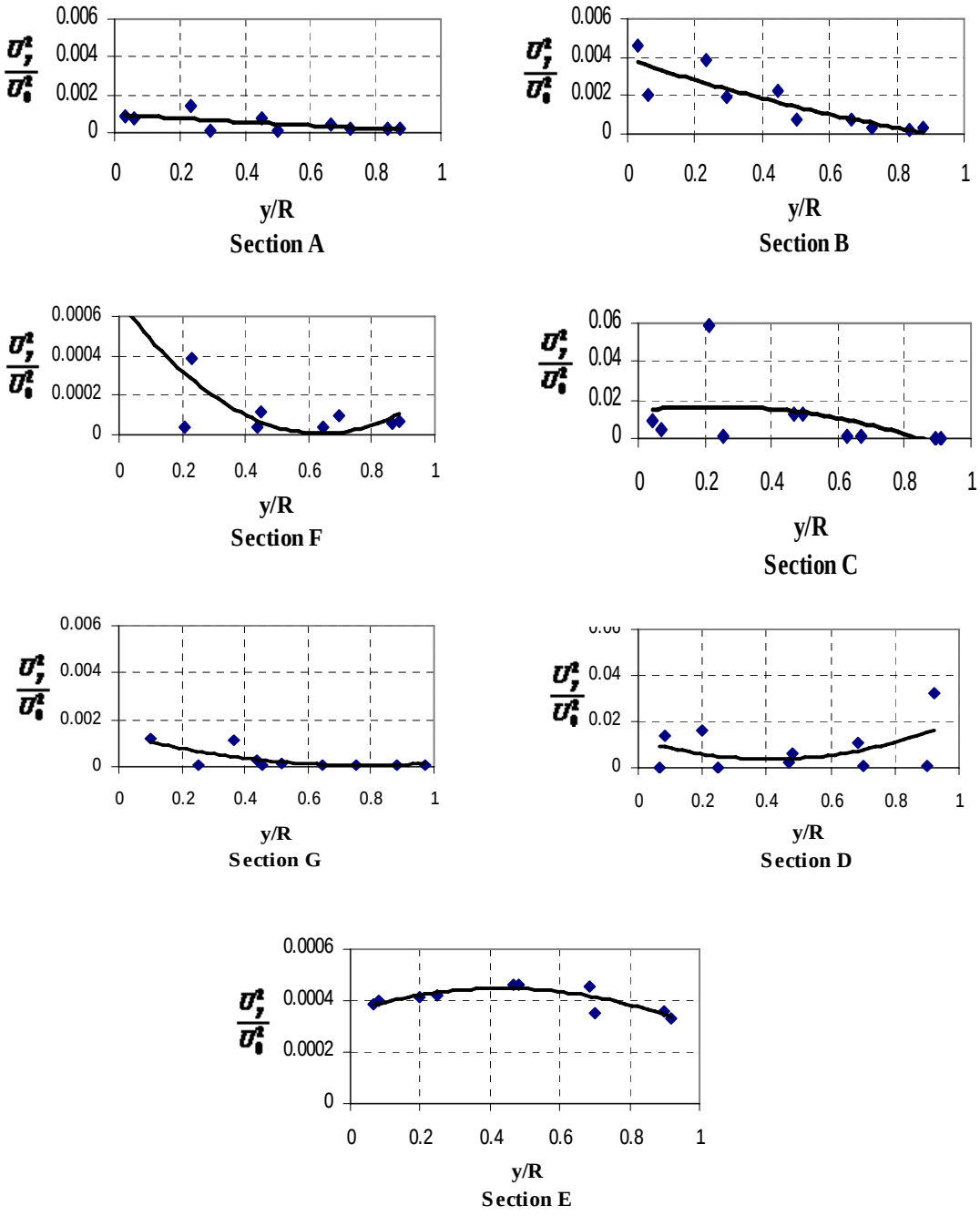

Figure 4.6 Variation of cross stream component ($U_y^{'}$) at Re = 27000 upstream of the reducer and Re = 41500 downstream of the reducer through sections, a, B, F, C, G, D and E.

4.3 Results and discussion for Re = 44000 and Re = 66000

The next batch of PIV measurements were taken at Re = 44000 and Re = 66000 upstream of the reducer and downstream of the reducer respectively. All the observation in the next lines are confined to close to the wall regions i.e. $y/R < 0.2$, unless otherwise stated.

In figure 4.7, the change in the magnitude of the fluctuating components is in agreement with cited literature. At section A and B of the figure 4.7 we observed no change in the value of stream wise component, fixed at 0.016. This confirms the degree of accuracy and repeatability of the PIV measurement system at these Re numbers. Further down the duct towards section F we noticed a decrease in stream wise component which remains at the same level in section C, (F and C are only 8 mm apart). In the section G there is a decrease in the component at a value of 0.004. In the next section D there is a further decrease of the stream wise velocity components at a value of 0.002. For the next section E no change in the value of the stream wise component is observed and the value remains fixed at 0.002. The above observations are in total agreement with the work done by Torbergsen and Krogstad (1998).

Similarly in figure 4.8 for the cross stream fluctuating components, there is a 4.5 times rise in the components from A to B, and a further rise in the magnitude by 4 times in the section F. In the section C there is a drop in the cross-stream component and this trend is continued to the section G, where the close to the wall value of the cross-stream component is 0.002 a drop from 0.003. In section D at the exit of the contraction the value of cross-stream component increased by a small amount. Downstream of the contraction at section E the cross-stream component is reduced to a value of 0.000015 (approximately). This decrease is in agreement with the work done by Torbergsen and Krogstad (1998).

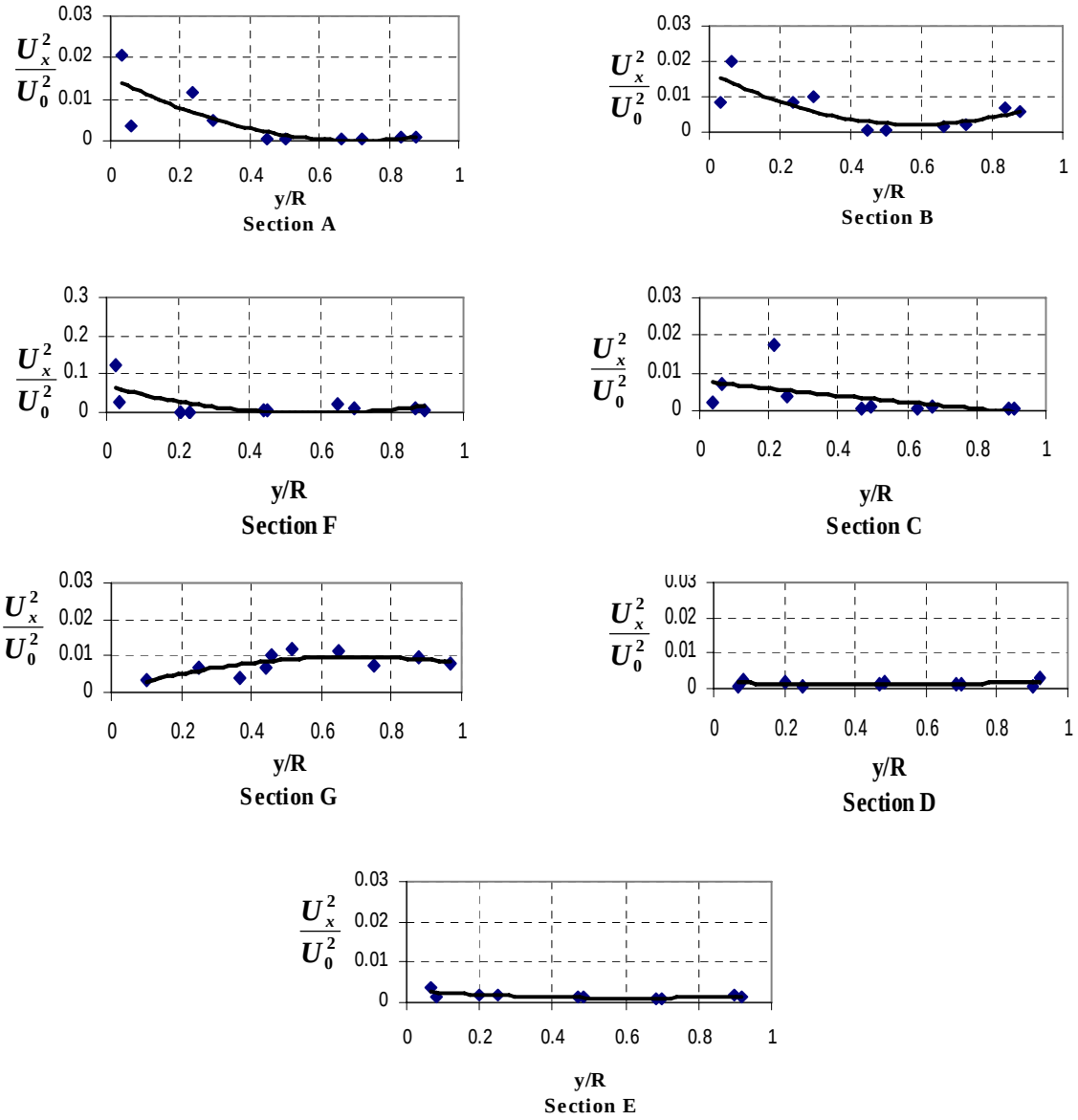

Figure 4.7 Variation of stream wise components (U_x) at Re = 44000 upstream of the reducer and Re = 66000 downstream of the reducer through sections, A, B, F, C, G, D and E.

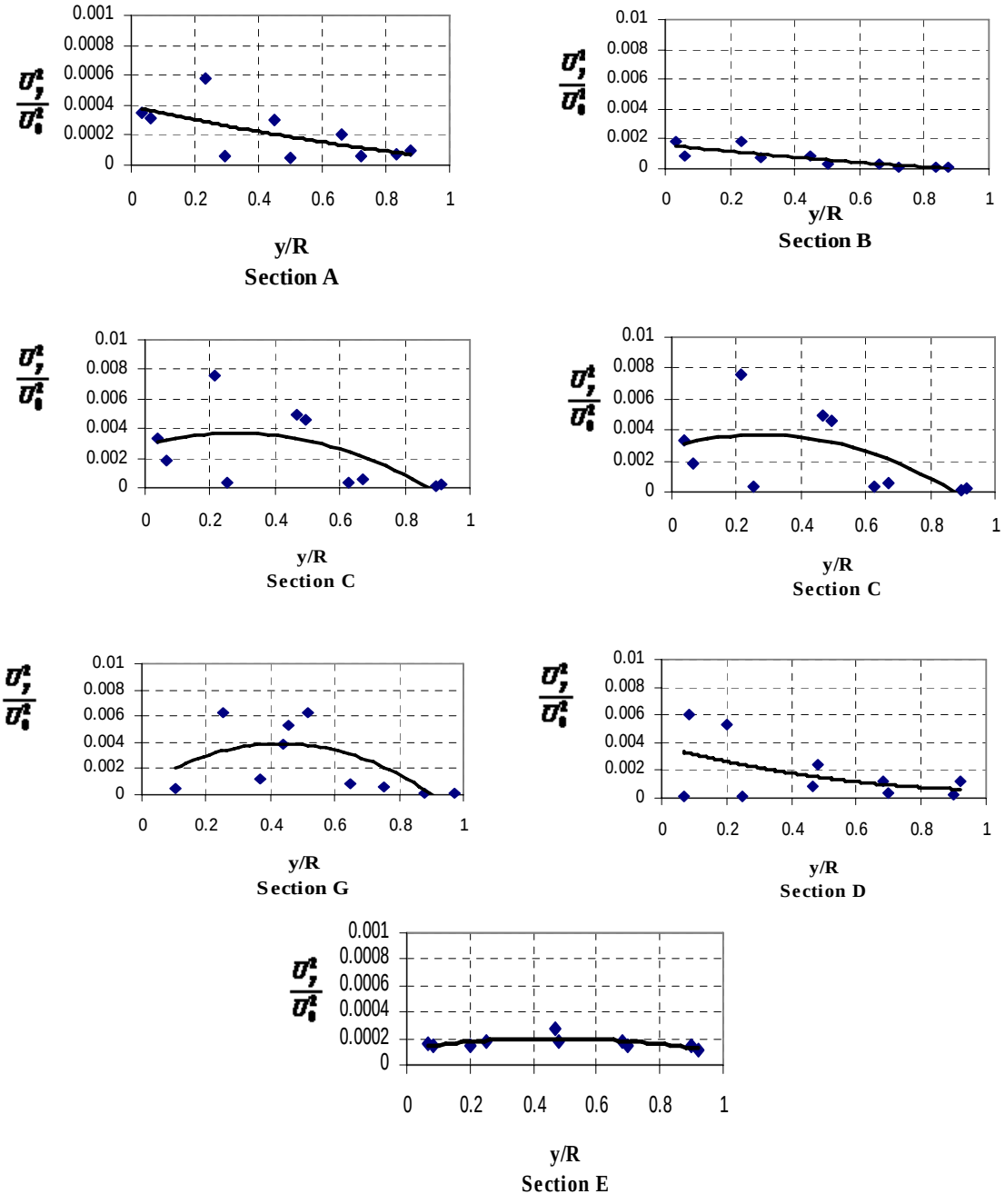

Figure 4.8 Variation of cross stream components (U_y) Re = 44000 upstream of the reducer and Re = 66000 downstream of the reducer **at through sections, A, B, F, C, G, D and E.**

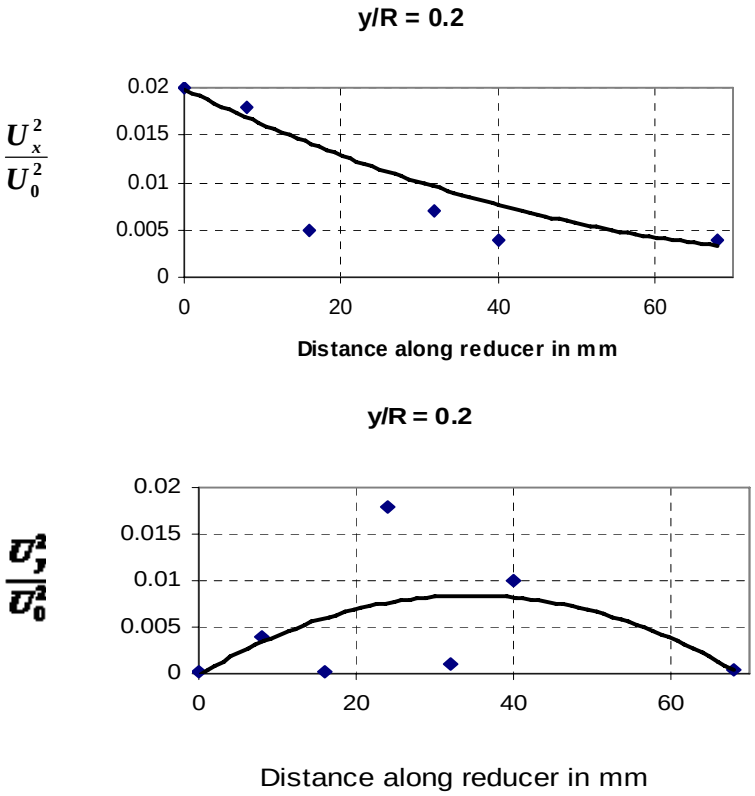

Figure 4.9 Overall changes in U and V fluctuating components at Re = 27000 upstream of the reducer and Re = 41500 downstream of the reducer along axial length of the reducer

The above figure shows the overall change of magnitude in the stream wise and cross stream components at a y/R of 0.2, Re = 27000 and Re = 41500 upstream of the reducer and downstream of the reducer respectively. These figures (figure 4.9 and 4.10) are mainly to add clarity for the reader so that reader can have a better picture of the changes in the components as the flow moves through reducer. It is recommended that more than 7 sections be analyzed in future to get a better understanding of these fluctuating components changes. The y-axis represents the magnitude of the stream wise fluctuating components and the x-axis shows the

distance in millimetres along the axial length of the reducer. Where 0 mm on x-axis represents section A and 68 mm represents section D. The scatter is high due to the sources of error in PIV measurement technique (see page 50 and 57 for sources of error in PIV measurement) but a general view can be formed which summarizes that a gradual decrease in the stream wise components is observed along the length of reducer, where as for cross stream components we noticed a gradual rise in the contraction and then a fall of the fluctuations at the exit of the reducer. The general trend is in consistent with the earlier findings.

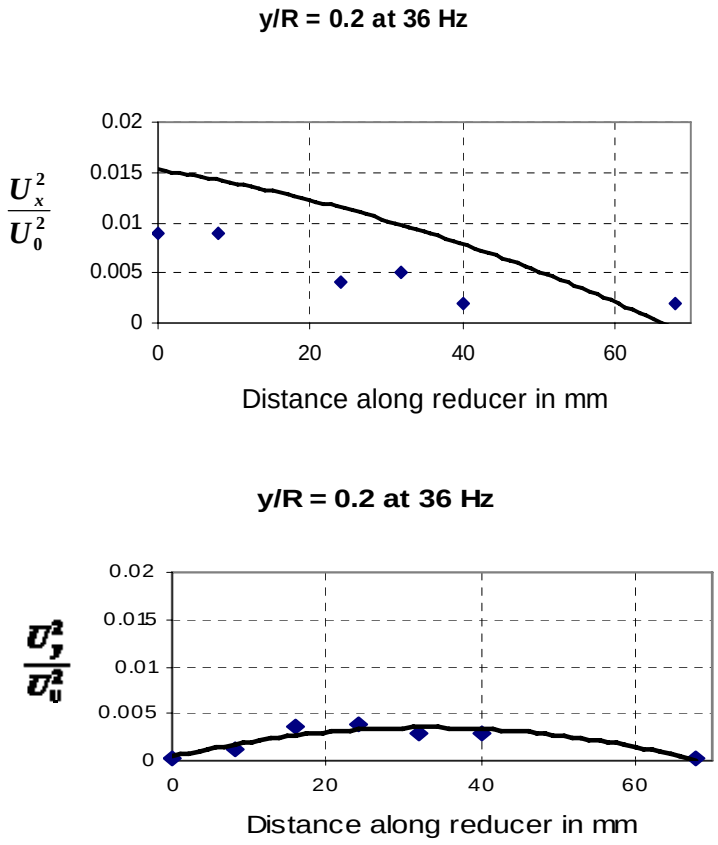

Figure 4.10 Overall changes in U and V fluctuating components at Re = 44000 upstream of the reducer and Re = 66000 downstream of the reducer along axial length of reducer

Similarly we see that at Re = 44000 and Re = 66000 upstream of the reducer and downstream of the reducer respectively there is a gradual fall in the magnitude of the stream wise components along the whole length of the reducer whereas a steady rise and then fall of the cross stream fluctuating component along the axial length of the reducer. This concludes the discussion for the PIV measurements and results for full view of the reducer at Re = 27000 and Re = 44000 in 101.8 mm of pipe section upstream of the reducer and Re = 41500 and Re = 66000 in 67 mm of pipe section at he downstream of the reducer.

4.4 Results for close to the wall PIV measurements

Close to the wall views of the reducer sections were exposed to study the role of turbulent bursting in scale growth mechanism. It is hypothesized that the frequency and intensity of the turbulent bursting (TB) into the boundary layer or close to the wall region decreases in the reducer as the flow passes through the reducer. It is theorized further that this reduced intensity of turbulent bursting is responsible for more scale growth in the contraction by eroding less scale and depositing more scaling particles into the sub-layer. Here it is the instantaneous shear stress at the wall that matters in the scale erosion and deposition. The instantaneous shear stress can be measured experimentally by using hot film anemometry technique. This method uses glued on probes (which are pasted on to the surfaces over which shear stress is to be measured) instead of normal hot wire probes for fluid flow velocity measurement.

For the purpose of finding the turbulent bursting into the sublayer using 2-D PIV, it was further assumed that this reduction in frequency of TB (number of occurrences of TB) can be detected by a decrease in the number of magnitude of instantaneous vectors pointing towards the wall. For example if we can detect more instantaneous vectors pointing towards the wall in straight pipe sections and less vectors pointing towards the wall in the contraction than we can assume that the frequency of the turbulent bursting in the contraction is reduced thus enhancing scale in the contraction or vice versa (please refer to page 49). This was assumed due to the limitations of our 2D PIV system's measurement capability in a very close to the wall region, though very accurate and precise detection of TB can be accomplished by other means such as 3 D Micro-PIV systems, using very small sized seeding particles (less than 5 microns) or/and using matched refractive index fluids etc (Uzol *et. al.,* 2002).

Three sections were magnified along the length of reducer one at the upstream of the contraction (section AA), one in the middle of the contraction (section BB) and one section at the downstream of the contraction (section CC) (figure 3.7, page 48). The axial wall length analysed were AA = 20 mm, BB = 29 mm and CC = 11 mm respectively.

4.5 Results and discussion for the section AA at Re = 27000

Figure 4.11 shows the instantaneous vectors drawn with their magnitude and associated angles. Only one image is taken as a sample out of 19 images to elaborate the procedure adopted for the detection of the TB. In total 5 TB activities were detected from 19 images analysed using the procedure explained earlier. The negative value for the angle shows the movement of vector towards the wall whereas the positive values are representative of the vectors pointing away from the wall. Only pairs of angles were selected in which one angle is positive and second angle is negative or vice versa. Table 4.1 and 4.2 contains the values for U_x', U_y', their magnitude and the angle θ in degrees for the ease of reader. The full file for all the sections AA, BB and CC is saved on the CD and is attached with the thesis.

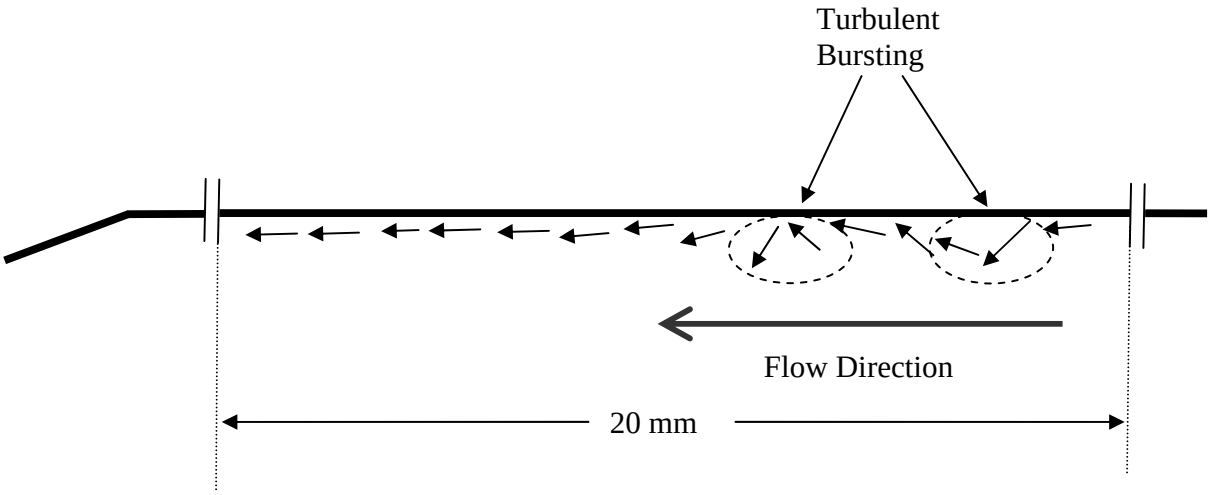

Figure 4.11 diagram illustrating the magnitude and directions of the fluctuating components (U_x' and U_y') for table 4.1 showing random occurrence of TB at Re = 27000 (vectors magnitude and directions are approximated)

Table 4.1 Values of the velocity fluctuations and their magnitude at Re = 27000 (101.8mm) and the associated angle. Values in italics represent TB.

	U_x'	U_y'	$\sqrt{\left(U_x'^2 + U_y'^2\right)}$	$Tan^{-1}\ U'_x/U'_y$
1	-0.0335	-0.00156	0.03353166	2.660655
2	-0.02139	-0.01386	0.0254921	***32.94687***
3	0.008688	-0.01303	0.015657771	***-56.3088***
4	0.052625	-0.0424	0.067578172	-38.8632
5	0.05973	-0.07066	0.092524061	-49.8016
6	0.046585	-0.0884	0.09992625	***-62.2245***
7	-0.03613	-0.05335	0.064435304	***55.9044***
8	-0.0816	-0.03747	0.089792107	24.66858
9	-0.09593	-0.03062	0.100695287	17.70855
10	-0.10829	-0.03416	0.11354887	17.51171
11	-0.11659	-0.00784	0.11685089	3.848443
12	-0.18639	-0.00652	0.186502006	2.002378
13	-0.27277	-0.00021	0.272770661	0.044528
14	-0.28669	0.001901	0.286696828	-0.37995
15	-0.31334	0.002579	0.313352558	-0.4716

Table 4.2 Values of the velocity fluctuations and their magnitude in the contraction at Re = 27000 (101.8) upstream of the contraction and Re = 41500 (67 mm) downstream of the

	U_x'	U_y'	$\sqrt{\left(U_x'^2 + U_y'^2\right)}$	$Tan^{-1}\ U'_x/U'_y$
1	-0.00383	0.027756	0.028019	***-103.96***
2	0.003633	0.022855	0.023142	***59.18218***
3	0.030354	0.02596	0.039941	18.74621
4	0.017385	0.028093	0.033037	36.46106
5	0.006978	0.01978	0.020974	***48.7822***
6	-0.0032	0.016296	0.016607	***-100.718***
7	-0.0073	0.037789	0.038488	-100.875
8	-0.00584	0.03063	0.031182	-101.023
9	-0.0207	0.031474	0.037674	-78.4733
10	-0.03189	0.028168	0.042545	-63.2652
11	-0.04893	0.018271	0.052227	***-42.2818***
12	-0.00117	-0.00353	0.003722	***49.93191***

contraction and their associated angles. Values in italics represent TB

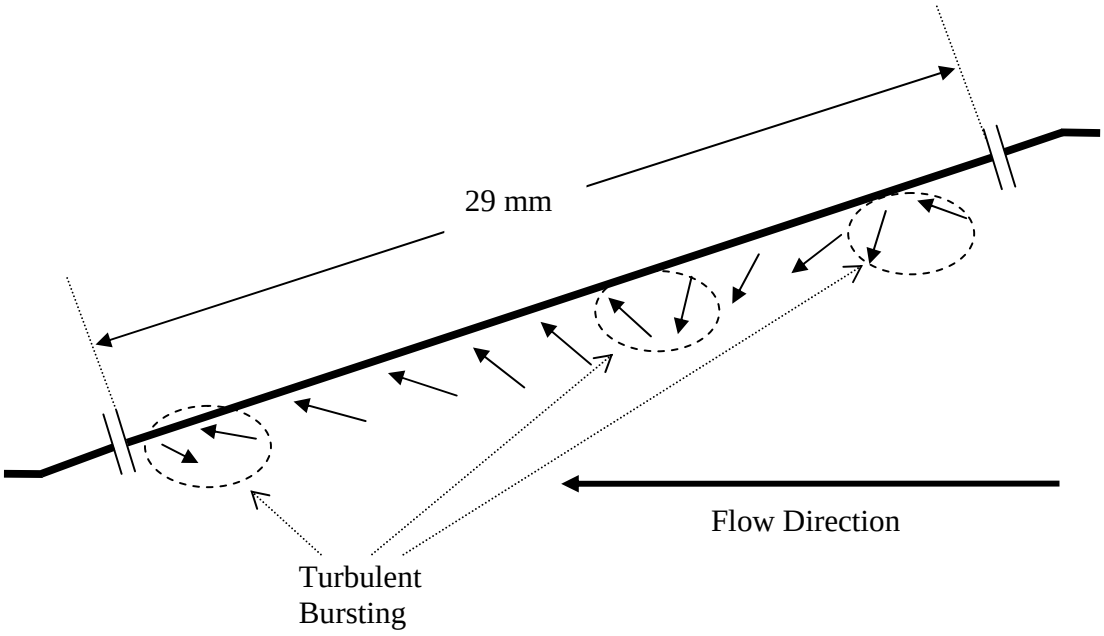

Figure 4.12 Diagram illustrating the magnitude and directions of the fluctuating components (U_x' and U_y') for table 4.2 showing random occurrence of TB at Re = 27000 upstream of contraction and Re = 41500 downstream of the contraction, (vectors magnitude and directions are approximated)

4.6 Results and discussion for the section BB at Re = 27000 and Re = 41500

Similarly the results for the section BB at 23 Hz for Re = 27000 and 41500 upstream and downstream of the contraction are plotted in figure 4.12. In total 18 images were analysed employing the same criteria as mentioned above for the detection of TB in section AA. The analysis revealed that the number of occurrences of TB or (frequency of TB) is increased in the contraction by almost 3 times for the same axial wall length. Total numbers of TB were found to be 17 for an axial length of 29 mm. (Figure 4.12)

4.7 Results for the remaining sections

On the same grounds of the analysis of the magnitude and orientation of the stream wise and cross stream velocity fluctuations ($U_x^{'}, U_y^{'}$), the numbers of TB's detected in the section CC at Re = 41500 were found to be 7. For the next batch of close to the wall measurements the numbers of TB's detected were 8 in section AA at Re = 44000, 22 in section BB at Re = 44000 and 66000, upstream and downstream of the contraction and 12 in the section CC at Re = 66,000.

Table 4.3 Relationship between the frequency of turbulent bursting and Re numbers in section AA, BB and CC of the reducer

Flow Rate (liters/sec)	Re no. in 101.8 mm pipe section	Re no. in 67 mm pipe section	Frequency of TB in Section AA	Frequency of TB in Section BB	Frequency of TB in Section CC
2.2	27000	-	5	-	-
2.2	27000	41500	-	17	-
2.2	-	41500	-	-	7
3.5	44000	-	8	-	-
3.5	44000	66000	-	22	-
3.5	-	66000	-	-	12

4.8 Concluding remarks

PIV post processing/analysis of both views i.e. full view of reducer and close to the wall readings clearly indicates a pattern whereby we can assume that increase in the number of occurrences of TB's (almost 3 time) was observed in the contraction. This is contrary to the assumption made earlier in a sense that if we presume the higher scale growth in the contraction is due to the decreased intensity of TB's in the contraction at the wall. It is not contrary if we realize that it's not the number of TB's but their magnitude that effects scale in the contraction. What we detected is the frequency or number of occurrences of TB. With the present PIV setup it's difficult to measure the magnitude since at a certain distance from the wall the average velocity start playing a role and our system is incapable of taking measurement at the boundary layer of the straight pipe and contraction of the reducer.

In fact what we observed is an increase in the frequency of the TB activity in the contraction, and an increased level of cross stream velocity fluctuations, which contributes to excessive sale growth in the contraction. Speaking in relation to particle detachment and attachment process, we found that the flow at the wall of the contraction appears to be more frequent with more numbers of TB events. This means that erosion of scale is inevitably faster in the contraction than in straight pipes. We assumed that erosion is detachment of the particles with high energy fluid (or high magnitude TB's). It is an experimental fact that scale growth rate is greater in the reducer which means that the deposition rate has increased much more substantially than the erosion rate. Keeping in mind the results found by Ilievski (Ilievski et. al., 2003), that the precipitation (crystallization) of gibbsite scale from Bayer liquor is flow independent at any flow regime (in other words it not diffusion controlled), it seems logical to conclude that most of the precipitation of Gibbsite happens on the surface of the suspended particles but not at the walls. The latter

should be true because the rate of flow independent processes is directionally proportional to the total area (at constant temperature) and the area of all suspended particles is many times greater than that of scale deposited on the wall. Hence the scale growth should go mainly through the delivery of the suspended particles to the wall by the fluid flow and subsequent adhesion of the particles to the wall. It is obvious that delivery of the particle to the wall is flow dependent. Therefore the scale deposition process is a flow dependent process and increased intensity and frequency of TB and higher cross stream fluctuations support the particles delivery to the wall and thus we have more scale in the axisymmetric contraction than in adjoining straight pipe sections for similar flow conditions.

Conclusion Chapter 5

> Nature is a self-made machine, more perfectly automated than any automated machine. To create something in the image of nature is to create a machine, and it was by learning the inner working of nature that man became a builder of machines.
>
> Eric Hoffer

Present experimental work attempts to answer one of the five hypothesis put forward in the first chapter i.e. the effect of localized velocities in the concentric reducer (3^{rd} hypothesis). The third hypothesis highlights the role of instantaneous fluctuating velocity components in the near wall region of a concentric reducer. These fluctuating velocity components were studied using 2-D PIV system as the flow moves from 101.8 mm pipe section to 67 mm section joined by a concentric reducer (dimensions given in figure 3.4, page 43). The study also explains the role of turbulent bursting in scale formation of the concentric reducer. Main points concluded are as under,

- During testing the role of velocity fluctuations it was observed that in the near wall region, y/R = 0.2 (where “y” is the local distance from the wall and “R” is the radius of section) there is an overall decrease in the stream wise velocity fluctuations at the same time an increase in the cross stream velocity fluctuations in the contraction as the flow passes through the reducer (Figure 4.10 page 73). These results are in good agreement with the earlier work (Torbergsen and Krogstad, 1998).

- The increased cross-stream fluctuating velocity components in the contraction should result in more frequent impacts of particles with the wall, hence promoting the scale growth.

- The analysis of the TB data revealed an increase in the TB activity in the contraction as compared with straight pipe sections (See table 4.3 page 80). The method used is to detect pairs of velocity fluctuations who with an angle of "incidence" to the wall and an angle of "reflection" from the wall (based on the definition of TB) greater than certain pre-set values is considered to be a TB (See page 48). Here it's worth mentioning that what was detected is the *frequency* of the TB occurring in the straight pipe sections before and after the contraction and in the contraction not the *intensity* of the TB. The scale removal component is the energetic fluid (high intensity TB's) impinging on the wall. The increased frequency of the TB may be playing the crucial role of carrying depositing particles across the turbulent boundary layer towards the wall thereby increasing residence time for the scaling particles in the contraction. This increased residence time in the boundary layer, in turn promoting excessive scale growth in the contraction.

- It is also noticed that our 2 D PIV is not suitable for measurements very close to the boundary layer but is suitable only for near wall region for the present circular geometry due to the vague demarcation of the fluid with the walls of the reducer model. This is due to the 90^0 orientation of the CCD camera with the laser light sheet. If the CCD camera is placed on top of the model the circular geometry of the reducer can not produce a clear wall distinction with the fluid. This is due to the refractive index difference of the fluid

(water) and reducer model (acrylic). To utilize PIV either solution with refractive index matching fluid should be used or a 3D micro PIV system should be employed as has been used by different researchers in the past like Uzol *et. al.,* 2002 and Ciu and Adrian, (1996).

- Our results imply that the rate of scale erosion in the contraction has increased but rate of scale deposition has increased even more substantially than the rate of erosion.

- Based on our results of flow distribution in the reducer we have concluded that scale deposition is a flow dependent process

5.1 Recommendations for Further work

The increased scale growth in the contraction can be explained fully if further research will be carried out in the following areas such as,

- The categorization of depositing particle due to their inertia in the straight pipes and contraction. Since inertia of the scaling particles can be a deciding factor in more scale growth. Due to the inertia of the depositing particles in the liquor they have more localized velocity to cross the turbulent boundary layer and start the process of nucleation.
- Introduction of the notch or squared grove at three locations in the reducer model (one before the entry of the reducer model, another one at the entry of the contraction and the last one at the exit to the contraction (entry of the smaller section pipe). This is to simulate operation of the contraction as per field conditions. The boundary layer separation phenomenon can produce pockets of re-circulating or even static fluid as a result of which the depositing particles have increased residence times which in turn is ideal for scale growth.
- Measurement of the shear stress very close to the wall of the contraction and straight pipe sections using hot film anemometry technique. Since the measurement of accurate fluid shear stress at the wall is crucial for the estimation of the lift forces required to remove depositing particles.
- Study of the increase in residence times of depositing particles using DNS studies.

- Effectively differentiating the working fluid with the wall of the reducer model for the present circular geometry.
- Use of 3D Micro PIV measurement systems along with LES or DNS study of the full reducer.

References Chapter 6

Addai-Mensah, J.; Gerson, A.; Prestidge, C. A. Ametov, I; and Ralston, J**.** ***"Interactions between gibbsite crystals in super-saturated caustic aluminate solutions"***, Ian Wark research Institute , U. of SA, Adelaide, Australia, Light metals (Warrendale, Pennsylvania) (1998), 159-166.

Addai-Mensah, J.; Prestidge, C. A.; and Ralston, J. ***"Inter-particle forces, inter-facial structure development and agglomeration of gibbsite particles in synthetic Bayer liquors"***, Mineral engineering, Vol 12, no. 6, 655-669, 1999.

Addai-Mensah, and Ralston, J**.** ***"The influence of interfacial structuring and forces on gibbsite interactions in Bayer liquor"*** submitted; J. Colloid and interface science, (1999)

Adomelt, P. and Renz, U. ***"The influence of liquid flow rate on particle deposition and detachment",*** Proceedings of "Fouling mitigation of industrial heat exchangers" San Luis Obispo, California, USA, June 1995.

Adrian, R. J. and Liu, Z. C. ***"Observation of vortex packets in direct numerical simulation of fully turbulent channel flow",*** Journal of visualization (2002), 5(1), 9-19.

Adrian, R. J.; Meinhart, C. D. and Tomkins, C. D. ***"Vortex Organization in the outer region of the turbulent boundary layer",*** J. of Fluid Mechanics (2000), 422, 1-54.

Angele, K. and Muhammad-Klingmann, Barbro***."The use of PIV in turbulent boundary layer Flows",*** Fluid Mechanics and its applications (2001), 59(IUTAM Symposium on geometry and statistics of Turbulence, 1999), 373-378.

Baldi, S. and Yianneskis, M.,"***On the direct measurement of turbulence energy dissipation in stirred vessels with PIV"*** Industrial and engineering chemistry research (2003), 42(26), 7006-7016.

Barker, D. B. and Fourney, M. E., ***"Measuring fluid velocity with speckle patterns***", Opt. Lett. 1, 1977, 135.

Beal, S. K., ***"Deposition of particles in turbulent flow on channel or pipe walls",*** Nuclear science and engineering" (1970), 40, 1-11

Blackburn, H. M. ***"Sidewall boundary layer instabilities in confined swirling flow"*** Conf. proceedings" Advances in turbulence" (Barcelona, 27-30 June 2000) selected for publishing in J of Turbulence. (May 2001)

Brown, N. "***Crystal growth and nucleation of aluminium tri-hydroxide from seeded caustic aluminate solutions",*** J. of Crystal Growth, 12 (1972), 39-45

Bugay, S.; Escudie, R. and Line, A. ***"Experimental analysis of hydrodynamics in axially agitated tank"***' AlChE Journal, (2002), 48(3) 463-475.

Canaan, R. E. and Hassan, Y. A. 1991, "***Simultaneous Velocity Filed Measurements of Bubbles and Surrounding Fluid by Pulsed Laser Velocimetry",*** *Laser Anemometry-ASME*, vol. 1, pp. 387-401.

Cleaver, J. W. and B.Yates, 1972, ***"The effect of detachment of colloidal particles from a flat substrate in a turbulent flow"***, Journal of colloid and interface science, 44 no. 3, 464-473.

Cleaver, J. W. and B.Yates, 1975, *'**The Effect of Re-entrainment on Particle Deposition**'*, *Chemical Engineering Science*, vol. 31, pp. 147-151.

Corino, E. R. and Brodkey, R. S. ***"A visual investigation of the wall region in turbulent flow"***, (1969) J of Fluid Mechanics 37, 1-30

Cui, M. M. and Adrian, R. J. ***"Refractive index matching and marking methods and marking methods for highly concentrated solid-liquid flows",*** Experiments in Fluids, 22 (1997) 261-264.

Dantec website ***http://www.dantecdynamics.com.***

Dudderar, T. D.; Meynart, R. and Simpkins, P. G., ***"Full field laser metrology for fluid velocity measurement",*** 1988, Opt. Laser Eng. 9, 163.

Dyer, K. R. and Soulsby, R. L. ***"Sand transport on a continental shelf",*** A Rev. Fluid Mechanic., 210, 295-324.

Escudie, R. and Line, A. ***"Experimental analysis of hydrodynamics in a radially agitated tank",*** AlChE Journal (2003) 49(3), 585-603.

Fox, R. W. and McDonald, A. T. "***Introduction to Fluid Mechanics",*** 5th Ed.

Grass, A. J., ***"Structural features of turbulent flow over smooth and rough boundaries"*** (1971) Journal of Fluid Mechanics, 50, 233-255

Gui, L. and Merzkirch, W. ***"A comparative study of the MQD method and several correlation-based PIV evaluation algorithms"***, Experiments in Fluids 28 (2000) 36-44.

Hosni, M. H. and Jones, B. W. "***Development of Particle Image Velocimetry for measuring Air Velocity in Large-Scale Room airflow Applications",*** *ASHRAE transactions: Symposia*, vol. HI-02-19-2 (RP-978), pp. 1164-72.

Huang, H 1998, "***An extension of digital PIV- Processing to double-exposed images"***, Experiments in Fluids, vol. 24, pp. 364-72.

Ilievski, D., ***"Development of a constant supersaturation, semi-batch crystallizer and its application to investigating crystal agglomeration"***, J. of Crystal Growth, 233(2001), 846-862.

Itakura, T. and Kishi, T***. "Open channel flow with suspended sediments",*** J. of Hydraulic. Div. ASCE, 106, 1325-1343

Kaftori, D.; Hetsroni, G. and Banerjee, S, ***"Particle behaviour in the turbulent boundary layer. Motion, deposition, and entrainment ",*** Physics Fluids 7 (5), May 1995, 1095-1106

Keane, R. D. and Adrian, R. J. ***"Optimization of particle image velocimeters, Part 1 Doubled pulsed Systems"*** Measurement of Science Technology 1: 1202-1215.

Kim-E, M. E.; Brown, R. A. and Armstrong, R. C. ***"The roles of inertia and shear-thinning in flow of an inelastic liquid through an axisymmetric sudden contraction"*** J. of Non-Newtonian fluid mechanics (1983), 13(3), 341-363.

Kline, S. J.; Reynolds, W.C.; Schraub, F. A.; and Rundstadler, P. W., ***"The structure of turbulent boundary layers"*** J of Fluid Mechanics, (1967) 30, 741.

Kline, S. J. and Robinson, S. K. ***"Turbulent boundary layer structure: Progress, status, and challenges"*** in A. Gyr(ed.), Structure of turbulence and drag reduction, Springer-Verlag, Berlin (1990).

Kovasznay, L. S. G. ***"Structure of the turbulent boundary layer"*** The physics of fluids supplement, 1967, S25-S30

Lee, M. Y. and Parkinson, G. M., ***"Growth rates of gibbsite single crystals determined using in situ optical microscopy",*** J of Crystal Growth, 199 (1999), 270-274.

Li, T.; Bedell, D.; Livk, I. and Ilievski, D. ***"Gibbsite crystal growth caustic aluminate solutions under different flow regimes"***, Hydrometallurgy 2003- Fifth international conference in honour of Professor Ian Ritchie, Vol. 2, Electrometallurgy and environmental hydrometallurgy.

Lindken, R.; Gui, L. and Merzkirch, W.1999, "***Velocity Measurements in Multiphase Flow by Means of Particle Image Velocimetry",*** *Chemical Engineering Technology*, vol. 22, pp. 202-206.

Liberzon, A.; Gurka, R. and Hetsroni, G. 2001, "***Vorticity characterization in a turbulent boundary layer using PIV and POD analysis"*** 4th International Symposium on Particle Image Velocimetry, Gottingen, Germany, September 17-19, 2001.

Ma, Q.; Nie, Y.; Bao, Y.; Wang, Y. and Shi, L. ***"Numerical simulation of hydrodynamics in stirred tank"***, Huagong Xuebao (Chinese edition) (2003) 54(5), 612-618.

Marchioli, C. and Soldati, A., "Mechanisms for particle transfer and segregation in turbulent boundary layer", J. of Fluid Mechanics, 468, 283 (2002).

McLaury, B. S. and Shirazi, S. A. ***"Predicting erosion in straight pipes"***, Proceedings of FEDSM, 1998 ASME fluids engineering division summer meeting, June 21-25. 1998, Washington, DC

Misra, C. and White, E. T. ***"Kinetics of crystallization of aluminium tri-hydroxide from seeded caustic aluminate solutions",*** Chemical engineering progress symposium series, 67(1971), 53-65.

Mousa, H. A. ***"Deposition of small particles on spherical collectors under turbulent flow conditions",*** Separation science and technology, (2002), 37(9), 2021-2035.

Narayanan, C. and Lakehal, D. ***"Mechanisms of particles deposition in a fully developed turbulent open channels flow",*** Physics of fluids, vol. 15, no. 3 March 2003.

Nawrath, S., Masters Thesis, ***"Investigation into the Relationship between Scale Growth Rate and Flow Velocity for a Supersaturated Caustic-Aluminate Solution,"*** Central Queensland University, Rockhampton Campus, Australia.

Papadoplous, G. and Hammad, K. J. ***"A PIV-based flow meter***", Dantec Measurement technology, Inc. ASME fluids engineering division summer meeting (FEDSM 2000), 270-275.

Prestidge, C. A. and Ametov, I. ***"Cations effect during aggregation and agglomeration of gibbsite particles under synthetic Bayer crystallization conditions",*** J. of Crystal Growth, (2000), 209(4), 924-933.

Queensland Alumina Ltd. Website, ***www.qal.com.au.***

Ranade, V. V.; Perrard, M.; Le Sauze, N.; Xuereb, C. and Bertrand, J. ***"Trailing vortices of Rushton turbine: PIV measurement and CFD simulations with snapshot approach"'*** Chemical engineering research and design (2001), 79(a1), 3-12.

Rao, K. N.; Narashima, R. and Badri-Narayanan, M.A., ***"The bursting phenomena in a turbulent boundary layer"***. J. of Fluid Mech., Vol. 48, 339-352 (1971)

Roach, G. I. D. and Cornell, J. B. "***Scaling in Bayer Refineries",*** The AusIMM Annual Conference, 24-28 March, 1996.

Roach, G. I. D. ; Cornell, J. B. and Griffin, Brendan J. ***"Gibbsite growth history – revelations of a new scanning electron microscope technique",*** Research and development, Alcoa of Australia limited, Australia. Light metals (1998), 153-158.

Rashidi, M.; Hetsroni, G. and Banerjee, S., 1990, ***"Particle-Turbulence Inter-action in a Boundary Layer"***, *Intl. Journal of Multi-phase flow*, vol. 16, no. 6, 935-49.

Rashidi, M., and Banerjee, S., 1990(a), ***"The effect of boundary conditions and shear rate on streak formation and breakdown in turbulent channel flow",*** Phys. Fluids. In press

Rothstein, J. P. and McKinley, G. H. ***"The axisymmetric contraction-expansion: the role of extensional rheology on vortex growth dynamics and the enhanced pressure drop",*** J. of Non-Newtonian fluid mechanics (2001), 98(1), 33-63.

Rothstein, J. P. and McKinley, G. H. ***"Extensional flow of a polystyrene Boger fluid through a 4:1:4 axisymmetric contraction/expansion",*** J. of Non-Newtonian fluid mechanics (1999), 86(1-2), 61-88.

Simpkins, P.G. and Dudderar, T. D. ***"Laser speckle measurement of transient Benard convection"***, J. of F. Mech., 1978, 89, 665.

Soulsby, R. L. and Wainwrights, B. L. S. A. ***"A criterion for the effect of suspended sediment on near-bottom velocity profiles",*** J. Hydraulic, Res, 1987, 25, 341-356.

Taylor, P. A. and Dyer, K. R., ***"Theoretical models of flow near the bed and their implications for sediment transport, in the sea,***" Vol. 6 (edited by Goldberg, E. D., McCave, I. N., O'Brien, J. J. and Steel, J. H.), 1977, 579-601, Wiley Inter-science, New York.

Tachibana, M.; Kawabata, N. and Sakamoto, M. ***"Laminar flow and pressure loss of power-law fluids in pipes with an axisymmetric sudden contraction"*** Nihon Reororji Gakkaishi (1987), 15(4), 210-219.

Tennekes, H and Lumley, J. L***. "A first course in Turbulence"*** MIT press, 1972

Thomas, D., (1997), ***"Swirling flow agitation"*** – QAL/CSIRO collaborative research program 2000, Presentation to QAL technical advisory committee – April, 2000.

Torbergsen, L. E. and Krogstad, Per-Age**., *"Axisymmetric Contraction of Fully Developed Pipe Flow"***, 13th Australian Fluid Mechanics Conference, Monash University, Melbourne, Australia. 13-18 December, 1998

TSI website ***http://www.tsi.com/fluid/products/piv/piv.htm.***

Uzol, O.; Chow, Y. C.; Katz, J. and Meneveau, C. ***"Unobstructed particle image velocimetry measurements within an axial turbo-pump using liquid and blades with matched refractive indices"***, Published online: 6th August 2002. Experiments in Fluids.

Westerweel, J., Draad A. A., J. G. Th. Van der Hoeven and Van Oord, J.1996, ***'Measurement of Fully Developed turbulent Pipe flow with Digital Particle Image Velocimetry',*** *Experiments in Fluids*, vol. 20, pp. 165-77.

Yung, B. P. K., Merry, H. and Bott, T. R.1989, ***"The Role of Turbulent Bursts in Particle Re-entrainment in Aqueous Systems"***, *Chemical Engineering Science*, vol. 44, no. 4, 873-82.

Appendix "A"

In this section detailed explanation of the method is discussed by which the stream wise and cross stream fluctuating velocity components were isolated from the PIV data. A CD containing an MS – Excel file is attached with the thesis also. The name of the file is "Thesis Data."

We use double frame double exposure technique to make PIV images. The two successive images are cross-correlated with each other to plot vectors on the PIV images. The Insight software was set to produce 1 vector along x-axis and 10 vectors along y-axis for all of the 7 sections in the reducer (Please see figure 41, 4.2, 4.3 and 4.4, page 63-66). A total of 700 vector plots were processed, fifty plots for section A, B, F, C, G, D and E at Re = 27000 reducer and Re = 41500 downstream of the reducer respectively and fifty plots for section A, B, F, C, G, D and E at Re = 44000 reducer and Re = 66000 downstream of the reducer respectively. These vector plots are then saved as vector files in Note Pad format in the PIV software. The Note Pad file contains information such as name of the file, time separation between the laser pulses, the micro-meter (μm) per pixel information, the cross correlation factor, x and y locations and their corresponding vector values (U and V) in metre/sec. A typical Note Pad format is shown in figure below. The Note Pad file is converted into excel file, to isolate U-component (stream-wise) of velocity and V-component (cross-stream) of velocity. The U and V component is isolated for each of the 700 files for all seven sections.

U and V components were separated which consisted of a total of 50 data points for each section A, B, F, C, G, D and E in the first 50 columns of the spread sheet. These data points were averaged arithmetically in the 51st column of the MS-Excel file. In the next 50 columns the arithmetic average value is subtracted from each of the 50 data points to get fluctuating components (U_x and U_y). These 50 fluctuating components were squared in the next 50 columns and then averaged in the 51st column. The squared value obtained is then divided with average velocity (volume flow/area of cross section). This division results in the non dimensionalized form or $\boldsymbol{U_x^2}/\boldsymbol{U_0^2}$. The value of $\boldsymbol{U_x^2}/\boldsymbol{U_0^2}$ is plotted against "y/R" ratio where "y" is the distance from the wall and "R" is the radius of the section.

```
TITLE="\2a.vec" VARIABLES= "X mm", "Y mm", "U m/s", "V m/s", "CHC" ZONE
  T="120.000000um/p, 120.000000um/p, 600.000000us " I=1, J=10 F=POINT
          93960.000000, 97320.000000, -0.066303, -0.013556, 1
           93960.000000, 89280.000000, -0.134113, 0.002401, 1
           93960.000000, 80280.000000, -0.160577, 0.002805, 1
           93960.000000, 72360.000000, -0.181339, 0.000489, 1
           93960.000000, 64320.000000, -0.190595, 0.000546, 1
           93960.000000, 56280.000000, -0.189320, 0.001929, 1
           93960.000000, 48360.000000, -0.184866, 0.001186, 1
           93960.000000, 39360.000000, -0.177436, 0.001497, 1
           93960.000000, 31320.000000, -0.151322, 0.001358, 1
           93960.000000, 23280.000000, -0.051263, 0.007028, 1
```

Figure 1 A sample vector output file by the TSI Insight ™ software in Note Pad

Appendix "B"

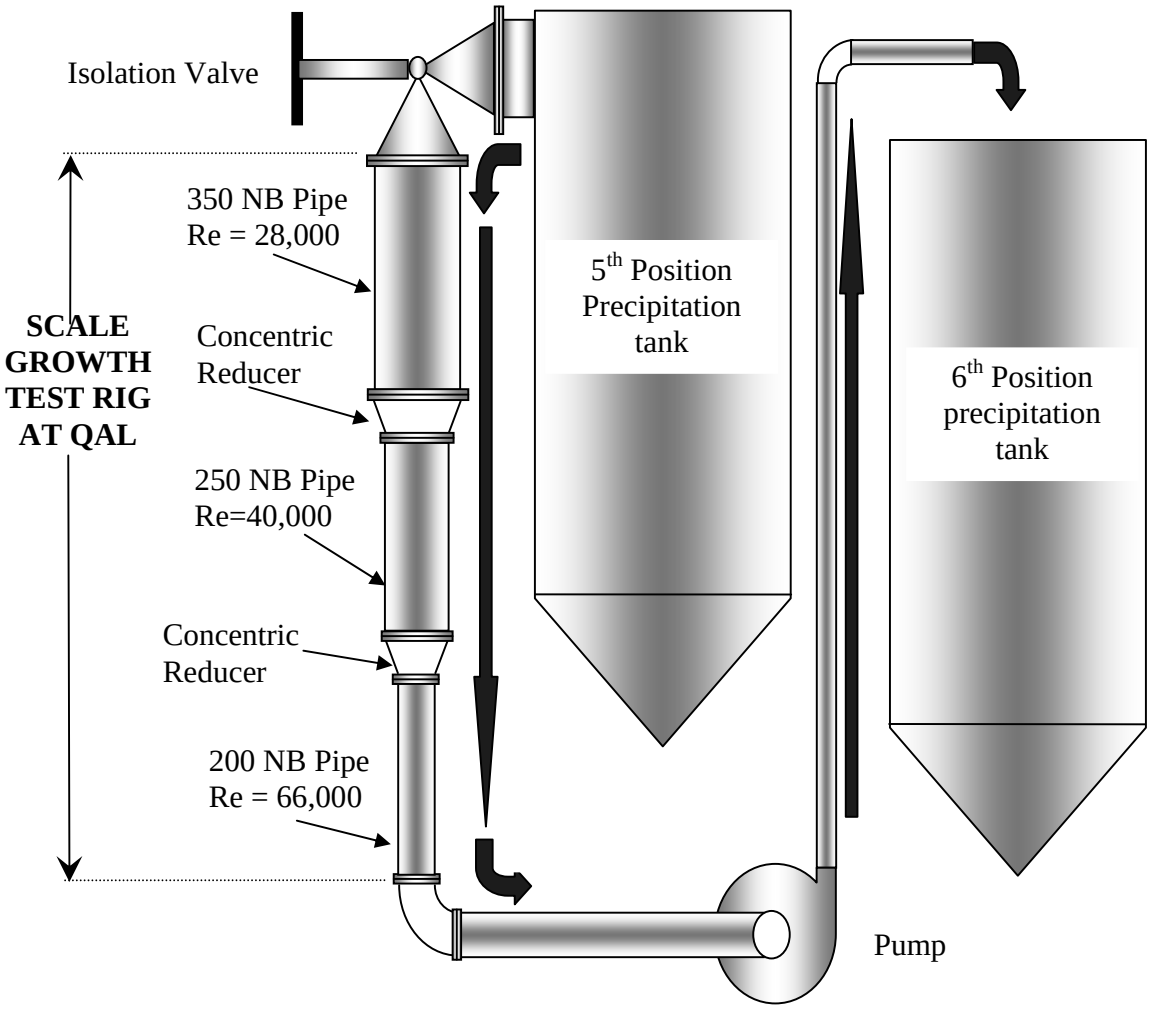

Figure appendix B

Gibbsite scale growth test rig in Precipitation section at QAL site

Appendix “C”

The percentage error of the PIV was determined by comparing the flow meter reading obtained from the digital read out of the flow meter and by integrating the stream wise velocity components values of 2 sections AA and BB at Re = 27000 and Re = 41500 upstream of the reducer and Re = 44000 and Re = 66000 downstream of the reducer respectively.

Arithmetic average of 2 (1 and 1*) stream wise velocity components near the upper and lower wall of the section is taken as shown in figure below. The 2 values are taken to get a mean value of stream-wise velocity value at a certain distance “ r ” from the center of flow. This if viewed at right angle to the plane of paper (flow moving towards or away from the reader) represent first annular ring at a distance “R_1” from the center.

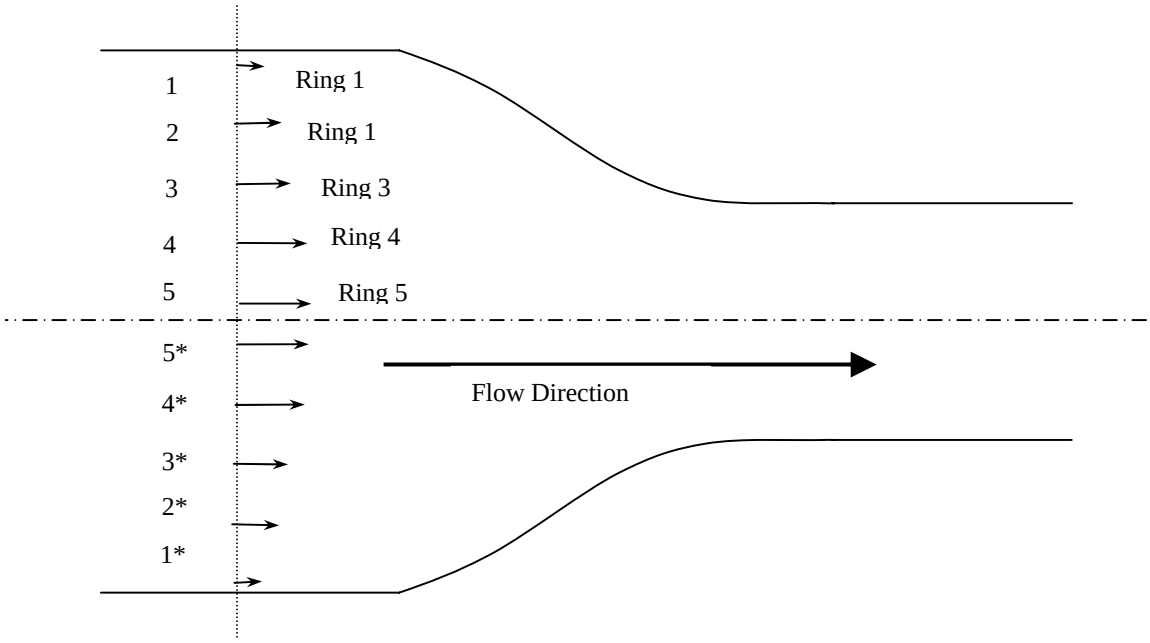

Figure Appendix “C”

Similarly, arithmetic averages of other values as 2-2*, 3-3*, 4-4* and 5-5* were calculated to get mean values for the stream wise velocity components at distances "R_2", "R_3", "R_4" and "R_5" respectively. Following formula is used to calculate the calculated volume flow rate.

$$Q = R_1 * V_1 + R_2 * V_2 + R_3 * V_3 + R_4 * V_4 + R_5 * V_5$$

The ratio of the flow meter reading for volumetric flow to the calculated volumetric flow using above formula is the experimental error of the PIV system.

Below is a sample MS – Excel file for Re = 27000 upstream of reducer and Re = 41500 downstream of the reducer used to calculate the volumetric flow rate at section AA of the concentric reducer.

23HZ Section AA

1	2	3	4	5	6	7	8	9	10	
-0.0549	-0.047	-0.065	-0.0964	-0.1069	-0.08693	-0.11101	-0.1031	-0.0725	-0.0725	
-0.1693	-0.14	-0.1624	-0.2068	-0.1814	-0.17467	-0.21898	-0.1971	-0.2203	-0.2203	
-0.2846	-0.275	-0.2443	-0.2453	-0.2385	-0.25416	-0.26491	-0.2255	-0.253	-0.253	
-0.3203	-0.336	-0.2846	-0.2899	-0.2915	-0.29667	-0.28811	-0.2492	-0.2689	-0.2689	
-0.3233	-0.341	-0.2887	-0.2914	-0.2952	-0.30754	-0.28592	-0.2452	-0.2698	-0.2698	
-0.3217	-0.35	-0.2938	-0.295	-0.2961	-0.30104	-0.29011	-0.247	-0.2694	-0.2694	
-0.3174	-0.345	-0.2923	-0.2952	-0.295	-0.29261	-0.3001	-0.2448	-0.2666	-0.2666	
-0.2976	-0.316	-0.2795	-0.2646	-0.2984	-0.2762	-0.28508	-0.2505	-0.2602	-0.2602	
-0.23	-0.181	-0.2245	-0.1608	-0.273	-0.19687	-0.24845	-0.2225	-0.2242	-0.2242	
-0.0837	-0.047	-0.1204	-0.0364	-0.1357	-0.08113	-0.10662	-0.0657	-0.0868	-0.0868	
-0.0018	-0.002	-0.0017	-0.0016	-0.0019	-0.00169	-0.00192	-0.0017	-0.0018	-0.0018	-0.00175

23HZ Section EE

-0.4516	-0.457	-0.4343	-0.4234	-0.4365	-0.44452	-0.48114	-0.4803	-0.4617	-0.4671	
-0.4652	-0.464	-0.4549	-0.4572	-0.4433	-0.45712	-0.47979	-0.4832	-0.4965	-0.4716	
-0.4809	-0.478	-0.473	-0.4774	-0.4515	-0.45776	-0.51322	-0.5038	-0.5316	-0.4943	
-0.5035	-0.465	-0.4942	-0.4771	-0.4723	-0.49547	-0.51182	-0.5139	-0.5399	-0.4901	
-0.51	-0.474	-0.4899	-0.4847	-0.5007	-0.51771	-0.5233	-0.5278	-0.5305	-0.5087	
-0.5081	-0.48	-0.4993	-0.4877	-0.4995	-0.51761	-0.51393	-0.5217	-0.5173	-0.5129	
-0.5036	-0.451	-0.492	-0.4867	-0.5048	-0.51483	-0.51762	-0.5191	-0.5009	-0.5193	
-0.4832	-0.434	-0.4881	-0.4837	-0.4798	-0.49713	-0.51127	-0.5193	-0.4891	-0.5102	
-0.447	-0.39	-0.4469	-0.4583	-0.4849	-0.44175	-0.50375	-0.51	-0.452	-0.4953	
-0.4011	-0.376	-0.4107	-0.4418	-0.4248	-0.38583	-0.46806	-0.4884	-0.4393	-0.4597	
-0.0017	-0.002	-0.0017	-0.0017	-0.0017	-0.00167	-0.0018	-0.0018	-0.0018	-0.0018	-0.00171

And further on next page

-0.06928	-8.5E-05				
-0.19964	-0.00078				
-0.29109	-0.00031				
-0.31884	-0.00054				
-0.32251	-8.1E-05	Cal. Value	Act. Value	%age Err	
	-0.0018	0.001801	0.0022	18.13885	
-0.42635	-0.00045				
-0.46518	-0.00046				
-0.24129	-0.00025				
-0.50349	-0.0005				
-0.51004	-6.6E-05	Cal. Value	Act. Value	%age Err	
	-0.00173	0.001727	0.0022	21.51701	

	1	2	3	4	5	6	7	8	9	10	11	12	13
A (U)	-0.331141	-0.325482	-0.381878	-0.302719	-0.370336	-0.320758	-0.345071	-0.38178	-0.476391	-0.299859	-0.334267	-0.323492	-0.316069
	-0.569168	-0.509125	-0.604294	-0.511588	-0.627442	-0.568678	-0.537735	-0.622793	-0.647856	-0.518487	-0.609047	-0.546954	-0.543741
	-0.668411	-0.658857	-0.673863	-0.673853	-0.681742	-0.700019	-0.677089	-0.682602	-0.690799	-0.678412	-0.689809	-0.675354	-0.668546
	-0.712136	-0.703557	-0.714309	-0.708979	-0.712516	-0.740736	-0.719508	-0.716983	-0.704684	-0.703197	-0.717924	-0.706395	-0.708949
	-0.742058	-0.730217	-0.735286	-0.742404	-0.725659	-0.741953	-0.725357	-0.732462	-0.713379	-0.722881	-0.725668	-0.740013	-0.727634
	-0.716294	-0.712994	-0.722581	-0.722941	-0.69616	-0.744868	-0.715219	-0.720213	-0.699369	-0.710163	-0.698887	-0.727585	-0.717419
	-0.692671	-0.690351	-0.692933	-0.693851	-0.691196	-0.706533	-0.699365	-0.698591	-0.690394	-0.692416	-0.682103	-0.69163	-0.687332
	-0.673703	-0.677014	-0.67837	-0.680897	-0.670626	-0.688826	-0.672431	-0.678512	-0.677574	-0.674782	-0.673342	-0.675195	-0.6586
	-0.612395	-0.597034	-0.543717	-0.561468	-0.545376	-0.55931	-0.564067	-0.619911	-0.631434	-0.566188	-0.588859	-0.629272	-0.612994
	-0.347639	-0.336615	-0.305527	-0.313097	-0.364485	-0.321705	-0.320627	-0.380392	-0.319615	-0.284108	-0.346889	-0.306477	-0.332021

14	15	16	17	18	19	20	21	22	23	24	25	26	27
-0.552158	-0.356319	-0.315131	-0.295039	-0.341012	-0.567798	-0.383941	-0.278309	-0.310938	-0.365734	-0.3044	-0.335346	-0.291669	-0.315663
-0.640035	-0.619838	-0.601845	-0.582249	-0.568604	-0.642916	-0.618819	-0.484327	-0.583592	-0.625034	-0.587928	-0.596344	-0.533144	-0.619172
-0.680536	-0.677645	-0.688407	-0.692315	-0.666645	-0.681224	-0.678811	-0.665	-0.690508	-0.690134	-0.67703	-0.676462	-0.672252	-0.680553
-0.703477	-0.713719	-0.716592	-0.718482	-0.69901	-0.724121	-0.703941	-0.699543	-0.734988	-0.7062	-0.718362	-0.721872	-0.722597	-0.706168
-0.720983	-0.754984	-0.722263	-0.729936	-0.717966	-0.738255	-0.731407	-0.71637	-0.744355	-0.716777	-0.751048	-0.750289	-0.747783	-0.728932
-0.720049	-0.723659	-0.701188	-0.709305	-0.70515	-0.723918	-0.72657	-0.711153	-0.717926	-0.737024	-0.740172	-0.721027	-0.726984	-0.71623
-0.697998	-0.702899	-0.693388	-0.686199	-0.693708	-0.694175	-0.696389	-0.707603	-0.69719	-0.700732	-0.709617	-0.697424	-0.690631	-0.698077
-0.688478	-0.687735	-0.678437	-0.663379	-0.665711	-0.673394	-0.673979	-0.694488	-0.681992	-0.690168	-0.682445	-0.685697	-0.666303	-0.679902
-0.657772	-0.611724	-0.612994	-0.612994	-0.612994	-0.492508	-0.597918	-0.603267	-0.602713	-0.646497	-0.642705	-0.579391	-0.522846	-0.612541
-0.386598	-0.322753	-0.326455	-0.305998	-0.302378	-0.32326	-0.354512	-0.333095	-0.294028	-0.293179	-0.423112	-0.293466	-0.306911	-0.324099

28	29	30	31	32	33	34	35	36	37	38	39	40	41
-0.321616	-0.320297	-0.322047	-0.266275	-0.323146	-0.342647	-0.308525	-0.351064	-0.311961	-0.288377	-0.276079	-0.33135	-0.266123	-0.375029
-0.543883	-0.575678	-0.593491	-0.541918	-0.576815	-0.592715	-0.512835	-0.631795	-0.592154	-0.484449	-0.598625	-0.594343	-0.612141	-0.551239
-0.672399	-0.685908	-0.672669	-0.638796	-0.681253	-0.683902	-0.683641	-0.685284	-0.702253	-0.665914	-0.683382	-0.68414	-0.679313	-0.682918
-0.711847	-0.711915	-0.706312	-0.687838	-0.708623	-0.69977	-0.708388	-0.706097	-0.719805	-0.699278	-0.704528	-0.713528	-0.709035	-0.727107
-0.742485	-0.732477	-0.727415	-0.715695	-0.732368	-0.722813	-0.741172	-0.724038	-0.735095	-0.740032	-0.718945	-0.73421	-0.740618	-0.747372
-0.719526	-0.724067	-0.714595	-0.732254	-0.725843	-0.731557	-0.716018	-0.716861	-0.739938	-0.734984	-0.704184	-0.72221	-0.747922	-0.72105
-0.697382	-0.701663	-0.700177	-0.700278	-0.706435	-0.710048	-0.69031	-0.694524	-0.715147	-0.699942	-0.68228	-0.700329	-0.71766	-0.696368
-0.687144	-0.669557	-0.673119	-0.676385	-0.686912	-0.691902	-0.68429	-0.673098	-0.677676	-0.679655	-0.667824	-0.685105	-0.702459	-0.687583
-0.612994	-0.412223	-0.438348	-0.61341	-0.623925	-0.655291	-0.651565	-0.512338	-0.612994	-0.591232	-0.581449	-0.603581	-0.640719	-0.650383
-0.286639	-0.289475	-0.291743	-0.383576	-0.320665	-0.322986	-0.331392	-0.328472	-0.305204	-0.301688	-0.309812	-0.315806	-0.3303	-0.34151

42	43	44	45	46	47	48	49	50	Arthmatic Average of 50 data points
-0.307803	-0.48029	-0.297732	-0.27193	-0.284954	-0.308232	-0.347126	-0.339275	-0.330139	-0.33789434
-0.532777	-0.648412	-0.499429	-0.478579	-0.498378	-0.569972	-0.576776	-0.629434	-0.62084	-0.57554866
-0.680179	-0.686703	-0.666836	-0.671643	-0.67539	-0.690207	-0.668582	-0.688125	-0.687582	-0.67907794
-0.701554	-0.701673	-0.71605	-0.704795	-0.709382	-0.720087	-0.709683	-0.714062	-0.711094	-0.71122792
-0.724712	-0.704671	-0.748279	-0.723932	-0.721566	-0.742655	-0.732508	-0.716193	-0.715765	-0.7312267
-0.713162	-0.709446	-0.742049	-0.71546	-0.717033	-0.736234	-0.736101	-0.705885	-0.706078	-0.7203501
-0.695564	-0.687684	-0.695582	-0.705487	-0.680264	-0.698802	-0.713189	-0.691427	-0.691868	-0.69695612
-0.67804	-0.662855	-0.683524	-0.678629	-0.673467	-0.675324	-0.682178	-0.68215	-0.681995	-0.67865702
-0.632356	-0.612994	-0.567772	-0.619561	-0.586484	-0.612994	-0.612152	-0.576479	-0.576479	-0.59277224
-0.362045	-0.291395	-0.304601	-0.362244	-0.294443	-0.329889	-0.326943	-0.329412	-0.329412	-0.32517386

(Average) - 1st data point	(Average) - 2nd data point						
0.00675334	0.01241234	-0.043984	0.035175	-0.032442	0.017136	-0.007177	-0.043886
0.00638066	0.06642366	-0.028745	0.063961	-0.051893	0.006871	0.037814	-0.047244
0.01066694	0.02022094	0.0052149	0.005225	-0.002664	-0.020941	0.001989	-0.003524
-0.00090808	0.00767092	-0.003081	0.002249	-0.001288	-0.029508	-0.00828	-0.005755
-0.0108313	0.0010097	-0.004059	-0.011177	0.005568	-0.010726	0.00587	-0.001235
0.0040561	0.0073561	-0.002231	-0.002591	0.02419	-0.024518	0.005131	0.000137
0.00428512	0.00660512	0.0040231	0.003105	0.00576	-0.009577	-0.002409	-0.001635
0.00495402	0.00164302	0.000287	-0.00224	0.008031	-0.010169	0.006226	0.000145
-0.01962276	-0.00426176	0.0490552	0.031304	0.047396	0.033462	0.028705	-0.027139
-0.02246514	-0.01144114	0.0196469	0.012077	-0.039311	0.003469	0.004547	-0.055218

15

-0.043886	-0.138497	0.038035	0.003627	0.014402	0.021825	-0.214264	-0.018425	0.022763	0.042855	-0.003118	-0.229904	-0.046047	0.059585
-0.047244	-0.072307	0.057062	-0.033498	0.028595	0.031808	-0.064486	-0.044289	-0.026296	-0.0067	0.006945	-0.067367	-0.04327	0.091222
-0.003524	-0.011721	0.000666	-0.010731	0.003724	0.010532	-0.001458	0.001433	-0.009329	-0.013237	0.012433	-0.002146	0.000267	0.014078
-0.005755	0.006544	0.008031	-0.006696	0.004833	0.002279	0.007751	-0.002491	-0.005364	-0.007254	0.012218	-0.012893	0.007287	0.011685
-0.001235	0.017848	0.008346	0.005559	-0.008786	0.003593	0.010244	-0.023757	0.008964	0.001291	0.013261	-0.007028	-0.00018	0.014857
0.000137	0.020981	0.010187	0.021463	-0.007235	0.002931	0.000301	-0.003309	0.019162	0.011045	0.0152	-0.003568	-0.00622	0.009197
-0.001635	0.006562	0.00454	0.014853	0.005326	0.009624	-0.001042	-0.005943	0.003568	0.010757	0.003248	0.002781	0.000567	-0.010647
0.000145	0.001083	0.003875	0.005315	0.003462	0.020057	-0.009821	-0.009078	0.00022	0.015278	0.012946	0.005263	0.004678	-0.015831
-0.027139	-0.038662	0.026584	0.003913	-0.0365	-0.020222	-0.065	-0.018952	-0.020222	-0.020222	-0.020222	0.100264	-0.005146	-0.010495
-0.055218	0.005559	0.041066	-0.021715	0.018697	-0.006847	-0.061424	0.002421	-0.001281	0.019176	0.022796	0.001914	-0.029338	-0.007921

25

0.026956	-0.02784	0.033494	0.002548	0.046225	0.022231	0.016278	0.017597	0.015847	0.071619	0.014748	-0.004753	0.029369	-0.01317
-0.008043	-0.049485	-0.012379	-0.020795	0.042405	-0.043623	0.031666	-0.000129	-0.017942	0.033631	-0.001266	-0.017166	0.062714	-0.056246
-0.01143	-0.011056	0.002048	0.002616	0.006826	-0.001475	0.006679	-0.00683	0.006409	0.040282	-0.002175	-0.004824	-0.004563	-0.006206
-0.02376	0.005028	-0.007134	-0.010644	-0.011369	0.00506	-0.000619	-0.000687	0.004916	0.02339	0.002605	0.011458	0.00284	0.005131
-0.013128	0.01445	-0.019821	-0.019062	-0.016556	0.002295	-0.011258	-0.00125	0.003812	0.015532	-0.001141	0.008414	-0.009945	0.007189
0.002424	-0.016674	-0.019822	-0.000677	-0.006634	0.00412	0.000824	-0.003717	0.005755	-0.011904	-0.005493	-0.011207	0.004332	0.003489
-0.000234	-0.003776	-0.012661	-0.000468	0.006325	-0.001121	-0.000426	-0.004707	-0.003221	-0.003322	-0.009479	-0.013092	0.006646	0.002432
-0.003335	-0.011511	-0.003788	-0.00704	0.012354	-0.001245	-0.008487	0.0091	0.005538	0.002272	-0.008255	-0.013245	-0.005633	0.005559
-0.009941	-0.053725	-0.049933	0.013381	0.069926	-0.019769	-0.020222	0.180549	0.154424	-0.020638	-0.031153	-0.062519	-0.058793	0.080434
0.031146	0.031995	-0.097938	0.031708	0.018263	0.001075	0.038535	0.035699	0.033431	-0.058402	0.004509	0.002188	-0.006218	-0.003298

0.025933	0.049517	0.061815	0.006544	0.071771	-0.037135	0.030091	-0.142396	0.040162	0.065964	0.05294	0.029662	-0.009232	-0.001381
-0.016605	0.0911	-0.023076	-0.018794	-0.036592	0.02431	0.042772	-0.072863	0.07612	0.09697	0.077171	0.005577	-0.001227	-0.053885
-0.023175	0.013164	-0.004304	-0.005062	-0.000235	-0.00384	-0.001101	-0.007625	0.012242	0.007435	0.003688	-0.011129	0.010496	-0.009047
-0.008577	0.01195	0.0067	-0.0023	0.002193	-0.015879	0.009674	0.009555	-0.004822	0.006433	0.001846	-0.008859	0.001545	-0.002834
-0.003868	-0.008805	0.012282	-0.002983	-0.009391	-0.016145	0.006515	0.026556	-0.017052	0.007295	0.009661	-0.011428	-0.001281	0.015034
-0.019588	-0.014634	0.016166	-0.00186	-0.027572	-0.0007	0.007188	0.010904	-0.021699	0.00489	0.003317	-0.015884	-0.015751	0.014465
-0.018191	-0.002986	0.014676	-0.003373	-0.020704	0.000588	0.001392	0.009272	0.001374	-0.008531	0.016692	-0.001846	-0.016233	0.005529
0.000981	-0.000998	0.010833	-0.006448	-0.023802	-0.008926	0.000617	0.015802	-0.004867	2.8E-05	0.00519	0.003333	-0.003521	-0.003493
-0.020222	0.00154	0.011323	-0.010809	-0.047947	-0.057611	-0.039584	-0.020222	0.025	-0.026789	0.006288	-0.020222	-0.01938	0.016293
0.01997	0.023486	0.015362	0.009368	-0.005126	-0.016336	-0.036871	0.033779	0.020573	-0.03707	0.030731	-0.004715	-0.001769	-0.004238

(Average)- 50th data point	((Average)-1st data point) squared	((Average) - 2nd data point) squared
0.00775534	4.56076E-05	0.000154066
-0.04529134	4.07128E-05	0.004412103
-0.00850406	0.000113784	0.000408886
0.00013392	8.24609E-07	5.8843E-05
0.0154617	0.000117317	1.01949E-06
0.0142721	1.64519E-05	5.41122E-05
0.00508812	1.83623E-05	4.36276E-05
-0.00333798	2.45423E-05	2.69951E-06
0.01629324	0.000385053	1.81626E-05
-0.00423814	0.000504683	0.0001309

0.001935	0.001237	0.001052	0.000294	5.15E-05	0.001926	0.019181	0.001447	1.32E-05	0.000207	0.000476	0.045909	0.000339	0.000518
0.000826	0.004091	0.002693	4.72E-05	0.00143	0.002232	0.005228	0.003256	0.001122	0.000818	0.001012	0.004158	0.001962	0.000691
2.72E-05	2.73E-05	7.1E-06	0.000439	3.96E-06	1.24E-05	0.000137	4.43E-07	0.000115	1.39E-05	0.000111	2.13E-06	2.05E-06	8.7E-05
9.49E-06	5.06E-06	1.66E-06	0.000871	6.86E-05	3.31E-05	4.28E-05	6.45E-05	4.48E-05	2.34E-05	5.19E-06	6.01E-05	6.21E-06	2.88E-05
1.65E-05	0.000125	3.1E-05	0.000115	3.45E-05	1.53E-06	0.000319	6.97E-05	3.09E-05	7.72E-05	1.29E-05	0.000105	0.000564	8.03E-05
4.98E-06	6.71E-06	0.000585	0.000601	2.63E-05	1.88E-08	0.00044	0.000104	0.000461	5.23E-05	8.59E-06	9.07E-08	1.09E-05	0.000367
1.62E-05	9.64E-06	3.32E-05	9.17E-05	5.8E-06	2.67E-06	4.31E-05	2.06E-05	0.000221	2.84E-05	9.26E-05	1.09E-06	3.53E-05	1.27E-05
8.24E-08	5.02E-06	6.45E-05	0.000103	3.88E-05	2.1E-08	1.17E-06	1.5E-05	2.82E-05	1.2E-05	0.000402	9.65E-05	8.24E-05	4.84E-08
0.002406	0.00098	0.002246	0.00112	0.000824	0.000737	0.001495	0.000707	1.53E-05	0.001332	0.000409	0.004225	0.000359	0.000409
0.000386	0.000146	0.001545	1.2E-05	2.07E-05	0.003049	3.09E-05	0.001686	0.000472	0.00035	4.69E-05	0.003773	5.86E-06	1.64E-06

25

0.001837	9.72E-06	0.052856	0.00212	0.00355	0.000727	0.000775	0.001122	6.49E-06	0.002137	0.000494	0.000265	0.00031	0.000251
4.49E-05	4.82E-05	0.004538	0.001872	0.008321	6.47E-05	0.002449	0.000153	0.000432	0.001798	0.001903	0.001003	1.67E-08	0.000322
0.000175	0.000155	4.61E-06	7.13E-08	0.000198	0.000131	0.000122	4.19E-06	6.84E-06	4.66E-05	2.18E-06	4.46E-05	4.66E-05	4.11E-05
5.26E-05	0.000149	0.000166	5.31E-05	0.000137	0.000565	2.53E-05	5.09E-05	0.000113	0.000129	2.56E-05	3.83E-07	4.72E-07	2.42E-05
1.67E-06	0.000176	4.94E-05	3.25E-08	0.000221	0.000172	0.000209	0.000393	0.000363	0.000274	5.27E-06	0.000127	1.56E-06	1.45E-05
0.000122	0.000231	1.27E-05	3.87E-05	8.46E-05	5.88E-06	0.000278	0.000393	4.58E-07	4.4E-05	1.7E-05	6.79E-07	1.38E-05	3.31E-05
0.000116	1.06E-05	7.73E-06	3.22E-07	0.000113	5.47E-08	1.43E-05	0.00016	2.19E-07	4E-05	1.26E-06	1.81E-07	2.22E-05	1.04E-05
0.000233	0.000168	2.77E-05	2.19E-05	0.000251	1.11E-05	0.000133	1.43E-05	4.96E-05	0.000153	1.55E-06	7.2E-05	8.28E-05	3.07E-05
0.000409	0.000409	0.010053	2.65E-05	0.00011	9.88E-05	0.002886	0.002493	0.000179	0.00489	0.000391	0.000409	0.032598	0.023847
0.000368	0.00052	3.66E-06	0.000861	6.27E-05	0.00097	0.001024	0.009592	0.001005	0.000334	1.16E-06	0.001485	0.001274	0.001118

0.000218	0.000218	2.26E-05	0.000863	0.000173	0.000673	0.002452	0.003821	4.28E-05	0.005151	0.001379	0.000905	0.020277	0.001613
1.6E-06	1.6E-06	0.000295	0.003933	0.003164	0.000276	0.008299	0.000533	0.000353	0.001339	0.000591	0.001829	0.005309	0.005794
4.73E-06	4.73E-06	2.33E-05	2.08E-05	3.85E-05	0.000537	0.000173	1.85E-05	2.56E-05	5.53E-08	1.47E-05	1.21E-06	5.81E-05	0.00015
6.79E-06	6.79E-06	0.000131	8.07E-06	2.63E-05	7.36E-05	0.000143	4.49E-05	5.29E-06	4.81E-06	0.000252	9.36E-05	9.13E-05	2.33E-05
1.3E-06	1.3E-06	7.08E-05	9.89E-05	5.17E-05	1.5E-05	7.75E-05	0.000151	8.9E-06	8.82E-05	0.000261	4.24E-05	0.000705	0.000291
3.02E-05	3.02E-05	0.000126	1.88E-05	1.22E-05	0.000384	0.000214	0.000261	3.46E-06	0.00076	4.9E-07	5.17E-05	0.000119	0.000471
8.98E-05	8.98E-05	0.000171	4.42E-05	5.92E-06	0.000331	8.92E-06	0.000215	1.14E-05	0.000429	3.46E-07	1.94E-06	8.6E-05	1.89E-06
6.81E-05	6.81E-05	0.000175	3.17E-05	3.09E-05	9.62E-07	9.96E-07	0.000117	4.16E-05	0.000567	7.97E-05	3.81E-07	0.00025	2.37E-05
0.00097	0.00097	0.003909	0.003457	0.00647	0.000409	2.37E-06	0.000128	0.000117	0.002299	0.003319	0.001567	0.000409	0.000625
2.03E-05	2.03E-05	4.79E-06	3.87E-05	1.09E-05	0.000399	0.000552	0.000236	8.78E-05	2.63E-05	0.000267	0.001359	0.001141	0.000423

					((Average) - 50th data point) squared	**Average of Squared value**
0.004351	0.002803	0.00088	8.52E-05	1.91E-06	6.01453E-05	0.00374469
0.009403	0.005955	3.11E-05	1.51E-06	0.002904	0.002051305	0.00218067
5.53E-05	1.36E-05	0.000124	0.00011	8.18E-05	7.2319E-05	8.02703E-05
4.14E-05	3.41E-06	7.85E-05	2.39E-06	8.03E-06	1.79346E-08	7.7206E-05
5.32E-05	9.33E-05	0.000131	1.64E-06	0.000226	0.000239064	0.000126307
2.39E-05	1.1E-05	0.000252	0.000248	0.000209	0.000203693	0.000148869
7.28E-05	0.000279	3.41E-06	0.000264	3.06E-05	2.5889E-05	6.66685E-05
7.85E-10	2.69E-05	1.11E-05	1.24E-05	1.22E-05	1.11421E-05	7.30818E-05
0.000718	3.95E-05	0.000409	0.000376	0.000265	0.00026547	0.002463797
0.001374	0.000944	2.22E-05	3.13E-06	1.8E-05	1.79618E-05	0.000754866

Average of squared values/Bulk velocity Squared

0.051367486
0.029913173
0.001101101
0.001059067
0.0017326
0.002042103
0.00091452
0.001002494
0.033796938
0.010354815

(Location of first (vector) data point / Radius at that section) or y/R value

0.0306	0.051367
0.2346	0.029913
0.449	0.001101
0.6633	0.001059
0.877	0.001733
0.836	0.002042
0.724	0.000915
0.5	0.001002
0.2959	0.018564
0.0612	0.010355